Bioremediation of Industrial VOC Air Pollutants

A Thesis submitted to the
College of Graduate Studies and Research
in partial fulfillment of the requirements for the
Degree of Doctor of Philosophy (Ph.D.)

In the
Department of Chemical Engineering
University of Saskatchewan
By
Hossein Nikakhtari

Permission to use

In presenting this thesis in partial fulfillment of the requirements for a doctorate degree of philosophy from the University of Saskatchewan, I agree that the Libraries of this University may make it freely available for inspection. I also agree that permission for extensive copying of this thesis for scholarly purposes may be granted by Dr. Gordon Hill who supervised my thesis, or in his absence, by the head of the Chemical Engineering Department or the Dean of the College of Graduate Studies. It is understood that due recognition will be given to me and to the University of Saskatchewan in any use of the material within this thesis. Any copying, publication, or use of this thesis or parts for financial gain is prohibited without my written permission.

Requests for permission to copy or to make other use of material in this thesis in whole or part should be addressed to:

Head of the Department of Chemical Engineering
University of Saskatchewan
Saskatoon, Saskatchewan
Canada, S7N 5A9

Acknowledgements

First of all, I would like to thank my supervisor Dr. Gordon A. Hill, who was ready to teach me, guide me, and advise me any time that I needed. Anytime there was an obstacle in our work, Dr. Hill had a good suggestion to overcome it. Besides, it was his encouragement and support that helped me to pursue this project to completion.

I would also like to thank the Iranian Ministry of Science, Research, and Technology for scholarship support for myself during this work.

I am grateful for the financial support provided by the Natural Sciences and Engineering Council of Canada (NSERC).

I appreciate valuable assistance that I received from the technicians and secretaries of the Chemical Engineering Department, University of Saskatchewan.

Finally, I would like to thank my family, who were a great support for me whenever I faced problems during this work.

Abstract

The External Loop Airlift Bioreactor (ELAB) with a packed bed in the riser section is the novel technology developed in this research, and its performance was examined by comparison to shake flasks and a well-mixed bioreactor.

Microbial growth on glucose (fast metabolism) and phenol (slow metabolism) was initially studied using *Pseudomonas putida* in shake flasks and also a mixed bioreactor considering both substrate and oxygen depletion. Mass transfer resistances for oxygen transfer through both a closure and headspace of shake flasks and also into the liquid phase were investigated. A new equation for prediction of K_La in shake flasks and new equations for prediction of k_Ga in shake flasks with closures are introduced. A combined model for oxygen mass transfer and microbial growth is shown to accurately predict experimental oxygen concentrations and oxygen yield factors during both slow and fast growth experiments in shake flasks better than any previous published models.

A small quantity of nylon mesh packing (96.3% porosity) inserted in the riser section of an ELAB was then investigated and found to increase the overall volumetric oxygen mass transfer coefficient by a factor of 3.73 compared to an unpacked riser. Problems due to absorption in the nylon packing led to the study of a stainless steel mesh packing (99.0% porosity) in the riser which was found to increase the overall volumetric mass transfer coefficients by an average factor of 2.45, 1.66, and 1.34 for oxygen, toluene, and benzene, respectively, compared to an unpacked riser. The packing increased gas holdup, decreased bubble size, and decreased liquid circulation rates in the bioreactor, all of which contributed to the dramatic improvement in mass transfer.

A dynamic, spatial model was developed to predict the mass transfer behavior between air bubbles and the continuous liquid phase in the ELAB with and without a packed bed. The model demonstrated superior accuracy compared to simulating the ELAB as a well-mixed vessel and also correctly predicted the cyclical behavior in the liquid phase oxygen or VOC concentrations. The mass transfer coefficient was determined as a best fitting parameter of the model. The oxygen mass transfer coefficient was found to increase to values approaching 0.021 s^{-1} (at 2.61 vvm aeration rate) using the small amount of packing. This is similar to values measured in well-

mixed bioreactors operating at the same aeration rates. A difference was observed between absorption and desorption rates of VOCs, which was explained by the decrease in gas bubble sizes in the presence of VOCs.

The ELAB with stainless steel mesh packing (99% porosity) was used for bioremediation of a phenol polluted air stream. The packing enhanced VOC and oxygen mass transfer rates and provided a large surface area for cell immobilization. Using a pure strain of *Pseudomonas putida*, batch and continuous runs at three different dilution rates were completed in this bioreactor with phenol polluted air as the only source of growth substrate. Essentially 100 % phenol removal was achieved in only one third of the bioreactor at a phenol loading rate of 33240 $mg/h.m^3$, superior to any previously reported biodegradation rates of phenol polluted air. Also a mathematical model has been developed and was shown to accurately predict steady state and quasi-steady state experimentally measured concentrations. This bioreactor seems to be a novel bioreactor with a high potential to continuously bioremediate VOC contaminated gas discharges at high loading rates.

Table of Contents

List of Tables

List of Figures

Chapter 1- Introduction

1.1 The Problem

1.1.1 Volatile Organic Compounds

Toxic Volatile Organic Compounds (VOCs) including many industrial hydrocarbons are dangerous environmental and/or health problems when present in the atmosphere beyond a certain concentration, which differs for each VOC. Sources of VOC emissions include industrial processes involved with solvents (basic and fine chemicals, degreasing of metals, paint production and application, printing, glues and adhesives, rubbers and plastics, etc.), or other industries (oil refineries, use of CFCs, production of alcoholic drinks, livestock operations, etc.). Another major source is motor vehicles which are used for transportation. Total emission quantity of non methane VOCs in 2003 was calculated to be 1400 kt which, although a very large number, is a 42% decrease compared to 1990 emissions (Citepa, 2005). The solution to VOC air pollution problems can often be undertaken at the source of emission. For instance, in the case of industries involved with solvents, a good action can be substitution of volatile solvents or reduction in losses by removing leaks. These techniques are not always possible or adequate to meet the limits established by regulations. Therefore elimination processes must often be used to purify waste gases (Citepa, 2005).

1.1.2 VOC Elimination Strategies

There are biological methods as well as classical techniques (such as thermal or catalytic incineration, adsorption, and scrubbing) to eliminate VOCs from waste gas streams.

Biological methods have some advantages including easy design and maintenance (low capital and running costs) and being environmentally friendly due to

producing harmless secondary byproducts (Daubert et al., 2001) that do not contribute to pollution. In biological systems, pollutants are usually oxidized to less harmful products such as CO_2, H_2O, and SO_4^{2-} (Woertz et al., 2001) mostly at ambient temperatures and pressures. The pollutant is used as the primary food source for microorganisms to grow and maintain their metabolic functions. The development of biological methods for treatment of air pollution started after that for water pollution because the aqueous phase is the living environment for microorganisms. For treatment of air pollution, pollutants need to be first transferred into the liquid phase and then assimilated by microorganisms. Nevertheless, new biological technologies have been shown to be effective and economical methods to degrade VOCs and odors in industrial effluents (Auria et al., 2000). Biological air treatment systems need to meet two main requirements to eliminate VOC air pollutants efficiently. They should first provide fast mass transfer of pollutants from the air phase to the liquid phase, and second fast metabolism of the pollutant by the microorganism in the liquid phase. Many types of biological systems have been invented to meet these goals, including bioscrubbers, trickling filters and biofilters.

1.2 Fundamentals of Biogrowth

1.2.1 Microbial Growth

A bacterial culture grows according to a first-order autocatalytic chemical reaction:

Rate of cells increase = μ (number or mass of cells)

which defines the rate constant, μ, usually called the specific growth rate. In mathematical terms:

$$\frac{dN}{dt} = \mu N \qquad \text{or} \qquad \frac{dX}{dt} = \mu X \tag{1.1}$$

Upon integration:

$$\ln N - \ln N_0 = \mu(t - t_0) \tag{1.2}$$

$$\mu = \frac{2.303(\log N - \log N_0)}{(t - t_0)} \tag{1.3}$$

which can be used to calculate μ.

Another commonly used parameter is the mean doubling time or generation time (t_d) which is the time required for the cell culture to double. If $N=2*N_0$ then $t - t_0 = td$. Substitution in Equation 1.3 yields:

$$\mu = \frac{\ln 2}{t_d} = \frac{0.693}{t_d} \tag{1.4}$$

For a bacterial culture under a non-growth limiting condition, the specific growth rate and doubling time are constants (Stanier et al., 1986) and this constant specific growth rate is often referred to as the maximum specific growth rate, $\mu_{\max}$.

1.2.2 Specific Growth Rate

Research has shown that specific growth rate of microorganisms is affected by substrate concentration, which is frequently expressed by the Monod equation:

$$\mu = \frac{\mu_{\max} S}{K_S + S} \tag{1.5}$$

Where K_S is a coefficient, equal to the substrate concentration when the specific growth rate is half of its maximum value (μ_{max}), as shown in Figure 1.1. According to the Monod equation, increasing the substrate concentration does not affect the specific growth rate after reaching the maximum value. However, it has normally been observed that the specific growth rate starts to decrease when substrate concentration passes a certain value. Improved models have been proposed to express this inhibitory effect of the substrate such as the Haldane equation:

$$\mu = \frac{\mu_{\max} S}{K_S + S + S^2 / K_I} \tag{1.6}$$

The specific growth rate is also affected by the product concentration, medium pH, temperature and oxygen supply. The optimum or critical values of these parameters differ for every microorganism (Lee, 1992).

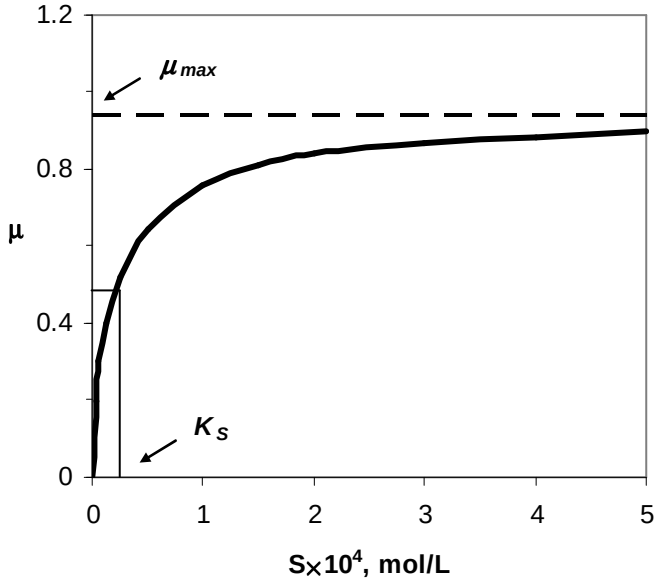

Figure 1.1 Variation of specific growth rate with limiting substrate concentration, μ_{max} = 0.935 h^{-1}, $K_S = 0.22 \times 10^{-4}$ mol/L (Lee, 1992, pp. 145).

1.3 Bioreactors

There are several types of bioreactors, some include different kinds of column bioreactors that are becoming popular for biological applications. The following text reviews some column bioreactors and finally discusses the External Loop Airlift Bioreactor (ELAB), the main bioreactor used in this work.

1.3.1 Bioscrubber versus Trickle-bed Bioreactor

Mass transfer of toluene from the gas to the liquid phase requires more energy in bioscrubbers than trickle-bed bioreactors. Bioscrubbers are more suitable for mass transfer of hydrophilic substrates rather than pollutants with high Henry coefficients that require large gas-liquid interfaces. Trickle-bed bioreactors provide a large gas-liquid interface that reduces the costs of mechanical mixing and air compression needed in bioscrubbers. Furthermore, trickle-bed bioreactors have a high volumetric degradation rate due to the microbial activity and high biomass concentration immobilized in the

biofilm. However, high biomass concentrations brings some problems such as clogging and channel formation, which in turn result in a reduction of interfacial area and an increase of required air pressure. Therefore, to maintain the capacity and continuity of a trickle-bed bioreactor for waste gas treatment, it is necessary to control biomass formation (Wubker et al., 1997).

The major disadvantage of trickle-bed bioreactors for waste gas treatment is the increase of biomass, which result in an increase in pressure drop, a decrease in the active surface of the biofilm, channel formation and clogging. Wubker et al. (1997) suggested two ways to maintain the volumetric degradation rate in trickle-bed bioreactors: 1. reduction of biomass formation rate and 2. removal of the extra biomass. Reduction of biomass formation rate has been achieved by limiting a nutrient such as phosphate or potassium. To prevent clogging of a bioreactor, Weber et al. (1996) tried limiting the nutrients available for growth, but as a consequence lower removal rates were observed. They then tried a different fungal culture in the bioreactor, and in this case the toluene removal rate under nutrient limiting conditions was found to be higher. As an alternative method, they also studied the application of a NaOH wash to remove excess biomass. Alonso et al. (1996) removed excessive biomass by media fluidization and also backwashing of the biofilter. Schonduve et al. (1996) suggested discontinuous trickling and addition of an inert salt (like NaCl) in trickle-bed bioreactors.

Laurenzis et al. (1998) developed a new trickle-bed bioreactor with discontinuous removal of the biomass and discontinuous trickling of liquid for elimination of chemicals from waste gases. Surplus biomass was removed from the packing material by mechanical shear. Using this method, they achieved high volumetric degradation rates (about 100 g toluene m^{-3} h^{-1}, at a loading of 150 g toluene m^{-3} h^{-1}). The pressure drop after biomass reduction was almost identical to the theoretical pressure drop for the packed bed without biomass.

1.3.2 Bubble Column or Airlift Bioreactor

The bubble column, airlift bioreactor or tower fermenter is a simple bioreactor without any moving parts in which the liquid is partially mixed by the rising bubbles dispersed from a sparger located in the bottom of the column. These bubbles provide

oxygen for cells and also substrate in the case of bioremediation of air pollutants. Bubble column bioreactors have several advantages over the stirred tank bioreactors including: ease of construction and operation, fewer chances of contamination and lower shear rates. The last one is particularly important for shear-sensitive cells. However, sometimes the rising bubbles do not provide adequate mixing for optimal growth and only the lower part of the bioreactor can maintain high cell concentrations. As the cell concentration increases, higher airflow rates are needed, which in turn can cause excessive foaming and higher residence times of bubbles. The bubbles can coalesce, as they rise in the column, which results in a decrease in the mass transfer rate. Bubble columns are limited to a very narrow range of operating conditions (Lee, 1992).

1.3.3 Loop Bioreactor

A loop bioreactor is a column bioreactor or fermenter with a liquid circulation loop. Different loop configurations are shown in Figure 1.2. The airlift loop bioreactor, in which the liquid circulation is provided by a density difference between the riser liquid containing air bubbles and the downcomer liquid without any bubbles (Figure 1.2(a), Lee, 1992) is the geometry used in this investigation.

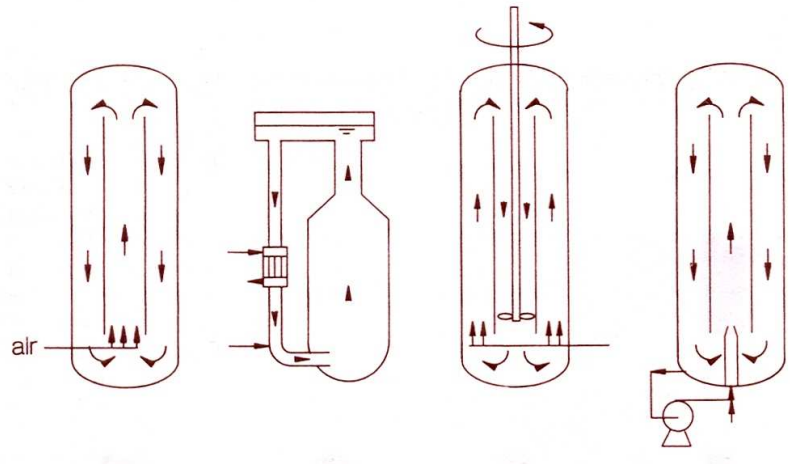

Figure 1.2 Loop bioreactors: (a) air-lift, (b) ICI pressure cycle, (c) stirred loop, and (d) jet loop (Lee, 1992, pp. 173).

1.3.4 ELAB

The External Loop Airlift Bioreactor (ELAB) is one type of air-lift loop bioreactor in which the net density difference of fluid in riser and downcomer sections of the bioreactor is the driving force causing liquid circulation in the bioreactor. There is no pump or impellers needed for circulating or mixing liquid. Compared to a bubble column, an ELAB improves mixing by circulating the liquid phase, which provides sufficient mixing for the slow process of fermentation. On the other hand, the turbulence in the liquid is reduced by damping out eddies found in bubble columns. The enhanced mixing in the loop airlift column forms a more homogeneous environment as compared to a bubble column. In continuous operations, a loop airlift bioreactor acts more closely to a well-mixed vessel as compared to an ordinary bubble column. To improve mass transfer between the gas and liquid phases in an ELAB, important hydrodynamic parameters to consider are the two-phase flow pattern, liquid physical properties, gas holdup, liquid circulation velocity, bubble sizes, bubble distribution, dispersion, and turbulence intensity (Cheremisinoff, 1996).

1.3.5 ELAB with porous sparger

A 75% enhancement of gas holdup and a threefold enhancement of the overall mass transfer coefficient have been found using a porous sparger instead of a 0.4 mm diameter standard orifice sparger (Cheremisinoff, 1996). However, there are two disadvantages involved in using a porous sparger: plugging of the tiny orifices by either microbial fouling or localized crystallization always occurs and the excess required power to pump air through the tiny porous openings.

1.3.6 ELAB with a Spinning Sparger

Fraser et al. (1993) used a rotating sparger with standard orifice diameters in an airlift bioreactor and generated small and uniform air bubbles. A schematic drawing of the ELAB with a spinning sparger is shown in Figure 1.3. This modification produced high, localized shear rates at the point of the gas stream entry and by locating the spinning sparger below the liquid circulation path, the flat plate sparger design did not

impact circulating microorganisms. Using baffles on the walls around the spinning sparger prevented occurrence of a vortex motion in the riser section of the column. Increasing the spinning rate increased the gas holdup and decreased the mean bubble diameters, which both contributed to a tripling of interfacial surface area in the riser section at the maximum rotational speed of 7.2 rev/s, and thereby enhanced the mass transfer rate. This technique reduced the demand for high gassing rate in the ELAB [47] and did not have the problems of plugging or high pressure drops that occur using a porous sparger.

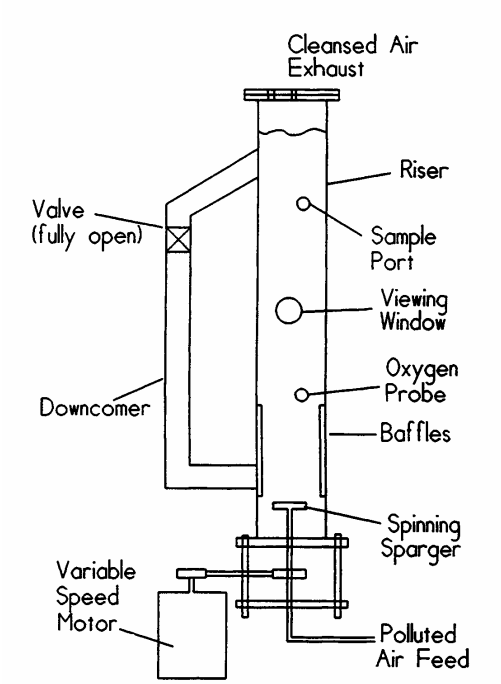

Figure 1.3 Schematic drawing of the ELAB with a spinning sparger (Wei et al., 1999).

1.3.7 ELAB with a Packed Bed

Mathison et al. (1992) investigated the ability of commercially available packing to enhance the biodegradation of water-soluble toxic organics in a packed bed bioreactor. They studied seven packing materials: nylon, HDPE, porcelain and acrylic rasching rings, crushed glass, sintered stainless steel and nylon pot scrubbers. They found that the mesh packing using plastic (likely nylon) provided the overall best design. They achieved 100% biodegradation efficiencies at 600 mg/L inlet phenol concentration and a low liquid flux. However, the highest biodegradation rate (about 8×10^{-5} kg/m^3·s)

was achieved at the highest liquid flux (2×10^{-3} m/s). They also showed that co-degradation of phenol and chlorophenols can take place using the packed bed column.

Meng et al. (2002 a) combined the ELAB and the packed bed bioreactor into one bioreactor. They inserted woven nylon packing in the riser section of the ELAB to represent the packed bed and the spinning sparger was employed to generate air bubbles. They found that the dependence of gas holdup on packing height was small. They reported the optimal hydrodynamic conditions for a packed ELAB occurred at a high packing porosity, observed to be 0.99, with full packing height between the top of the gas sparger and the downcomer inlet. These conditions would permit high, immobilized biomass holdup attached to the packing, highest gas holdup to improve mass transfer, and large void spaces to reduce plugging and liquid frictional losses.

1.4 Some Other Aspects of Column Bioreactors

1.4.1 Measurement of Gas Holdup

The gas holdup is the most important factor in the study of hydrodynamics and mass transfer in airlift bioreactors. These bioreactors typically operate in the bubble flow regime. The gas holdup or the gas void fraction is defined as the volume fraction of the gas phase in the gas-liquid mixture. The volume of dispersed phase can be related to the height of this mixture, but in practice it is difficult to measure this height due to the fluctuation of fluid, especially at higher gas flow rates. The pressure gradient method (Chisti, 1989) is widely used to determine the overall gas holdup in airlift bioreactors. The problem in using this method is that energy dissipation between the two pressure measurement ports is responsible for some of the pressure gradient.

Meng et al. (2002 b) developed an inclined, oil-filled, manometric tube to measure the volume expansion in the riser section of an ELAB due to gas holdup. An inclined glass tube with a 3 mm internal diameter was installed on the ELAB at the same height as that of the liquid phase when there was no gas holdup in the ELAB. After

introducing air into the ELAB, the height of gas liquid dispersion was higher than the original height of the liquid phase. The difference between these two heights is a direct measurement of the overall gas holdup. Using the inclined tube method, the overall gas holdup was shown to be very close to the results determined using a gamma ray density method. But significant disagreements were found between this method and the pressure gradient method due to frictional pressure losses in the riser section of the bioreactor. A combination of the inclined tube and pressure gradient methods can be a simple way to measure frictional energy losses in a bubbling column (Meng et al., 2002 b).

1.4.2 Dynamic Mixing and Oxygen Transfer

Fraser et al. (1994) developed a model that predicts the dynamic oxygen-transfer rates in the ELAB at different air flow rates and sparger spinning speeds. As the orifice speed in the sparger increased from 0.30 m/s to 0.99 m/s, the required time to reach 30% of dissolved oxygen saturation level dropped from 81 to 45 s. By increasing the air superficial velocity from 0.48 to 0.84 cm/s, the required time to reach 30% of dissolved oxygen saturation level dropped by another 10 s to 35 s. The increased orifice speed reduced air bubble size and increased gas holdup while the increased air superficial velocity increased gas holdup, which all contributed to enhance the oxygen mass transfer coefficient, $k_L a$.

1.4.3 Lag Phase Kinetic Model

Microbial cells have to adjust to the surrounding environment before they can actively metabolize a substrate. This lag phase can happen when there is a sudden change in the cell environment such as temperature, type of substrate or even substrate concentration. Tarighian et al. (2001) used a lag phase model during the lag phase and the Monod model after the lag phase to express cell growth kinetics:

$$\mu = \mu_L[1 - \exp(-\frac{S}{K_S})] \qquad t<t_L \qquad (1.7)$$

This model was shown to represent batch growth, start-up continuous flow growth and step-up concentration changes in a continuous flow bioreactor. Under controlled conditions (inoculum amount and phenol concentration), the lag time for

Pseudomonas putida was 10.5 h but this value increased by increasing the phenol concentration.

1.4.4 A New Gas/Liquid Contactor

In most cases, microbial degradation occurs in the aqueous phase; therefore, for bioremediation of air pollutants, the first step is moving gaseous compounds into a liquid phase before their elimination. However, because of low VOC solubilities, high residence times are needed which leads to increased bioreactor size. Daubert et al. (2001) introduced a new gas/liquid contactor called an "aero-ejector" to sweep the liquid phase along by a gaseous flow. The high turbulence created inside the aero-ejector created a high dispersion of the liquid into the gas and a close contact between the two phases, which in turn enhanced the mass transfer rate. This technique seemed to be effective particularly when gaseous compounds had diluted concentrations (less than 10^{-2} kg·m^{-3}). When used for a gas stream with a high flow rate (more than 3 m^3·s^{-1}), toxic compounds were transferred into a liquid with a small volume (with a volume ratio higher than 500) for further biological treatment. A bioreactor then can be used to eliminate the dissolved compounds (Daubert et al., 2001).

1.5 Bioremediation Experiments in the ELAB

1.5.1 Biodegradation of Phenol-Polluted Air in an ELAB

Using an ELAB, Ritchie et al. (1995) found phenol to be completely absorbed into water below the detectable outlet air concentrations (2 mg/m^3 of air) at the highest air superficial velocities and longest run times used in their experiments. They used a 12.3 L ELAB for the bioremediation of phenol-contaminated air with a phenol loading of 1800 to 16200 mg/(h·m^3). In this range, phenol removal from air and its biodegradation in the liquid phase was essentially complete.

1.5.2 Bioremediation of Contaminated Air in an ELAB

Wei et al. (1999) used *Pseudomonas putida* (ATCC 17484) to bioremediate p-cresol and *Acetobacter aceti* (ATCC 15973) to metabolize ethanol in an ELAB. They showed that the ELAB is an effective bioreactor for bioremediation of highly soluble, semi-volatile and volatile organic chemicals from contaminated air. They also found that batch biokinetics for phenol (Ritchie and Hill, 1995), p-cresol and ethanol could be used to predict the dynamic behavior of the ELAB. Using a modeling approach, they determined that a volatile organic chemical can be bioremediated at high loading rates (up to 220 $g/m^3 \cdot h$ for ethanol) using a very slow growing microorganism. This required careful adjustment of the initial biomass inoculum and continuous operation at a very low dilution rate in steady-state mode.

1.5.3 Bioremediation of Toluene in an ELAB

Harding et al. (2001) used the ELAB with a spinning sparger to bioremediate toluene, a commonly emitted pollutant with high volatility and low solubility. They found *Pseudomonas putida* can successfully degrade toluene in an ELAB. There was no significant increase in mass transfer of toluene into the liquid medium when the sparger speed was increased over 310 rpm. Toluene was degraded more efficiently when the culture had previous exposure to the substrate. In fed-batch liquid operation, successful degradation was limited by nutrient availability. Slurry of activated carbon was observed to act as a buffer and minimized the effects of shock loadings and it also minimized the amount of toluene escaping in the exit gas stream.

1.6 Hydrodynamic Correlations for the ELAB

The following empirical and semi empirical correlations have been reported to reasonably predict important parameters in the ELAB by earlier researchers.

Correlation for gas holdup in the ELAB:

$$\varepsilon_{GR} = 1.06 \times J_{GR}{}^{0.701}(1+U_T)^{0.379} \quad \text{without packing} \tag{1.8}$$

$$\varepsilon_{GR} = (-2.75 + 0.272 \times h_p + 4.03 \times \phi_s) \times J_{GR}{}^{0.701}(1+U_T)^{0.379} \quad \text{with packing} \tag{1.9}$$

Correlation for liquid velocity in the riser:

$$U_{LR} = C_F \times E \tag{1.10}$$

where:

$$E = \left(\frac{\varepsilon_{GR}}{(1-\varepsilon_{GR})^{-2} + (A_R / A_D)^2} \right)^{0.92} \tag{1.11}$$

C_F (m/s) represents the effect of friction on velocity, while E represents the gas holdup driving force for liquid circulation as developed by Chisti et al. (1989). In Equation 1.10, the frictional term is calculated by:

$$C_F = 19.1 \quad \text{without packing} \tag{1.12}$$

$$C_F = -54.3 - 7.53 \times h_p + 71.4 \times \phi_s \quad \text{with packing} \tag{1.13}$$

Correlation for axial dispersion:

Axial dispersion is normally expressed by the dispersion coefficient (*D*) and for circulating columns, by the dimensionless Bodenstein number (*Bo*), which is defined as:

$$Bo = \frac{U_{LR} \times L}{D} \tag{1.14}$$

The Bodenstein number was about 47 for no packing in an ELAB, but when packing is placed in the ELAB, the Bodenstein number falls depending on the packing height and porosity (Meng et al., 2002 a).

Correlation for interfacial area:

Interfacial area, like gas holdup, is affected by both the air flow rate and the rotation speed of the sparger (Fraser et al., 1994):

$$a = 179 \times J_{GR}{}^{0.49}(1+U_T)^{1.34} \tag{1.15}$$

1.7 Standard Error

Throughout chapters of this thesis mean values have been reported as: mean value ± one standard error. With assumption of a normal distribution, this interval has a 68.26% confidence level. In biological studies, it is common to use this level of confidence.

1.8 Objectives

It is not always possible to prevent emissions of toxic VOCs in the gas effluents of industries that deal with these compounds. In these cases, industries search for economical and simple technologies to purify their effluent gases. Bioremediation of organic air pollutants is a cheap, easy and attractive method for elimination of VOCs compared to classical elimination methods. Research is continuing to make bioremediation methods even cheaper and easier to carry out. Any enhancement in VOC and oxygen mass transfer into the liquid phase and VOC degradation in the liquid phase can lead to a smaller and more cost-effective bioreactor. With this in mind, a novel bioreactor is introduced in this project and its mass transfer and bioremediation performance is investigated.

The first step to start this work involved mass transfer and biodegradation studies in shake flasks and a well-mixed bioreactor using the selected microorganism. Shake flask and well-mixed bioreactor studies are commonly performed to understand the growth behavior of microorganisms prior to studying their behavior in novel bioreactors, the packed bed ELAB in this case. Biogrowth experiments in shake flasks and well-mixed bioreactors were performed with both glucose and phenol as growth substrates. Every microorganism grows very well on glucose. Therefore, glucose is the best starting substrate as a comparison point for growth studies of any microorganism on any other substrate. Growth on glucose is faster than on VOCs, which is shown in kinetic growth

parameters such as the specific growth rate. Kinetic parameters are a good basis for comparison of growth on VOC substrates.

The main objective of this project is to study the mass transfer and bioremediation of some organic industrial air pollutants in a novel bioreactor, which is a combination of the External Loop Air Lift Bioreactor (ELAB) and a Packed Bed column. This bioreactor is expected to have two complementing features. The first feature involves the enhancement of oxygen and VOCs mass transfer rate from the air phase into the liquid phase. Enhancement of either oxygen or VOCs mass transfer rate can result in faster bioremediation of VOCs with higher loading rates. The second feature is enhancement in the biodegradation rate due to a high biomass concentration located in an immobilized biofilm that will be developed on the packing of the ELAB. Oxygen and three organic chemicals: phenol, toluene, and benzene have been used to investigate enhancements in mass transfer. Phenol is soluble in water and has relatively low volatility, so it can be considered as a semi-volatile organic chemical. Toluene and benzene have low solubilities in water and are more volatile, so they are good examples of volatile organic chemicals. For bioremediation studies, phenol has been used as a model air pollutant. Mathematical mass transfer and bioremediation models are also developed in this study.

Specifically, the objectives of this work are divided into the following headings:

- Growth study in shake flasks and a well-mixed bioreactor.
- Oxygen mass transfer study in the ELAB with and without a packed bed.
- VOCs mass transfer study in the ELAB with and without a packed bed.
- Phenol bioremediation in the ELAB with a packed bed.

The order of chapters in this thesis is in accordance with these objectives. Chapter Two and Three include the results of the first objective, growth studies in shake flasks and a well-mixed bioreactor, and determination of growth parameters of the microorganism used in this thesis, *Pseudomonas putida*. Chapters Four and Five include studies on the second objective, oxygen mass transfer, while Chapter Six is about the third objective, VOCs mass transfer in the ELAB with and without a packed bed. Finally, Chapter Seven presents results on the last objective, phenol bioremediation in the ELAB with a packed bed.

1.8 Nomenclature

a	Interfacial area in bioreactor (m^2/m^3)
A_D	Downcomer cross sectional area (m^2)
A_R	Riser cross sectional area (m^2)
Bo	Bodenstein number (dimensionless)
C_F	Friction loss variable (m/s)
D	Axial dispersion coefficient (m^2/s)
E	Gas holdup function
h_p	Packing height (m)
J_{GR}	Superficial gas velocity in the riser section (m/s)
K_S, K_I	Constants for cell growth kinetics
L	Length of circulation loop (m)
N	Cell number
N_0	Initial cell number
S	Substrate concentration (mg/L)
t	time (s)
t_0	start time (s)
t_d	Doubling or generation time (s)
t_L	Lag phase time (h)
U_{LR}	Riser section liquid velocity (m/s)
U_T	Orifice speed (m/s)
X	Cell density (mg/L)
ε_{GR}	Overall gas holdup
ϕ_s	Packing porosity
μ	Specific cell growth rate (h^{-1})
μ_L	Lag phase specific cell growth rate (h^{-1})
μ_{max}	Maximum specific cell growth rate (h^{-1})

1.9 References

Alonso, C.; Suidan, M. T.; Sorial, G. A.; Smith, F. L.; Biswas, P.; Smith, P. J.; Brenner, R. C. Gas Treatment in Trickle-Bed Biofilters: Biomass, How Much Is Enough? *Biotechnol. Bioeng.* **1997** *54*, 583-594.

Auria, R.; Frere, G.; Morales, M.; Acuna, M. E.; Revah, S. Influence of Mixing and Water Addition on the Removal Rate of Toluene Vapors in a Biofilter, *Biotechnol. Bioeng.* **2000** *68*, 448-455.

Cheremisinoff, N. P. Mixed Flow Hydrodynamics. Gulf Publishing Co., Houston 1996, pp. 499-519.

Chisti, M. Y. Airlift Bioreactors. Elsevier Science Publishers, New York 1989, pp. 203-206.

Citepa website, http://www.citepa.org/pollution/sources_en.htm#cov, and http://www.citepa.org/techniques/cov_en.htm, 2005.

Daubert, I.; Lafforgue, C.; Maranges, C.; Fonade, C. Feasibility Study of a Compact Process for Biological Treatment of Highly Soluble VOCs Polluted Gaseous Effluent. *Biotechnol. Prog.* **2001**, *17*, 1084-1092.

Fraser, R. D.; Hill, G. A. Hydrodynamic Characteristics of a Spinning Sparger, External Loop Airlift Bioreactor. *Can. J. Chem. Eng.* **1993**, *71*, 419-425.

Fraser, R. D.; Ritchie, B. J.; Hill, G. A. Dynamic Mixing and Oxygen Transfer in Small, Airlift Loop Bioreactor. *Biotechnol. Prog.* **1994**, *10*, 543-574.

Harding, R.; Hill, G. A. Bioremediation of Toluene in an External Loop Airlift Bioreactor. M.Sc. Thesis Report, 2001.

Laurenzis, A.; Heits, H.; Wubker, S. M.; Heinze, U.; Friedrich, C.; Werner, U. Continuous Biological Waste Gas Treatment in Stirred Trickle-Bed Reactor with Discontinuous Removal of Biomass. *Biotechnol. Prog.* **1998**, *57*, 497-503.

Lee, J. M. Biochemical Engineering. Prentice-Hall, 1992, pp. 144-174.

Mathison, S.; Hill, G. A. Effect of Packing Material on Phenol Biodegradation. U of S Report for Cyntech Resource Services Ltd., 1992.

Meng, A. X.; Hill, G. A.; Dalai, A. K. Hydrodynamic Characteristics in an External Loop Airlift Bioreactor Containing a Spinning Sparger and a Pached Bed. *Ind. Eng. Chem. Res.* **2002**, a. *41*, 2124-2128.

Meng, A. X.; Hill, G. A.; Dalai, A. K. Modified Volume Expansion Method for Measuring Gas Holdup, *Can. J. Chem. Eng.* **2002**, b. *80*, 194-199.

Ritchie, B. J.; Hill, G. A. Biodegradation of Phenol-Polluted Air Using an External Loop Airlift Bioreactor. *J. Chem. Thech. Biotechnol.* **1995,** *62*, 339-344.

Schonduve, P.; Sara, M.; Friedl, A. Influence of Physiologically Relevant Parameters on Biomass Formation in a Trickle-Bed Bioreactor Used for Waste Gas Cleaning. *Appl Microbiol Biotechnol.* **1996**, *45*, 286-292.

Stanier R. Y.; Ingraham, J. L.; Wheelis, M. L.; Painter, P. R. The Microbial World. 5th Ed., Prentice-Hall, 1998, pp. 183-184.

Tarighian, Alireza; Hill, Gordon; Lin, Yen-Han. Lag Phase Model for Transient Growth of *Pseudomonas putida* on Phenol. *Can. J. Chem. Eng.* **2001**, *79*, 732-736.

Weber, F. J.; Hartmans, S. Prevention of Clogging in a Biological Trickle-Bed Reactor Removing Toluene from Contaminated Air. *Biotechnol. Bioeng.* **1996**, *50*, 91-97.

Wei, V. Q.; Hill, G. A.; Macdonald, D. G. Bioremediation of Contaminated Air Using an External Loop Airlift Bioreactor. *Can. J. Chem. Eng.* **1999**, *77*, 955-962.

Woertz, J. R.; Kinney, K. A.; Mclntosh, N. D. P.; Szaniszlo, P. J. Removal of Toluene in a Vapor-Phase Bioreactor Containing a Strain of *Exophiala Iecanii-corni*. *Biotechnol. Bioeng.* **2001**, *75*, 550-558.

Wubker, S. M.; Laurenzis, A.; Werner, U.; Friedrich, C. Controlled biomass Formation and kinetics of Toluene Degradation in a Bioscrubber and in a Reactor with a Periodically Moved Trickle-Bed. *Biotechnol. Bioeng.* **1997**, *55*, 686-692.

Chapter 2 - Modelling Oxygen Transfer and Aerobic Growth in Shake Flasks and Well-Mixed Bioreactors

A similar version of this chapter has been copyrighted and published in the **Canadian Journal of Chemical Engineering**:

Nikakhtari, H.; Hill, G. A. Modelling Oxygen Transfer and Aerobic Growth in Shake Flasks and Well-Mixed Bioreactors. *Can. J. Chem. Eng.* **2005**, *83*, 493-499.

Contribution of the PhD candidate

Experiments were planned by Hossein Nikakhtari and Gordon A. Hill, and were performed by Hossein Nikakhtari. Modeling and computer program development were done by Hossein Nikakhtari with consulting by Gordon A. Hill. All text of the published paper was created by Hossein Nikakhtari with Gordon Hill providing editorial guidance.

Contribution of this chapter to the overall study

Before beginning any mass transfer and bioremediation work in the ELAB, studies of oxygen mass transfer and growth of the selected microorganism were undertaken in shake flasks and a well-mixed bioreactor to provide a basis for comparison of the performance of the ELAB. This initial work was aimed at a study of the microorganism characteristics and determination of growth parameters. Growth of the microorganism considering both oxygen and substrate depletions were investigated using both glucose and phenol. Glucose is a fast metabolism substrate on which every microorganism grows easily and fast. Therefore, starting a growth study of a microorganism on glucose provides a good basis for any further study on that microorganism. In this chapter growth parameters of *Pseudomonas putida* (ATCC 23973) were determined under oxygen and substrate depletion conditions and a new

model to predict oxygen mass transfer coefficients in the liquid phase of a shake flask was developed.

Additional experimental details

The apparatus set up to measure oxygen concentration in the liquid phase of a bioreactor (shake flask in this case) is shown in Figure 2.01.

(a) (b) (c)

Figure 2.01 Apparatus set up for oxygen mass transfer: (a) Deaeration of the liquid by bubbling nitrogen gas into the liquid, (b) Measurement of oxygen concentration in the liquid of the shake flask on the shaker using an oxygen probe during both oxygen mass transfer or biogrowth experiments, and (c) Oxygen meter connected to the computer.

The sensitivity analysis which is used in this chapter is according to the following procedure, which shows μ is sensitive to μ_{max} much more than K_S or K_m, and μ is sensitive to K_S or K_m only when there is a very low concentration of substrate (S) or oxygen (C).

$$\mu = \frac{\mu_{\max} S}{S + K_S} \times \frac{C}{C + K_m} \tag{2.3}$$

By differentiation:

$$\frac{\partial \mu}{\partial \mu_{\max}} = \frac{SC}{(S + K_S)(C + K_m)} \tag{2.01}$$

$$\frac{\partial \mu}{\partial K_S} = \frac{-1}{(S + K_S)^2} \frac{\mu_{\max} SC}{(C + K_m)} \tag{2.02}$$

$$\frac{\partial \mu}{\partial K_m} = \frac{-1}{(C + K_m)^2} \frac{\mu_{\max} SC}{(S + K_S)} \tag{2.03}$$

By dividing:

$$I = \frac{\dfrac{\partial \mu}{\partial \mu_{\max}}}{\dfrac{\partial \mu}{\partial K_S}} = -\frac{S + K_S}{\mu_{\max}} \tag{2.04}$$

$$II = \frac{\dfrac{\partial \mu}{\partial \mu_{\max}}}{\dfrac{\partial \mu}{\partial K_m}} = -\frac{C + K_m}{\mu_{\max}} \tag{2.05}$$

Using reasonable values for μ_{max}, K_S, and K_m equal to 0.37 h^{-1}, 1 mg/L and 0.25 mg/L respectively (same values used in this chapter), it is easy to see from Equations 2.04 and 2.05 that $\frac{\partial \mu}{\partial K_S}$ or $\frac{\partial \mu}{\partial K_m}$ is comparable to $\frac{\partial \mu}{\partial \mu_{\max}}$, only when *S* or *C* is below 0.5 mg/L. In that case *I* or *II* is less than 2.

Narrow neck Pyrex (Germany) or Kimex (U.S.A.) brand shake flasks were used in this study and had a constant flask angle equal to 74.5 ± 1.5°. This angle is shown in Figure 2.02. This consistent geometry allows calculating stationary liquid surfaces in the flask as a function of flask and liquid volume as discussed in this chapter.

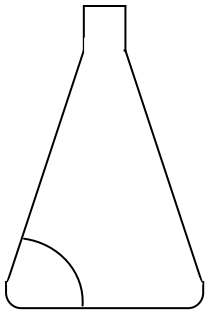

Figure 2.02 Shake flask angle.

2.1 Abstract

Oxygen transfer is an important aspect of aerobic metabolism. In this work, microbial growth on glucose (fast metabolism) and phenol (slow metabolism) has been studied using *Pseudomonas putida* in shake flasks and a mixed bioreactor considering both substrate and oxygen depletion. Under typical operating conditions, the highest mass transfer coefficient (K_La) for the aerated well-mixed bioreactor was found to be 50.8 h^{-1}, while the maximum non-aerated shake flask K_La was 21.1 h^{-1}. The presence of media and/or dead cells did not have significant effect on measured values of K_La. A new equation for prediction of K_La in shake flasks with an absolute average deviation of 11.1% is introduced, and a combined model for oxygen mass transfer and microbial growth is shown to fit experimental data during growth on glucose and phenol in both shake flasks and the mixed bioreactor with an absolute average deviation of 19.3 %.
Keywords: Oxygen Transfer, Shake Flasks, Bioreactors, Microbial Growth, Modelling

2.2 Introduction

Oxygen availability is an important factor for most metabolic reactions in aerobic microorganisms. Even though many studies have been performed in shake flasks before scaling up to mixed bioreactors, there is little information about oxygen mass transfer in shake flasks and comparisons with mixed bioreactors. Instantaneous data acquisition of the oxygen transfer rate in shake flasks has only recently been reported (Anderlei and Buchs, 2001). Tolosa et al. (2002) reported an optical sensor as a noninvasive monitoring method of dissolved oxygen in shake flasks, which is accurate under 60% of the saturated dissolved oxygen concentration. Gupta and Rao (2003) used this method to determine oxygen mass transfer coefficients in shake flasks and stirred-tank fermentors. They also studied the effects of plugs and baffles on this coefficient. Oxygen mass transfer during the aerobic growth of different microorganisms in shake flasks and well-mixed bioreactors with determination of the oxygen mass transfer coefficient has

been the subject of several studies (Schell et al., 2001 and Klasson et al., 1998). Maier and Buchs (2001) have compared five different correlations previously reported for the prediction of the oxygen mass transfer coefficient (K_La) in shake flasks, and showed over 150% deviation among these correlations. Andrews et al. (1984) reported higher K_La values in fermentation broths than in cell-free liquids, especially at high cell concentrations. Yagi and Yoshida (1975) investigated enhancement of oxygen absorption into fermentation broth with respiration of microorganisms. According to their research, except for extreme cases, respiration has no effect on K_La values.

One of the oxygen mass transfer resistances in shake flasks is the sterile plug. Mrotzek et al. (2001) developed a new method to determine the mass transfer resistance of different sterile closures. They measured the water evaporation rate of the shaking flask, using different kinds of sterile plugs, and reported dependence of this resistance mainly on the neck geometry and to a lesser extent on the plug material and density. On the other hand, Schuttz (1964) reported that density of cotton plugs in shake flasks can affect the oxygen diffusion rate from outside into the shake flask headspace.

In this study, the rate of oxygen uptake in shake flasks and a well-mixed bioreactor are compared. Dual oxygen and substrate limitation conditions are then generated by growing the same microorganism on either glucose or phenol in both vessels. Finally, a new oxygen mass transfer model is combined with cell growth models to accurately predict the transient behaviour of biomass, oxygen and substrate concentrations during batch growths in shake flasks and well-mixed bioreactors.

2.3 Experimental Methods

2.3.1 Microorganism and Media

Pseudomonas putida (ATCC 23973) was used for all microbial growth experiments (obtained from Dr. Wayne Brown, McGill University). It was maintained on nutrient broth agar and stored at 4 °C. For each growth experiment, a fresh culture was initially grown in media broth on the substrate of interest, and then used for

inoculation. The growth media consisted of (mg in 1 L reverse osmosis water; analytical reagent grade chemicals, BDH, Toronto): K_2HPO_4, 750; KH_2PO_4, 840; $(NH_4)_2SO_4$, 474; NaCl, 60; $CaCl_2$, 60; $MgSO_4$, 60; $Fe(NH_4)SO_4$, 20; and 1 ml of trace mineral solution. The trace mineral solution consisted of (mg in 1 L reverse osmosis water): $ZnSO_4.7H_2O$, 200; $MnCl_2$, 60; H_3BO_3, 600; $CoCl_2$, 400; $CuCl_2$, 20; $NiCl_2$, 40; Na_2MoO_4, 60. The pH of the media solution was 7.0.

2.3.2 Mass Transfer and Batch Growth Procedures

All experiments were carried out at room temperature (22 ºC ± 2 ºC). For determination of oxygen mass transfer coefficients, absorption of oxygen into de-aerated water, broth media without cells, or broth media with dead cells was measured over time in shake flasks and in the well-mixed bioreactor (model BioFlo C30, New Brunswick Scientific, Edison, NJ) using an oxygen meter (model 50175, Hach company, Loveland, CO) with a membrane probe (model 50180, Hach company, Loveland, CO). The probe diameter was 12 mm and 20 mm of the probe tip was dipped into the liquid during all experiments. The oxygen meter was connected to a computer using WinWedge® data acquisition software. For oxygen mass transfer experiments, each solution was de-aerated by nitrogen gas and then absorption of oxygen was measured over a wide range of flask sizes, mixing speeds and aeration rates in both shake flask and well-mixed bioreactors (Table 2.1). For the preparation of media with dead cells, after cultures reached their highest cell density, the broth was sterilized at 121 ºC for 15 min. Oxygen concentrations were also measured during growth experiments to determine oxygen yield factors as described below.

Several batch growth experiments were performed to obtain the characteristics of glucose metabolism by *Pseudomonas putida* in shake flasks and a well-mixed bioreactor under different mixing and aeration rates. Similar experiments were subsequently performed using phenol in place of glucose as the substrate. Shake flask growth experiments were carried out using a rotary shaker (model 542, Fermentation Design, Allentown, PA) at rates up to 160 rpm and with a shaking amplitude of 6 mm. Four sizes of Erlenmeyer shake flasks were used: 250, 500, 1000 and 2000 ml containing media broth from 125 ml to 1200 ml with either 3 or 50 ml inoculum taken from a fresh

culture using the same media and substrate. A 2 liter fermenter with 115 mm vessel diameter (model BioFlo C30, New Brunswick Scientific, Edison, NJ) was used as a well-mixed bioreactor and operated with 500 ml broth and 10 ml inoculum under different conditions: 120 to 450 rpm mixing speed and 0 to 1.0 L/min aeration. The turbine impeller (50 mm diameter) position was adjusted according to well-mixed, vessel design strategies (Ho and Oldshue, 1987). Low mixing rates were used to induce poor oxygen transfer and study its effect on bacteria's growth. Mixing at 450 rpm provided Westerterp's minimum criteria for homogeneity in the bioreactor (Westerterp et al., 1963). All bioreactors were connected to atmosphere through 10 mm diameter and 40 mm length, lightly packed (0.02 g/mL glass wool) filters. Long hypodermic needles were inserted into the growth vessels and used to withdraw samples. In all growth experiments, the media broth contained either an initial concentration of 1000 mg/L glucose or 300 mg/L phenol.

One of the oxygen mass transfer experiments in a shake flask and also one in the mixed bioreactor were randomly chosen for replication studies. For these two conditions, each experiment was completely replicated 6 times.

2.3.3 Analysis

Biomass concentrations were measured at 600 nm wavelength using a spectrophotometer (model Spectronic 1001 plus, Milton Roy, Rochester, NY). Optical density was converted to cell dry weight using a previously prepared calibration curve. Samples were filtered and used immediately for phenol analysis or stored in a freezer for later glucose analysis. For measurement of phenol, optical density of the filtered sample was measured at 280 nm. Then absorbance was converted to phenol concentration using a prepared calibration curve. Glucose concentrations were determined using a glucose enzymatic measuring kit (model 115, Sigma, St. Louis), in which glucose undergoes an oxidization reaction that produces hydrogen iodonitrotetrazolium chloride that in turn is measured colorimetrically at 520 nm.

To measure stationary liquid surface area in a shake flask, the circumference of the liquid surface was measured using a flexible rope, and then the diameter and surface area of the liquid surface were calculated.

2.4 Oxygen Mass Transfer Model

The K_La values for water, media, and media with dead cells were determined assuming all vessels were well-mixed and using the equation of Merchuk et al. (1990):

$$\frac{C - C^*}{C_0 - C^*} = \frac{e^{-K_L a \times t} - \tau \times K_L a \times e^{-t/\tau}}{1 - \tau \times K_L a} \tag{2.1}$$

Considering first order response for the oxygen probe and fitting the first order response equation to experimental data, the probe response time was determined to be 7.9 ± 0.5 s, which had only 2.6% deviation from the value previously reported for this probe (Bi et al., 2001). Once the probe delay time was known, Equation 2.1 was fit to the experimental data by a least squares method and K_La was obtained as a parameter of this minimization process.

2.5 Cell Growth Model

Cell growth kinetics with dual limitations (substrate and oxygen concentrations) can be expressed as a multiplication of two Monod equations (one for substrate and the other for oxygen, as is seen in Equation 2.3), as proposed by Tong and Fan (1988):

$$\frac{dX}{dt} = \mu X \tag{2.2}$$

$$\mu = \frac{\mu_{\max} S}{S + K_S} \times \frac{C}{C + K_m} \tag{2.3}$$

Substrate consumption kinetics can be expressed using the substrate yield factor (assumed constant):

$$\frac{dS}{dt} = -\frac{1}{Y_{XS}} \frac{dX}{dt} \tag{2.4}$$

Oxygen concentration is affected by both mass transfer and consumption according to:

$$\frac{dC}{dt} = -\frac{1}{Y_{XC}}\frac{dX}{dt} + K_L a(C^* - C) \qquad (2.5)$$

In some literature, the first term on the right hand side of Equation 2.5 is referred to as $Q_{O2}X$ (Cho and Wang, 1990).

Since glucose and phenol concentrations were high throughout most of the batch runs, K_S only affects the dynamics of the system for a small interval near the end of the run when the substrate concentration is almost depleted. K_S was set equal to 1 mg/L for both glucose and phenol as used earlier by Tarighian et al. (2003). K_m is also known to be a low value for *Pseudomonas putida*. In this work, K_m was set equal to 0.25 mg/L, which is three times the average critical oxygen value for this bacterium (Bailey and Ollis, 1986; Blakebrough, 1967). Since the oxygen mass transfer coefficient ($K_L a$) was known from oxygen mass transfer experiments, Equations 2.2 to 2.5 could be solved simultaneously (using a 4th order Runge-Kutta numerical method on Excel®) to determine the best fit values of the three model parameters (μ_{max}, Y_{XS}, and Y_{XC}) for both glucose and phenol.

Sensitivity analysis revealed the solutions are sensitive to K_S or K_m only when S is a comparable value to K_S or C to K_m, which covers negligible intervals of the whole growth process. But the solutions are extremely sensitive to μ_{max}, Y_{XS}, and Y_{XC} during the whole growth process.

2.6 Results and Discussion

2.6.1 Mass Transfer of Oxygen

Figure 2.1 shows a close fit of Equation 2.1 to dissolved oxygen concentration data for a typical mass transfer run. Best fit values of $K_L a$ are shown in Table 2.1 and were obtained by minimizing the squared error between Equation 2.1 and the data for each oxygen transfer experiment. Six replicate experiments revealed standard errors of the mean $K_L a$ to be 3.9%. The $K_L a$ values for media and media with dead cells (400

mg/L) were normally slightly below the K_La values measured with water, but at the 95% confidence limits these decreases were not significant. In contrast, comparison of mean K_La values for shake flasks and the bioreactor operating at different conditions of mixing and aeration showed significant trends. The highest K_La value was 50.8 h^{-1} and occurred in the bioreactor for mixing at 450 rpm and aeration at 1.0 L/min (2.0 vvm). This value agrees with typical published values for oxygen mass transfer coefficients in well-mixed bioreactors with low ionic strength fermentation media at these aeration rates and mixing speeds as thoroughly investigated by Robinson and Wilke (1973). Surprisingly, a high oxygen mass transfer rate of 21.1 h^{-1} also occurred for a shake flask operated with no aeration, minimal liquid volume (125 mL in 500 mL Erlenmeyer flask) and high shaking speed (160 rpm). This indicates that good surface aeration in shake flask cultures may produce aerobic growth kinetics similar to conditions that would be found in scaled up, well-mixed bioreactors. Measured K_La values were then modeled as functions of mixing and aeration rates. For the well-mixed bioreactor, models for the prediction of K_La are well documented in textbooks (Ho and Oldshue, 1987) and can be written in the form:

$$K_L a = A_0 \times (N)^{A_1} \times (Q)^{A_2} \tag{2.6}$$

Constants of Equation 2.6 were determined by fitting all the K_La data collected for the Bioflo bioreactor and were determined to be 5.76×10^{-3}, 1.48 and 0.253 for A_0, A_1 and A_2 respectively. These constants as well as those in Equations 2.7 and 2.8 are unit dependent as shown in the Nomenclature section.

It is known that the oxygen mass transfer rate is dependent on shaking speed, the volume of both flask and liquid, and the liquid surface area (Tolosa et al., 2002; Kanokwaree and Doran, 1997). In this work, an empirical equation for prediction of K_La in shake flasks is introduced which is a function of the stationary liquid surface area (A) and turbulence factor (T) which in turn are functions of liquid and flask volumes and the shaking speed. Actual liquid surface area during motion of the flask is not easy to measure, but it is a function of stationary liquid surface area and turbulence factor, which are embedded in this model. First, the stationary liquid surface area was calculated as a function of the Erlenmeyer flask and liquid volumes, which in any experiment are known values, according to:

$$A = \alpha \times (V - L)^{2/3} \tag{2.7}$$

The coefficient of Equation 2.7 (α) was determined to be 142.0 by fitting of several measured liquid surface areas, for flask sizes from 250 mL to 2000 mL, as shown in Figure 2.2.

A second empirical equation was developed for the turbulence factor in the shake flask, which was considered to be a function of the ratio of the flask volume to the liquid volume multiplied by the shaking speed according to:

$$T = \frac{V^{\beta}}{L} \times \frac{N}{60} \tag{2.8}$$

The coefficient of Equation 2.8 (β) was found to be 0.463 by error minimization of measured $K_L a$ data at different operating conditions of flask volumes, liquid volumes and shaking speeds. $K_L a$ in shake flasks was finally expressed as a linear function of A multiplied by T and coefficients of the linear equation were determined by best fit of the experimental $K_L a$ data:

$$K_L a = 0.0182 \times (A \times T) \tag{2.9}$$

The constant of this equation is unit dependent and the equation covers shake flask sizes from 250 mL to 2000 mL. The absolute average error between the experimental data and prediction was found to be 11.1%, but Figure 2.3 shows generally a good fit of Equation 2.9 to all the experimental data.

Four correlations reviewed by Maier and Buchs (2001) were tested for the experimental data of this study but none of them was able to cover the whole range of data with any comparable accuracy to Equation 2.9. Veljkovic et al.'s equation, using an optimized coefficient of 0.032 (by minimizing the error method), had the best compatibility:

$$K_L a = 0.032 \times N \left(\frac{V}{L} \right)^{0.845} \tag{2.10}$$

Equation 2.10 showed an absolute average error of 31.8% in comparison to experimental data. Henzler and Schedel (1991) equation is much more complicated than Equation 2.9 and uses more parameters:

$$K_L a = 0.24 \times 3600 \times \frac{N}{60} \sqrt{D_F} \left(\frac{g^3}{\upsilon} \right)^{1/3} \left(\frac{d^3}{L/1000} \right)^{8/9} \left(\frac{1}{\upsilon} \right)^{1/2} \left(\frac{2}{d^3 g} \right)^{8/27} \left(\frac{\sqrt{d_0 d}}{g} \right)^{0.5} \quad (2.11)$$

Equation 2.11, using an optimized coefficient of 0.24 for the mass transfer of oxygen in water, showed an absolute average error of 36.25%. The results of Equations 2.10 and 2.11 are shown in Figure 2.3, which show significant scatter as compared to Equation 2.9 developed in this study.

2.6.2 Growth of *Pseudomonas putida*

Having the ability to predict $K_L a$ for all operating conditions, the three differential equations for cell growth, substrate utilization and dissolved oxygen consumption (Equations 2.2, 2.4 and 2.5) were now solved and best fit to all the experimental growth data to achieve μ_{max}, Y_{XS}, and Y_{XC} as model parameters for both glucose and phenol batch cultures. The best fit values of these parameters are shown in Table 2.2. The kinetic constants are close to values reported for other strains of *Pseudomonas putida* (Tarighian et al., 2003; Reardon et al., 2000). As expected, μ_{max} for glucose is much higher than for phenol. The oxygen yield factor (Y_{XC}) for glucose is higher than for phenol, which is in line with the molecular demand for conversion of these substrates to biomass and CO_2.

Figures 2.4 shows typical experimental data and predictions of biomass, glucose, and oxygen concentrations during batch growth of *Pseudomonas putida* on glucose while Figure 2.5 shows similar results when phenol was the growth substrate. As can be seen, the combined oxygen mass transfer and biogrowth models are able to predict the experimental data reasonably accurately for both the qualitative effects and quantitative values of these variables. The absolute average deviation of the model is 29.2%, 13.7%, and 14.9% for the prediction of biomass, substrate and oxygen concentrations respectively. An absolute average deviation from experimental data can be considered equal to 19.3% for the whole model. A relatively weak prediction of oxygen absorption into water in Figure 2.4 after 7.2 h is because of the closure effect that is a barrier against oxygen mass transfer into the shake flask headspace, and has been ignored in this stage of the study. This issue is fully discussed in the next chapter. The dip of oxygen

concentration during rapid exponential growth and subsequent oxygen limited growth can be seen in Figure 2.4 for the case of growth on glucose in a shake flask when the oxygen transfer rate is low, however a similar growth situation in the well-mixed bioreactor does not reach this oxygen limiting condition, which is shown in Figure 2.6. For the case of growth on phenol, both the shake flask (Figure 2.5) and well-mixed bioreactor did not reach oxygen limited conditions due to the much slower growth rate on phenol compared to glucose. Oxygen depletion is critical and can limit high cell density cultures. The model presented here can be a useful predictive tool to anticipate and avoid such culture conditions.

2.7 Conclusions

Oxygen mass transfer rates in shake flasks could be comparable to those achieved in a well-mixed bioreactor when both high flask to liquid volume ratios and shaking turbulence were used. A new predictive model for the oxygen transfer rate in Erlenmeyer shake flasks has been presented and is applicable when no oxygen limitation occurs into the shake flasks. However, the rates may eventually become limited by restricted oxygen diffusion through plugs in the flasks. The combined model for oxygen transfer and cell growth accurately predicted the transient concentrations of cell mass, substrate and oxygen in both shake flasks and a well-mixed bioreactor over a wide range of operating conditions. Use of this combined model will allow the determination of the suitability of shake flask cultures to predict the subsequent behaviour of cultures in well-mixed bioreactors.

2.8 Nomenclature

A	liquid surface area (cm^2)
A_0, A_1, A_2	constants in Equation 2.6
C	dissolved oxygen concentration (mg/L)
C_0	initial dissolved oxygen concentration (mg/L)
C^*	equilibrium dissolved oxygen concentration (mg/L)
D_F	effective diffusion coefficient of oxygen in liquid phase (m^2/s)
d	maximum shake flask diameter (m)
d_0	shaking diameter (m)
g	gravitational acceleration (m/s^2)
K_La	volumetric oxygen mass transfer coefficient (h^{-1})
K_S, K_m	constants in Equation 2.3 (mg/L)
L	liquid volume in the shake flask (L)
N	impeller rotation or shaking speed (rpm)
Q	aeration rate (L/min)
Q_{O2}	specific oxygen uptake rate (mg oxygen/ mg cell-h)
S	substrate concentration (mg/L)
T	turbulence factor
t	time (s)
V	volume of shake flask (L)
X	cell density (mg/L)
Y_{XS}	substrate yield factor (mg cell/ mg substrate)
Y_{XC}	oxygen yield factor (mg cell/ mg oxygen)
Greek Symbols	
α	constant in Equation 2.7
β	constant in Equation 2.8
μ_{max}	maximum specific growth rate (h^{-1})
ν	kinematic viscosity of liquid phase (m^2/s)
τ	response time (s)

2.9 References

Anderlei, T.; Buchs, J. Device for Sterile Online Measurement of the Oxygen Transfer Rate in Shaking Flasks. *Biochem. Eng. J.* **2001** *7*, 157-162.

Andrews, G. F.; Fonta, J. P.; Marrotta, E.; Stroeve, P. The Effects of Cells on Oxygen Transfer Coefficients. II. Analysis of Enhancement Mechanisms. *Chem. Eng. J.* **1984** *29*, 47-55.

Bailey, J. E.; Ollis, D. F. Biochemical Engineering Fundamentals, 2nd ed.; McGraw-Hill: New York, NY 1986, pp. 467-468.

Bi, Y.; Hill, G. A.; Sumner, R. J. Enhancement of the Overall Volumetric Oxygen Transfer Coefficient in a Stirred Tank Bioreactor Using Ethanol. *Can. J. Chem. Eng.* **2001** *79*, 463-467.

Blakebrough, N. (ed.) Biochemical and Biological Engineering Science. Vol. 1; Academic Press, Inc.: New York 1967, pp. 81.

Cho, M. H.; Wang, S. S. Practical Method for Estimating Oxygen Kinetic and Metabolic Parameters. *Biotechnol. Prog.* **1990** *6*, 164-167.

Gupta, A.; Rao, G. A Study of Oxygen Transfer in Shake Flasks Using a Non-Invasive Oxygen Sensor. *Biotechnol. Bioeng.* **2003** *84*, 351-358.

Henzler, H. J.; Schedel, M. Suitability of the Shaking Flask for Oxygen Supply to Microbiological Cultures. *Bioprocess Eng.* **1991** *7*, 123-131.

Ho, C. R.; Oldshue, J. Y. Biotechnology Processes Scale-up and Mixing; AIChE: New York, NY 1987.

Kanokwaree, K.; Doran, P. M. Extent to Which External Oxygen Transfer Limits Growth in Shake Flask Culture of Hairy Roots. *Biotechnol. Bioeng.* **1997** *55*, 520-526.

Klasson, K. T.; Lundback, K. M. O.; Clausen E. C.; Gaddy, J. L. In Situ Global Method for Measurement of Oxygen Demand and Mass Transfer. *Appl. Biochem. Biotechnol.* **1998** *70-72*, 527-533.

Maier, U. Buchs, J. Characterization of the Gas-Liquid Mass Transfer in Shaking Bioreactors. *Biochem. Eng. J.* **2001** *7*, 99-106.

Merchuck, J. C.; Yona, S.; Siegel, M. H.; Zvi A. B. The First-Order Approximation to the Response of Dissolved Oxygen Electrodes for Dynamic K_La Estimation. *Biotechnol. Bioeng.* **1990** *35*, 1161-1163.

Mrotzek, C.; Anderlei, T.; Henzler, H. J.; Buchs, J. Mass Transfer Resistance of Sterile Plugs in Shaking Bioreactors. *Biochem. Eng. J.* **2001** *7*, 107-112.

Reardon, K. F.; Mosteller, D. C.; Bull, R. J. D. Biodegradation Kinetics of Benzene, Toluene, and Phenol as Single and Mixed Substrates for *Pseudomonas putida* F1. *Biotechnol. Bioeng.* **2000** *69*, 385-400.

Robinson, C. W.; Wilke, C. R. Oxygen Absorption in Stirred Tanks. *Biotechnol. Bioeng.* **1973** *15*, 755-782.

Schell, D. J.; Farmer, J.; Hamilton, J.; Lyons, B.; McMillan, J. D.; Saez, J. C.; Tholudur, A. Influence of Operating Conditions and Vessel Size on Oxygen Transfer During Cellulase Production. *Appl. Biochem. Biotechnol.* **2001** *91-93*, 627-642.

Schultz, J. S. Cotton Closure as an Aerobic Barrier in Shake Flask Fermentations. *Appl. Microbiol.* **1964** *12*, 305-310.

Tarighian, A.; Hill, G. A.; Headley, S.; Pedras, S. Enhancement of 4-chlorophenol biodegradation using glucose. *Clean Technol. Environ. Policy* **2003** *5*, 61-65.

Tolosa, L.; Kostov, Y.; Harms P.; Rao, G. Noninvasive Measurement of Dissolved Oxygen in Shake Flasks. *Biotechnol. Bioeng.* **2002** *80*, 594-597.

Tong, C. C.; Fan, L. S. Concentration Multiplicity in a Draft Tube Fluidized-Bed Bioreactor Involving Two Limiting Substrates. *Biotechnol. Bioeng.* **1988** *31*, 24-34.

Yagi, H.; Yoshida, F. Enhancement Factor for Oxygen Absorption into Fermentation Broth. *Biotechnol. Bioeng.* **1975** *17*, 1083-98.

Westerterp, K. R.; van Dierendonck L. L.; de Kraa, J. A. Interfacial Areas in Agitated Gas-Liquid Contactors. *Chem. Eng. Sci.* **1963** *18*, 157-176.

Table 2.1 Best fit K_La values from all oxygen mass transfer runs.

Vessel	Size (L)	Liquid (L)	Aeration (L/min)	Mixing speed (rpm)	K_La (h^{-1})
Flask	2	1.5	0	100	2.0
Flask	0.25	0.175	0	140	2.6
Flask	2	1.0	0	100	5.3
Flask	0.25	0.125	0	140	6.8
Flask	0.5	0.125	0	60	7.0
Flask	1	0.50	0	110	7.5
Flask	2	1.0	0	140	8.8
Flask	0.5	0.25	0	160	9.1
Flask	0.5	0.125	0	80	9.6
Flask	1	0.30	0	110	13.7
Flask	2	0.50	0	100	14.9
Flask†	0.5	0.125	0	140	15.6
Flask*	0.5	0.125	0	140	17.4
Flask††	0.5	0.125	0	140	19.2
Flask	0.5	0.125	0	160	21.1
Bioflo	2.0	0.50	0.10	120	4.1
Bioflo††	2.0	0.50	0.25	150	7.7
Bioflo	2.0	0.50	0.25	120	7.9
Bioflo†	2.0	0.50	0.25	150	8.8
Bioflo	2.0	0.50	0.65	120	9.5
Bioflo	2.0	0.50	0.25	150	10.0
Bioflo	2.0	0.50	0.10	300	13.0
Bioflo	2.0	0.50	1.0	120	14.3
Bioflo	2.0	0.50	0.25	300	16.7
Bioflo	2.0	0.50	0.65	300	20.3
Bioflo††	2.0	0.50	0.25	350	21.9
Bioflo	2.0	0.50	1.0	300	22.6
Bioflo†	2.0	0.50	0.25	350	23.3
Bioflo	2.0	0.50	0.10	450	26.3
Bioflo*	2.0	0.50	0.25	350	27.2
Bioflo	2.0	0.50	0.25	450	39.6
Bioflo	2.0	0.50	0.65	450	46.1
Bioflo	2.0	0.50	1.0	450	50.8

* repeated 6 times and reported the average value
† media
†† media and dead cells

Table 2.2 Mean value of biokinetic parameters and standard errors.

Substrate	μ_{max} (h^{-1})	Y_{XS} (mg cells/ mg substrate)	Y_{XC} (mg cells/ mg oxygen)
Glucose	0.37 ± 0.03	0.30 ± 0.03	0.78 ± 0.09
Phenol	0.088 ± 0.012	0.73 ± 0.12	0.36 ± 0.09

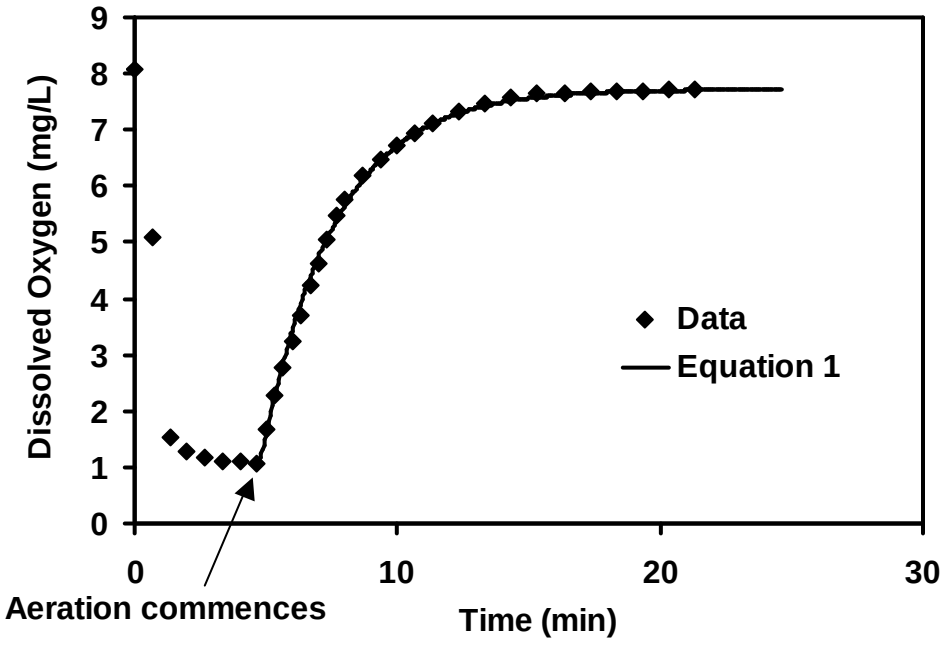

Figure 2.1 Comparison of mass transfer model (Equation 2.1) to experimental data (medium with dead cells, 0.25 L/min aeration and 300 rpm mixing speed in bioreactor).

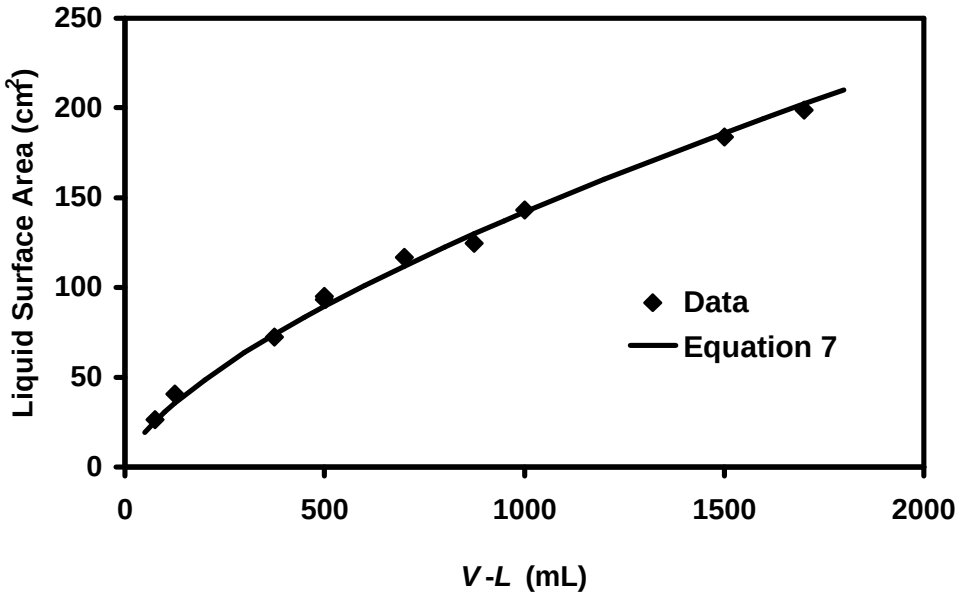

Figure 2.2 Comparison of liquid surface area model (Equation 2.7) to experimental data, for flask sizes from 250 mL to 2000 mL.

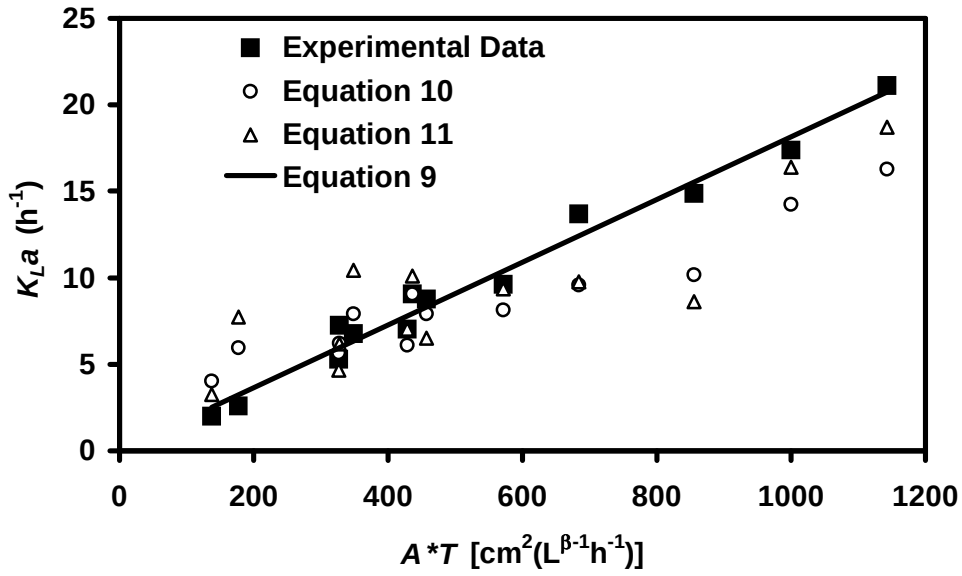

Figure 2.3 Comparison of oxygen volumetric mass transfer coefficient model for shake flasks (Equation 2.9, developed in this study), Veljkovic et al's equation (Equation 2.10) and Henzler and Schedel's equation (Equation 2.11) to experimental data.

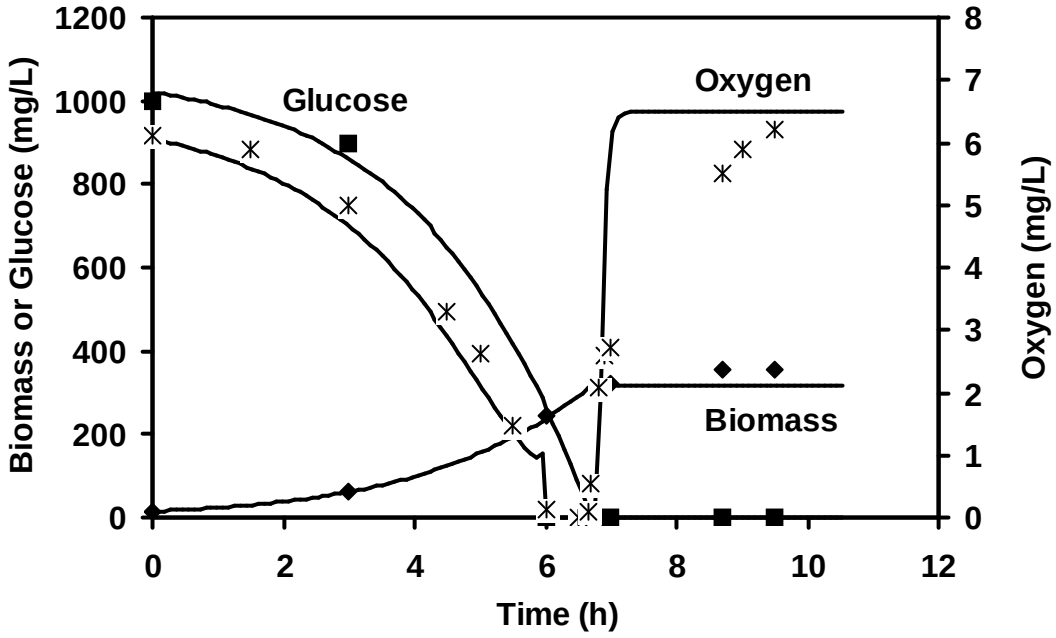

Figure 2.4 Model and experimental data for growth of biomass, consumption of glucose, and depletion and absorption of oxygen in 500 mL shake flask (125 mL medium, 1000 mg/L glucose, 140 rpm shaking speed).

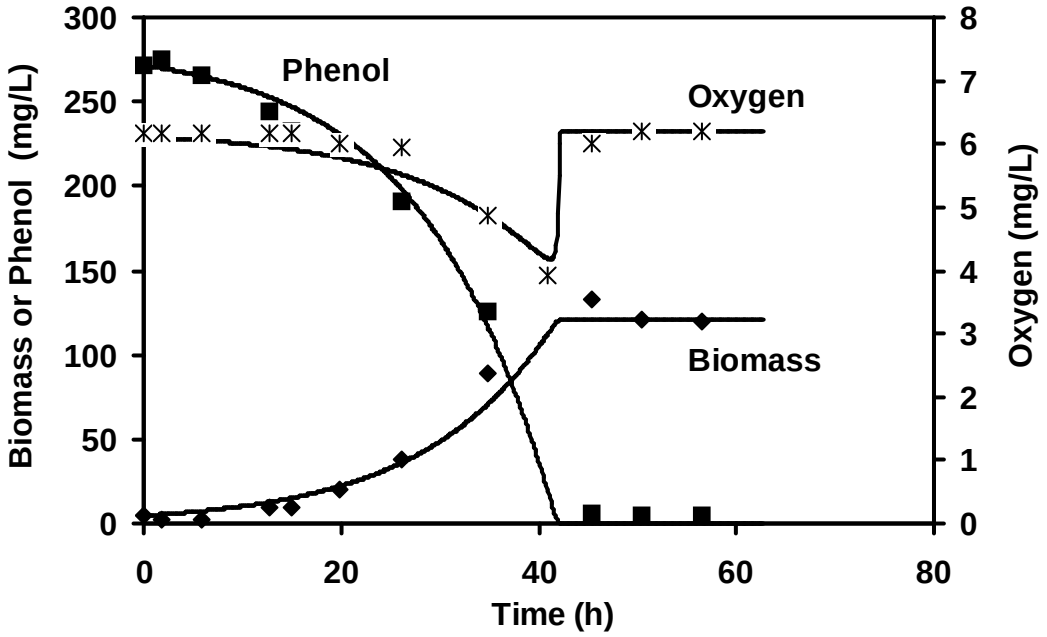

Figure 2.5 Model and experimental data for growth of biomass, consumption of phenol, and depletion and absorption of oxygen in 500 mL shake flask (125 mL medium, 300 mg/L phenol, 140 rpm shaking speed).

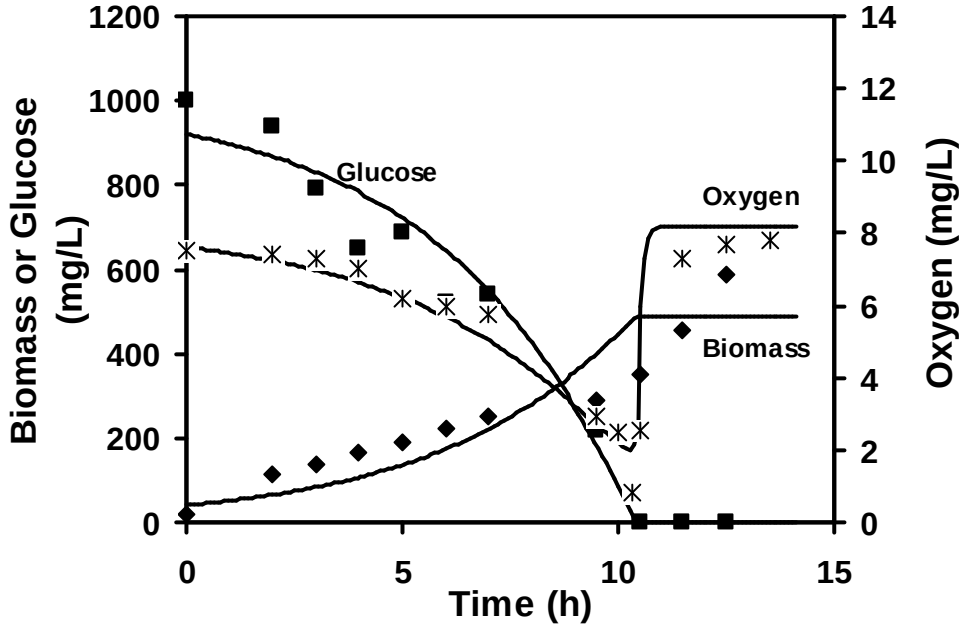

Figure 2.6 Model and experimental data for growth of biomass, consumption of glucose, and depletion and absorption of oxygen in well-mixed bioreactor (500 mL medium, 1000 mg/L glucose, 0.25 L/min aeration, 300 rpm mixing speed).

Chapter 3 - Closure Effects on Oxygen Transfer and Aerobic Growth in Shake Flasks

A similar version of this chapter has been copyrighted and accepted for publication in the journal of **Biotechnology and Bioengineering**:

Nikakhtari, H.; Hill, G. A. Closure Effects on Oxygen Transfer and Aerobic Growth in Shake Flasks. *Biotechnol. Bioeng.* submitted in Nov. 2005.

Contribution of the PhD candidate

Experimental design and experiments were planned and performed by Hossein Nikakhtari. Modeling and computer program development were done by Hossein Nikakhtari with advice from Gordon A. Hill. All written text was prepared by Hossein Nikakhtari with Gordon A. Hill providing editorial guidance.

Contribution of this chapter to the overall study

This chapter is a continuation of the previous chapter but with the development of an improved model to predict the growth parameters of microorganism in shake flasks. In this improved model, resistance of the shake flask closure against oxygen mass transfer has been considered. The hypothesis was that closure of a shake flask can provide a resistance against oxygen mass transfer and affect the determined growth parameters, which was not considered in the previous chapter. The aim of this chapter was to determine the magnitude of error which occurs in growth parameters estimations without considering closure effects, determine accurate growth parameters by including closure effects, and finally to determine the critical shake flask conditions that start to affect the accurate determination of growth parameters. This study provides a basis for determining growth parameters accurately in shake flasks. Some new equations to

predict oxygen mass transfer coefficient through the closure and headspace of shake flask were also developed.

Additional experimental details

The apparatus set up in this chapter was similar to the one in the previous chapter. Figure 3.01 shows a picture of oxygen concentration measurements in the liquid phase of a shake flask with a foam plug closure.

Figure 3.01 A photograph of a shake flask with foam plug closure and oxygen probe in the liquid phase.

3.1 Abstract

Oxygen mass transfer in shake flasks is an important aspect limiting the culture of aerobic microorganisms. In this work, mass transfer of oxygen through a closure and headspace of shake flasks is investigated. New equations for prediction of $k_G a$ in shake flasks with closures are introduced. Using *Pseudomonas putida*, microbial growth on glucose (fast metabolism) and phenol (slow metabolism) in shake flasks with closures were studied, considering both substrate and oxygen restrictions. A combined model for oxygen mass transfer and microbial growth is shown to accurately predict experimental oxygen concentrations and oxygen yield factors during the growth experiments more accurately than previous models.

Keywords: Oxygen Transfer, Shake Flask, Closures, Microbial Growth, Modelling

3.2 Introduction

Shake flasks are widely used for batch cultures of aerobic microorganisms. Oxygen availability is a crucial factor for the metabolic growth of aerobic microorganisms. Knowledge of oxygen transfer is also critical for scale-up purposes. Schultz (1964) demonstrated limited growth of *Bacillus megaterium* due to oxygen restrictions in a shake flask. Even though many studies have been performed in shake flasks, there is little information about oxygen mass transfer in shake flasks, especially in the gas phase through a closure and into the headspace of the flask. Mrotzek et al. (2001) developed a new method of measuring the water evaporation rate in shake flasks using different kinds of sterile plugs to determine the mass transfer resistance of sterile closures. They found dependence of the mass transfer resistance mainly on the neck geometry and to a lesser extent on the plug material and density. On the other hand,

Schuttz (1964) reported that the densities of cotton plugs in shake flasks can affect the oxygen diffusion rate from outside into the shake flask headspace. Instantaneous data acquisition of the oxygen transfer rate in shake flasks has recently been reported (Anderlei and Buchs, 2001). Tolosa et al. (2002) reported an optical sensor as a noninvasive monitoring method of dissolved oxygen in shake flasks, which was found to be accurate under 60% of the saturated dissolved oxygen concentrations. Gupta and Rao (2003) used this method to determine oxygen mass transfer coefficients in shake flasks and stirred-tank fermentors and investigated effects of plugs and baffles on these coefficients. They defined an equivalent oxygen mass transfer coefficient including both liquid and gas phase coefficients. For the gas phase mass transfer coefficient, they considered only diffusivity of oxygen through three kinds of plugs (sponge, cotton and milk filter). Veglio et al. (1998) used a similar method and reported no interaction among three factors of stirring speed, liquid volume, and weight of the cotton closure. They reported positive effects of stirring, temperature and flask neck diameter, but a negative effect of liquid volume on the oxygen mass transfer coefficient. Henzler and Schedel (1991) followed the same procedure to study the oxygen flow rate into a shake flask during a cell culture (*Streptomyces tendae*). They reported up to eight times more resistance in the gas/liquid interface rather than the sterile plug. Van Suijdam et al. (1978) studied oxygen diffusion through standard cotton plugs and milk filter disk pads without considering shaking of the flask. They observed turbulent eddies in the cotton plugs could account for enhanced mass transfer compared to only diffusion. Tribe et al. (1994) noted that neglecting the membrane probe's response time during a gas-out experiment caused a significant error on the calculated oxygen mass transfer coefficients even when the probe response time is much smaller than the inverse of the mass transfer coefficient. Nikakhtari and Hill (2005) studied oxygen mass transfer in the liquid phase of shake flasks and introduced a new model for the prediction of this mass transfer coefficient. Using this mass transfer model combined with a cell growth model, three growth parameters: maximum growth rate, μ_{max}, substrate and oxygen yield factors, Y_{XS}, and Y_{XC}, could be accurately determined from aerobic shake flask experiments.

In this study, the effects of closures on oxygen mass transfer rate in shake flasks are investigated. An oxygen mass transfer model which included both the closure and

headspace was combined with a cell growth model to accurately predict the transient behaviour of biomass, oxygen and substrate concentrations during batch growths in shake flasks. This model was verified on dual oxygen and substrate limitation conditions generated by growing *Pseudomonas putida* on either glucose or phenol in shake flasks. The improved model is found to predict oxygen concentration profiles and yield factors more accurately than other models available in the literature.

3.3 Experimental Methods

3.3.1 Microorganism and Media

Pseudomonas putida (ATCC 17484) was used for all microbial growth experiments. It was maintained on nutrient broth agar and stored at 4 °C. For growth experiments, a fresh culture was initially grown in media broth on the substrate of interest, and then used for inoculation. The growth media consisted of (mg in 1 L reverse osmosis water; analytical reagent grade chemicals, BDH, Toronto): K_2HPO_4, 750; KH_2PO_4, 840; $(NH_4)_2SO_4$, 474; NaCl, 60; $CaCl_2$, 60; $MgSO_4$, 60; $Fe(NH_4)SO_4$, 20; and 1 ml of trace mineral solution. The trace mineral solution consisted of (mg in 1 L reverse osmosis water): $ZnSO_4.7H_2O$, 200; $MnCl_2$, 60; H_3BO_3, 600; $CoCl_2$, 400; $CuCl_2$, 20; $NiCl_2$, 40; Na_2MoO_4, 60. The pH of the media solution was 7.

3.3.2 Mass Transfer and Batch Growth Procedures

All experiments were carried out at room temperature (22 ± 2 ºC). For determination of oxygen mass transfer coefficients in the gas phase, first the water and gas phases in the flask were de-aerated using nitrogen gas, which was sparged into the liquid phase of the flask using a coarse fritted sparger. Then a closure was quickly inserted into the flask opening (or without any closure) and then absorption of oxygen into the water was measured over time using an oxygen meter (model 50175, Hach

company, Loveland) with a membrane probe (model 50180, Hach company, Loveland). The probe diameter was 12 mm and was positioned so that 20 mm of the probe tip was dipped into the liquid during all experiments. The oxygen probe was passed through the closure (rubber stopper or foam plug) and sealed to the closure material so that no oxygen could bleed into the flask between the probe and closure. The probe was always installed vertically into the middle of the flask to minimize its effect as a baffle. The oxygen meter was connected to a computer using WinWedge® data acquisition software. After installation of the probe in the shake flask, the monitored oxygen concentrations started to drop. The shaking was commenced once the probe showed a stable, minimum oxygen concentration. Experiments were carried out over a wide range of flask sizes, liquid amounts, and shaking speeds for four types of closures: no closure, foam plugs (Identi-Plugs, Jaece Industries, North Tonawanda, NY), glass wool holder with no filling, and glass wool holder with 1 g glass wool (Table 3.1). A schematic drawing of the glass wool holder and its dimensions are shown in Figure 3.1. Shaking started at 80 rpm because the oxygen mass transfer was too slow at lower speeds such that probe fluctuations made mass transfer determination impossible. Oxygen concentrations were also measured during glucose and phenol growth experiments to determine oxygen yield factors as will be described.

All shake flask growth experiments were carried out using a rotary shaker (model 542, Fermentation Design, Allentown) at 100 rpm shaking rate and with shaking amplitude of 25 mm. Size of the Erlenmeyer shake flasks were 500 ml containing 220 ml media broth inoculated with 3 ml inoculum taken from a fresh culture using the same media and substrate. All shake flasks were connected to atmosphere through a foam plug closure. Long hypodermic needles were inserted through the foam plugs into the growth vessels and used to withdraw samples. In all growth experiments, the media broth contained either an initial concentration of 1000 mg/L glucose or 300 mg/L phenol.

3.3.3 Analysis

Biomass concentrations were measured at 620 nm wavelength using a spectrophotometer (UVmini-1240, Shimadzu, Kyoto, Japan). Optical density was converted to cell dry weight using a previously prepared calibration curve. Samples were

filtered and used immediately for phenol analysis or stored in a freezer for later glucose analysis. For measurement of phenol, optical density of the filtered sample was measured at 280 nm. Then absorbance was converted to phenol concentration using a prepared calibration curve. Glucose concentrations were determined using a biochemistry analyzer (model 2700/115V, YSI Incorporated, Yellow Springs, Ohio).

3.4 Model

3.4.1 Oxygen Mass Transfer Model

Assuming the liquid phase in all vessels was well-mixed, a first order response equation that includes the probe response time can be used for the variation of the liquid phase oxygen concentrations (Merchuk et al., 1990):

$$\frac{C - C_i}{C_0 - C_i} = \frac{e^{-k_L a \times t} - \tau \times k_L a \times e^{-t/\tau}}{1 - \tau \times k_L a} \tag{3.1}$$

Assuming the gas phase was well-mixed, a first order response equation can be used for the variation of the gas phase oxygen concentrations:

$$\frac{y^* - y_i}{y^* - y_{i0}} = e^{-k_G a \times t} \tag{3.2}$$

Henry's law relates equilibrium concentrations at the air-water interface:

$$y_i = HC_i \tag{3.3}$$

The air-liquid mass transfer coefficient was determined using an earlier model (Nikakhtari and Hill, 2005):

$$k_L a = 0.0182 \times (A \times T_L) \tag{3.4}$$

$$A = 142 \times (V - L)^{2/3} \tag{3.5}$$

$$T_L = \frac{V^{0.463}}{L} \times \frac{N}{60} \tag{3.6}$$

The probe response time was determined earlier (7.9 ± 0.5 s). Measuring oxygen concentrations in the liquid phase and using Equations 3.1 and 3.3, oxygen

concentrations in the flask headspace were calculated. Fitting these gas phase concentrations to Equation 3.2 by a least squares method, $k_G a$ was determined as a best-fit parameter. This gas phase oxygen mass transfer coefficient includes resistances due to the flask neck and the closure.

3.4.2 Cell Growth Model

The prediction of cell growth includes the same growth kinetic model used earlier (Nikakhtari and Hill, 2005) but now combined with oxygen mass transfer limitations to both the headspace and the liquid phase. Growth kinetics was limited by either low amounts of organic substrate or dissolved oxygen. This dual limitation was modeled by combining either Haldane inhibition (for phenol as used earlier by Hill and Robinson, 1975) and Monod kinetics (for oxygen); or using a dual Monod model for glucose and oxygen (Tong and Fan, 1988):

$$\frac{dX}{dt} = \mu X \tag{3.7}$$

$$\mu = \frac{\mu_{\max} S}{S + K_S + S^2 / K_i} \times \frac{C}{C + K_m} \tag{3.8}$$

Substrate consumption kinetics can be expressed using the substrate yield factor (assumed constant):

$$\frac{dS}{dt} = -\frac{1}{Y_{XS}} \frac{dX}{dt} \tag{3.9}$$

Oxygen concentration in the liquid phase is affected by both mass transfer and consumption according to:

$$\frac{dC}{dt} = -\frac{1}{Y_{XC}} \frac{dX}{dt} + k_L a (C_i - C) \tag{3.10}$$

Oxygen concentration at the gas-liquid interface is governed by Henry's law while the oxygen concentration in the headspace (assumed to be the same as that at the gas-liquid interface) is due to flow into the headspace through the flask neck and closure and flow of oxygen into the liquid phase:

$$y_i = HC_i \tag{3.11}$$

$$\frac{dy_i}{dt} = k_G a(y^* - y_i) - k_L a(C_i - C) \quad (3.12)$$

where y* is the oxygen concentration in the atmospheric air (mg/L). From earlier studies, K_S and K_m were set at 1 and 0.25 mg/L for all experiments, and K_i at ∞ and 470 mg/L for glucose and phenol respectively (Tarighian et al., 2003; Nikakhtari and Hill, 2005). Since the oxygen mass transfer coefficients (k_La and k_Ga) were known from oxygen mass transfer experiments, Equations 3.7 to 3.12 could be solved simultaneously (using a 4th order Runge-Kutta numerical method on Excel®) to determine the best fit values of the three model parameters (μ_{max}, Y_{XS}, and Y_{XC}) for both glucose and phenol as reported in our earlier study (Nikakhtari and Hill, 2005).

3.5 Results and Discussion

3.5.1 Mass Transfer of Oxygen

Best fit values for gas mass transfer coefficients (k_Ga) are listed in Table 3.1, which were obtained by minimizing the squared error between Equation 3.2 and the gas phase data for each oxygen transfer experiment. Figure 3.2 shows a good fit of Equations 3.1 and 3.2 to dissolved and gas phase oxygen concentration data for a typical mass transfer run. Figure 3.3 combines the results of gas phase mass transfer coefficients for the shake flask without a closure. The gas phase volumetric mass transfer coefficient is a function of turbulence in the flask. Similar to the liquid phase, an empirical gas phase turbulence factor (T_G) was defined as a function of flask to liquid volume ratio and shaking rate as:

$$T_G = \frac{V}{L} \times N^{\alpha} \quad (3.13)$$

In the shake flask without a closure, k_Ga values were fit to an exponential equation and the parameter of Equation 3.13 (α) was determined to be 1.80 by minimizing the sum of squared errors. The exponential function is valid under T_G = 11000 ± 400:

$$k_G a = 0.176 \times e^{0.00020 \times T_G}, \qquad R^2 = 0.989 \tag{3.14}$$

When either flask to liquid volume ratio or shaking rate increases such that T_G exceeds 11000, $k_G a$ values showed wide scatter with a dramatic increase in values, which can be seen in Table 3.1 For T_G above 11000, $k_G a$ has an overall average value of 86.8 ± 15.7 h^{-1}, which suggests under these conditions resistance against oxygen mass transfer in the gas phase is negligible. It can be concluded that at low shaking rates and high liquid to flask volume ratios, resistance of the shake flask neck without any closure against oxygen mass transfer into the headspace of the flask can be considerable. This feature has generally been neglected in earlier studies (Gupta and Rao, 2003; Henzler and Schedel, 1991; Van Suijdam et al., 1978; Veglio et al., 1998). It will be shown later that if $k_G a$ is less than 1 h^{-1}, it is important to take this coefficient into account.

When foam plugs were used as closures, the $k_G a$ values and the best linear fit to these values at lower T_G values are shown in Figure 3.4. The best value for α in this case was found to be 1.31 and a linear equation was fit to the experimental data when T_G < 1260:

$$k_G a = 0.0013 \times T_G - 0.157, \quad R^2 = 0.962 \tag{3.15}$$

At higher T_G values, the gas phase oxygen mass transfer coefficient does not vary significantly and fluctuates around an average value of 1.66 ± 0.03 h^{-1}. This reveals that at higher T_G values, the oxygen mass transfer rate reaches a maximum and does not depend on turbulence of the gas phase in the flask. Lower α in this case reveals that the shaking rate has a lower effect on $k_G a$ when a foam plug is used as a closure. In other words, when no closure was used, shaking creates more turbulence in the neck of flask which increases oxygen transfer at increased shaking rates. Using foam plugs as closures normally resulted in a decrease in $k_G a$ values compared to flasks without any closures over the range of parameters tested in this work. Figure 3.5 shows that $k_G a$ values of both cases are similar at low T_G values (below about 800) but as the turbulence factor is increased, enhanced mass transfer occurs in the shake flasks without the foam plug closures.

When a neoprene stopper with an empty glass wool holder was used as a closure for the shake flask, $k_G a$ values were found to be very low, fluctuating around an average value of 0.076 ± 0.004 h^{-1}. The same trend was observed when 1 g of glass wool was

inserted in the holder with an average $k_G a$ value of 0.065 ± 0.006 h^{-1}. Even though $k_G a$ value in the case of 1 g glass wool was 14.7% less than its value in the case of 0 g glass wool, a t-test with 95% confidence interval showed that this difference was not meaningful. The same statistical test also showed that there was not any significant difference among $k_G a$ values when any of the three parameters affecting T_G (flask volume, liquid volume, or shaking speed) was changed. These results reveal that in the case of using a holder, diffusion through the narrow neck of the holder is the main resistance against oxygen mass transfer in the gas phase, and increasing turbulence in the gas phase does not reduce this resistance. Adding a small amount of glass wool to the holder does not increase this resistance significantly.

3.5.2 Biogrowth Experiments

A foam plug closure was used for three replications of glucose (a fast metabolism substrate) and three replications of phenol (a slow metabolism substrate) consumption by *Pseudomonas putida* in shake flasks under a low shaking speed condition (100 rpm). The experiments were modeled using both the old model, without consideration of air phase oxygen mass transfer (Nikakhtari and Hill, 2005), and the new model (Equations 3.7-3.12), and three parameters of models (μ_{max}, Y_{XS}, and Y_{XC}) were determined as best fitting parameters. The results are shown in Table 3.2. Concentration distributions predicted by the new model for substrate, biomass, and oxygen in both liquid and gas phases in one of glucose experiments are shown in Figure 3.6. It can be seen that model predictions closely follow the experimental data points. Oxygen concentration distributions in the liquid phase predicted by the old model are also shown in this figure, and it is clear the fit is not as accurate as the new model. The main effect of using the new model was on the dissolved oxygen curve when the substrate is depleted and the dissolved oxygen concentration starts to increase. By using the new model, this increase was slower due to the resistance of the foam plug, the curve matched experimental data better. This improved fit resulted in an increase in all three growth parameters of the model as shown in Table 3.2. T-test with a 95% confidence interval showed that in the both cases of glucose and phenol experiments, increases in μ_{max} and Y_{XS} values were not meaningful. On the other hand, in both cases, there was a

significant increase in Y_{XC} values (48.3% and 84.6% for glucose and phenol experiments respectively). This reveals that using the new model and taking into account oxygen flow resistance through the flask neck and closure, has improved the estimates for Y_{XC} significantly.

It is seen from Figure 3.6 that once the oxygen became depleted in the liquid phase, the gas phase oxygen concentration in the flask starts to decrease at a higher rate, which is due to a higher driving force to the liquid phase. After a while, when depletion of oxygen concentration in the gas phase occurs, mass transfer in the gas phase becomes the controlling step for oxygen availability. The new model is able to predict this complex variation in the gas phase oxygen concentrations in the headspace of the shake flask. This demonstrates the importance of considering the gas phase mass transfer coefficient in metabolism studies in shake flasks under oxygen restrictions.

This new model was then used on data of an earlier study (Nikakhtari and Hill, 2005) for which 1 g glass wool had been inserted in the holder for shake flask cultures. The new model did not affect the reported values for μ_{max} and Y_{XS} but affected reported values for Y_{XC} significantly. The changes in Y_{XC} values for growth on both glucose and phenol are shown in Table 3.3.

Using this new model, a critical value of about 1 h^{-1} was found for k_Ga, above which there is no significant advantage in using the improved model, even when high shaking rates and low liquid volumes are used, under which conditions k_La has the highest values (up to 17.4 h^{-1}, Nikakhtari and Hill, 2005). This means that when k_Ga is larger than 1 h^{-1}, there is no significant resistance in the gas phase in comparison to the liquid phase against oxygen mass transfer in shake flask cultures.

3.6 Conclusions

New equations for the prediction of oxygen mass transfer coefficients in the gas phase of Erlenmeyer shake flasks have been presented. An improved combined model for oxygen transfer and cell growth, considering both liquid and gas phase oxygen mass

transfer resistances, accurately predicted the transient concentrations of oxygen in both liquid and gas phases of shake flasks. Shake flask closures were found to have significant effects on the determination of oxygen yield factors when there is an oxygen depletion during a growth experiment. It was shown that the improved model introduced in this work is able to fit experimental oxygen concentrations and predict oxygen yield factors with improved accuracy compared to models employed earlier in the literature.

3.7 Nomenclature

A	liquid surface area (cm^2)
C	dissolved oxygen concentration in the liquid phase (mg/L)
C_0	initial oxygen concentration in the liquid phase (mg/L)
C_i	interfacial oxygen concentration in the liquid phase (mg/L)
H	Henry's constant
k_La	oxygen mass transfer coefficient in the liquid phase (h^{-1})
k_Ga	oxygen mass transfer coefficient in the gas phase (h^{-1})
K_S, K_i, K_m	constants in Equation 3.8 (mg/L)
L	liquid volume in the shake flask (L)
N	shaking speed (rpm)
S	substrate concentration (mg/L)
T_L	liquid phase turbulence factor
T_G	gas phase turbulence factor
t	time (s)
V	volume of shake flask (L)
X	cell density (mg/L)
y_i	interfacial oxygen concentration in the gas phase (mg/L)
y_{i0}	initial interfacial oxygen concentration in the gas phase (mg/L)
y^*	oxygen concentration in the atmospheric air (mg/L)
Y_{XS}	substrate yield factor (mg cell/ mg substrate)

Y_{XC} oxygen yield factor (mg cell/ mg oxygen)

Greek Symbols

α constant in Equation 3.13

μ specific growth rate (h^{-1})

μ_{max} maximum specific growth rate (h^{-1})

τ response time (s)

3.8 References

Anderlei T.; Buchs J. Device for Sterile Online Measurement of the Oxygen Transfer Rate in Shaking Flasks. *Biochem. Eng. J.* **2001** *7*, 157-162.

Gupta A.; Rao G. A Study of Oxygen Transfer in Shake Flasks Using a Non-Invasive Oxygen Sensor. *Biotechnol. Bioeng.* **2003** *84*, 351-358.

Henzler H. J.; Schedel M. Suitability of the Shaking Flask for Oxygen Supply to Microbiological Cultures. *Bioprocess. Eng.* **1991** *7*, 123-131.

Merchuk J. C.; Yona S.; Siegel M. H.; Zvi A. B. The First-Order Approximation to the Response of Dissolved Oxygen Electrodes for Dynamic K_La Estimation. *Biotechnol. Bioeng.* **1990** *35*, 1161-1163.

Mrotzek C.; Anderlei T.; Henzler H. J.; Buchs J. Mass Transfer Resistance of Sterile Plugs in Shaking Bioreactors. *Biochem. Eng. J.* **2001** *7*, 107-112.

Nikakhtari H.; Hill G. A. Modelling Oxygen Transfer and Aerobic Growth in Shake Flasks and Well-Mixed Bioreactors. *Can. J. Chem. Eng.* **2005** *83*, 493-499.

Schultz J. S. Cotton Closure as an Aerobic Barrier in Shake Flask Fermentations. *Appl. Microbiol.* **1964** *12*, 305-310.

Tarighian A.; Hill G. A.; Headley S.; Pedras S. Enhancement of 4-chlorophenol biodegradation using glucose. *Clean Technol. Environ. Policy.* **2003** *5*, 61-65.

Tolosa L.; Kostov Y.; Harms P.; Rao G. Noninvasive Measurement of Dissolved Oxygen in Shake Flasks. *Biotechnol. Bioeng.* **2002** *80*, 594-597.

Tribe L. A.; Briens C. L.; Margaritis A. Determination of the Volumetric Mass Transfer Coefficient (k_La) Using the Dynamic "Gas Out-Gas In" Method: Analysis of Error Caused by Dissolved Oxygen Probes. *Biotechnol. Bioeng.* **1995** *46*, 388-392.

Van Suijdam J. C.; Kossen N. W. F.; Joha A. C. Model for Oxygen Transfer in a Shake Flask. *Biotechnol. Bioeng.* **1978** *20*, 1695-1709.

Veglio F.; Beolchini F.; Ubaldini S. Empirical Models for Oxygen Mass Transfer: a Comparison between Shake Flask and Lab-Scale Fermentor and Application to Manganiferous Ore Bioleaching. *Process Biochem.* **1998** *33*, 367-376.

Table 3.1 Best fit $k_G a$ values from all oxygen mass transfer runs.

Closure	Flask size (L)	Liquid volume (L)	Shaking speed (rpm)	$k_G a$ (h^{-1})
Nothing	0.5	0.125	80	2.08
Nothing	0.5	0.125	120	55.6
Nothing	0.5	0.125	160	148
Nothing	0.5	0.25	80	0.60
Nothing	0.5	0.25	120	2.49
Nothing	0.5	0.25	160	95.3
Nothing	1	0.25	80	3.58
Nothing	1	0.25	100	11.3
Nothing	1	0.25	120	94.4
Nothing	1	0.25	160	147
Nothing	1	0.5	80	0.60
Nothing	1	0.5	100	1.10
Nothing	1	0.5	120	117
Nothing	1	0.5	160	102
Nothing	1	0.75	80	0.427
Nothing	1	0.75	100	0.630
Nothing	1	0.75	120	0.852
Nothing	1	0.75	160	93.0
Foam plug	0.5	0.125	80	1.56
Foam plug	0.5	0.125	100	1.65
Foam plug	0.5	0.125	120	1.67
Foam plug	0.5	0.125	140	1.75
Foam plug	0.5	0.25	80	0.60
Foam plug	0.5	0.25	100	0.96
Foam plug	0.5	0.25	120	1.08
Foam plug	1	0.25	80	1.44
Foam plug	1	0.25	100	1.61
Foam plug	1	0.25	120	1.60
Foam plug	1	0.5	80	0.594
Foam plug	1	0.5	100	0.960
Foam plug	1	0.5	120	1.32
Foam plug	1	0.75	80	0.415
Foam plug	1	0.75	100	0.60
Foam plug	1	0.75	120	0.84
Glass wool	0.5	0.125	80	0.057
Glass wool	0.5	0.125	100	0.077
Glass wool	0.5	0.125	120	0.063
Glass wool	0.5	0.125	140	0.064

Glass wool	0.5	0.125	200	0.064
Glass wool	0.5	0.125	220	0.062
Glass wool	0.5	0.25	140	0.083
Glass wool	0.5	0.25	160	0.089
Glass wool	0.5	0.25	180	0.099
Glass wool	0.5	0.25	220	0.089
Glass wool	1	0.5	120	0.084
Glass wool	1	0.5	220	0.061
Glass wool	1	0.75	120	0.096
Glass wool	1	0.75	220	0.078
Glass wool-1 g	0.5	0.125	140	0.063
Glass wool-1 g	0.5	0.125	180	0.063
Glass wool-1 g	0.5	0.125	220	0.063
Glass wool-1 g	0.5	0.25	180	0.109
Glass wool-1 g	0.5	0.25	200	0.080
Glass wool-1 g	0.5	0.25	220	0.077
Glass wool-1 g	1	0.25	120	0.040
Glass wool-1 g	1	0.25	220	0.039
Glass wool-1 g	1	0.5	140	0.050
Glass wool-1 g	1	0.5	220	0.053
Glass wool-1 g	1	0.75	120	0.073
Glass wool-1 g	1	0.75	220	0.069

Table 3.2 Mean value of biokinetic parameters and standard errors for *Pseudomonas putida* (17484). Foam plugs used as shake flask closures.

Substrate	New model (Equations 3.7 to 3.12)			Old model		
	μ_{max}	Y_{XS}	Y_{XC}	μ_{max}	Y_{XS}	Y_{XC}
	(h^{-1})	(mg cells/ mg substrate)	(mg cells/ mg oxygen)	(h^{-1})	(mg cells/ mg substrate)	(mg cells/ mg oxygen)
Glucose	0.282 ± 0.02	0.248 ± 0.008	0.043	0.262 ± 0.02	0.239 ± 0.008	0.029
Phenol	0.175 ± 0.007	0.372 ± 0.022	0.024	0.169 ± 0.005	0.346 ± 0.025	0.013

Table 3.3 Mean value of oxygen yield factor and standard errors for *Pseudomonas putida* (23973). Glass wool in holder used as shake flask closures.

Substrate	Y_{XC} – Old model (mg cells/ mg oxygen)	Y_{XC} – New model (mg cells/ mg oxygen)	Increase %
Glucose	0.78 ± 0.09	1.07 ± 0.04	37.2
Phenol	0.36 ± 0.09	0.49 ± 0.07	36.1

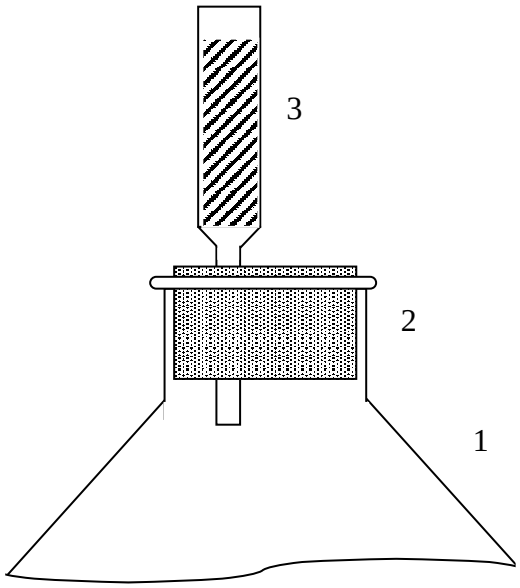

1. Shake flask
2. Neoprene rubber stopper
3. Glass wool holder (Inside diameter at bottom: 5 mm, Inside diameter at top: 20 mm, Length of the section filled with glass wool: 55 mm, Length of the narrow bottom tube: 50 mm)

Figure 3.1 Schematic drawing of the shake flask with glass wool and holder as closure.

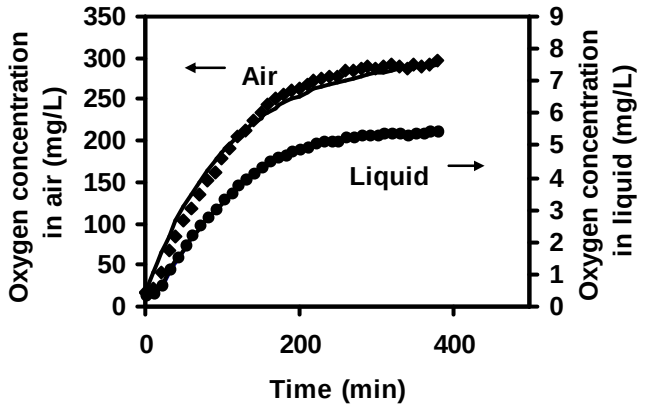

Figure 3.2 Comparison of the oxygen mass transfer model (Equation 3.1 and 3.2) to experimental and calculated data (flask volume 1 L, liquid volume 0.5 L, shaking rate 80 rpm, without closure) solid lines represent the model.

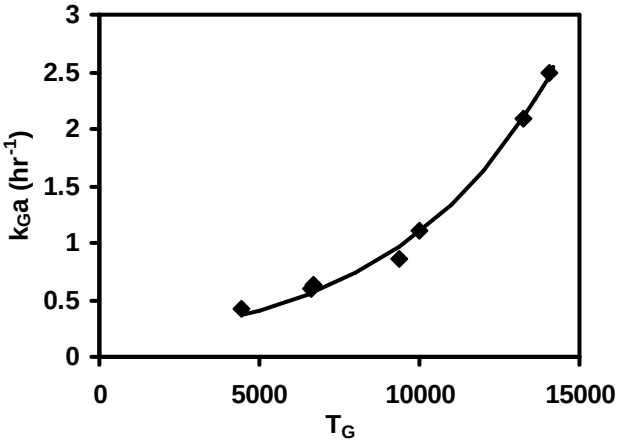

Figure 3.3 Gas phase mass transfer coefficients for the shake flask without a closure at low turbulence conditions.

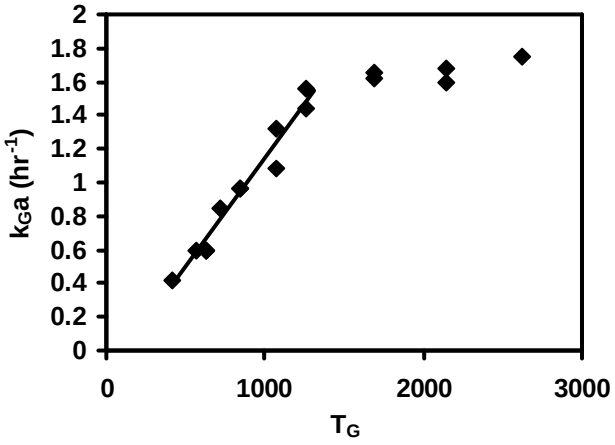

Figure 3.4 Gas phase mass transfer coefficients for the shake flask with foam plugs as closures, solid line represents Equation 3.12.

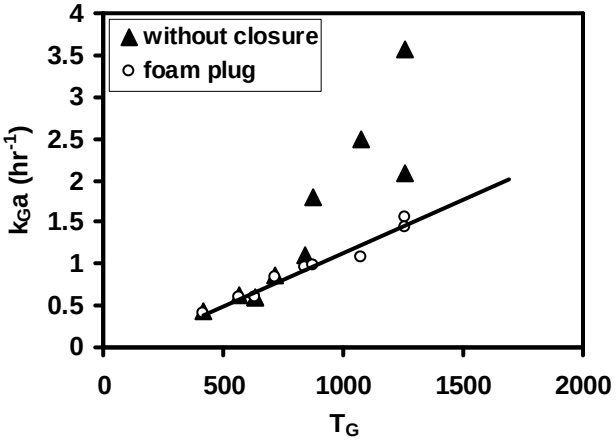

Figure 3.5 Gas phase mass transfer coefficients for the shake flask without closure and with foam plugs as closures, solid line represents Equation 3.12.

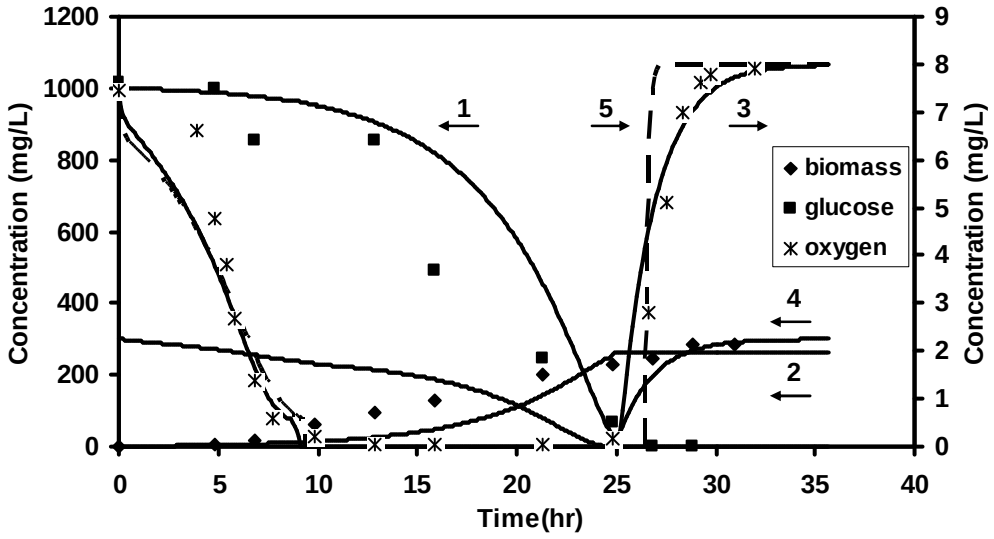

1. Substrate
2. Biomass
3. Oxygen in the liquid phase
4. Oxygen in the gas phase
5. Oxygen in the liquid phase – Old model

Figure 3.6 Model and experimental data for growth of biomass, consumption of glucose, and depletion and absorption of oxygen in 500 mL shake flask (250 mL medium, 1000 mg/L glucose, 100 rpm shaking speed), solid lines represent the new model, dashed line represents the old model.

Chapter 4 - Enhanced Oxygen Mass Transfer in an External Loop Airlift Bioreactor Using a Packed Bed

A similar version of this chapter has been copyrighted and published in the journal of **Industrial and Engineering Chemistry Research**:

Nikakhtari, H.; Hill, G. A. Enhanced Oxygen Mass Transfer in an External Loop Airlift Bioreactor Using a Packed Bed. *Ind. Eng. Chem. Res.* **2005**, *44*, 1067-1072.

Contribution of the PhD candidate

Experiments were planned by Hossein Nikakhtari and Gordon A. Hill, and were performed by Hossein Nikakhtari. Modeling and computer program development were performed by Hossein Nikakhtari with advice from Gordon A. Hill. All written text of the published paper was created by Hossein Nikakhtari with Gordon Hill providing editorial guidance.

Contribution of this chapter to the overall study

The main idea of this project was inserting a packed bed in the riser section of an ELAB and investigating three important enhancement effects: 1. Enhancement of oxygen mass transfer rate, 2. Enhancement of VOC mass transfer rate, both by providing larger mass transfer surface area, and 3. Enhancement of the bioremediation process by providing an immobilization surface for biofilm developemtn with a high active bacteria concentration on the packed bed. In this chapter, the enhancement of oxygen mass transfer rate using a nylon mesh packing in the riser section of the ELAB is studied. The same ELAB as Meng et al. (2002) had used earlier was used in this chapter, therefore the same hydrodynamic equations introduced by Meng et al. (2002) were used in the modelling part of work. In this chapter, using nylon mesh packing, enhancement of

oxygen mass transfer rate was determined and a mathematical model to predict the oxygen mass transfer coefficient was developed.

Additional experimental details

The ELAB used in this chapter is exactly the same as the one used earlier by Meng et al. (2002) A photograph of the nylon mesh packing used in this work is shown in Figure 4.01.

Figure 4.01 A photograph of the nylon mesh packing.

4.1 Abstract

A small quantity of nylon mesh packing inserted in the riser section of an External Loop Airlift Bioreactor (ELAB) was found to increase the overall volumetric oxygen mass transfer coefficient by a factor of 3.73 compared to an unpacked riser. The packing increased gas holdup, decreased bubble size, and decreased liquid circulation rates in the bioreactor, all of which contributed to the dramatic improvement in oxygen mass transfer.

A dynamic, spatial model was developed to predict the mass transfer behavior between air bubbles and the continuous liquid phase in the ELAB with and without a packed bed. The model demonstrated superior accuracy compared to simulating the ELAB as a well-mixed vessel and also correctly predicted the cyclical behavior in liquid oxygen concentrations. The oxygen mass transfer coefficient was determined as a best fitting parameter of the model and was found to increase to 4.2×10^{-3} s^{-1} using a small amount of packing (96.3 percent porosity) compared to the unpacked ELAB. This is similar to values measured in well-mixed bioreactors operating at the same aeration rates. The ELAB containing a packed bed is a novel bioreactor with much higher mass transfer and increased surface area for cell immobilization, and therefore has potential to greatly enhance gas-liquid fermentations and other gas-liquid biochemical operations.

Key words: Mass Transfer, Optimization, Airlift Bioreactor, Packed Bed, Modeling.

4.2 Introduction and Background

For the past three decades, airlift bioreactors have been used both at research and industrial scales for aqueous fermentation and bioremediation purposes. We have reported on their use for bioremediation of both hydrophilic (Ritchie and Hill, 1995; Wei et al., 1999) and hydrophobic (Harding et al., 2003) air pollutants. Because oxygen has

low aqueous solubility and is in high demand by exponentially growing microorganisms, the oxygen mass transfer rate is an important feature for aerobic fermentation and bioremediation processes. The oxygen mass transfer coefficient, K_La, is directly proportional to the rate at which oxygen can be transferred from the air phase to the aqueous medium. Although considering the ELAB as a completely stirred reactor is frequently used to predict oxygen mass transfer coefficients (Fraser et al., 1994; Wang et al., 2003), it is not accurate for a larger ELAB, especially when there is a low liquid circulation rate. Also, in some studies the variation of gas phase concentration has been neglected throughout the vessel (Dhaouadi et al., 2001). This can be a reasonable assumption for oxygen mass transfer, but not for the mass transfer of volatile organic hydrocarbons that may drop from high inlet concentrations to near zero at the outlet of the ELAB.

Oxygen K_La values fall below 100 h^{-1} in well-mixed bioreactors when pure water is used as the aqueous phase, but mixing solutes in the water can increase this value up to 1000 h^{-1} (Bi et al., 2001; Robinson and Wilke, 1974). By using high aeration rates, K_La values for oxygen in bubble columns and loop bioreactors can reach similar values as those reported for well-mixed tanks (Bello et al., 1985). However, at aeration rates similar to those used in well-mixed tanks, K_La values tend to be an order of magnitude smaller in columns compared to well-mixed bioreactors due to poor mass transfer. Although, several methods have been reported to enhance oxygen mass transfer rates in column reactors at low aeration rates (Xu et al., 2002; Godo et al., 1999; Su and Heindel, 2004; Fraser and Hill, 1993), in this study it is shown that simply using a small amount of nylon packing significantly increases the oxygen mass transfer coefficient in an ELAB. A dynamic model was used to determine mass transfer coefficients and predict the dynamic oxygen profiles throughout the vessel both with and without the packed bed.

4.3 Experimental Apparatus and Procedures

The same ELAB used earlier (Meng et al., 2002) was used in this work except that a stationary sparger was used since Meng et al. (2002) reported that the spinning sparger does not significantly improve hydrodynamic behaviour in the presence of packing. Figure 4.1 shows a schematic diagram of the ELAB with packed bed. Specifications for the experimental column are listed in Table 4.1. Woven nylon mesh (density = 647 kg/m^3 and fiber diameter 6.9×10^{-4} m) was used as packing. The packing dry weight, height and porosity were 0.164 kg, 1.09 m and 0.963 respectively.

A constant airflow rate of 9.17×10^{-6} m^3/s was used and measured by a calibrated rotameter. The corresponding air superficial velocity (J_{GR}) was 0.00147 m/s. A Hach model 50175 dissolved oxygen meter was used to measure the dissolved oxygen concentration in water. The probe was placed 10 cm below the water surface at the top of the riser section. Oxygen concentrations were recorded every 10 s with a ± 0.2 ppm repeatability. Tap water was used as the continuous phase and was de-aerated using nitrogen gas. Analysis of tap water in the city of Saskatoon, SK is shown in Table 4.2. Air, as the dispersed phase, was then instantaneously connected to the sparger and entered the ELAB through the sparger. This procedure was performed both with and without packing installed in the riser section of the ELAB.

4.4 Model

It is known that sparger orifice diameter does not significantly affect hydrodynamic parameters, such as gas hold up and circulation time (Freitas et al., 2000). The equations needed to predict the hydrodynamics of this ELAB were reported by Meng et al. (2002). Gas holdup relationships are:

$$\theta_{GR} = 1.06 J_{GR}^{\ 0.701} \quad \text{.. without packing} \qquad (4.1)$$

$$\theta_{GR} = (-2.75 + 0.272 h_P + 4.03\phi_S) J_{GR}^{\ 0.701} \quad \text{.. with packing} \qquad (4.2)$$

These equations were obtained over a range of packing heights of 0.05 – 0.8 m, porosities of 0.90 – 0.99, and gas superficial velocities of 0.003 – 0.016 m/s (Meng et al., 2002). To determine the liquid velocity in the riser section:

$$U_{LR} = C_F E \tag{4.3}$$

where E is the gas holdup driving force for liquid circulation, given by:

$$E = \left(\frac{\theta_{GR}}{(1-\theta_{GR})^{-2} + (A_R / A_D)^2}\right)^{0.92} \tag{4.4}$$

and C_F is the friction resistance for liquid flow, given by:

$$C_F = 19.1 \qquad \text{.. without packing} \tag{4.5}$$

$$C_F = -54.3 - 7.53 h_P + 71.4 \phi_S \qquad \text{.. with packing} \tag{4.6}$$

The axial mixing in the ELAB is evaluated by the Bodenstein number:

$$Bo = U_{LR} L / D \tag{4.7}$$

The Bodenstein number was reported by Fraser and Hill (1994) to be 47 in an ELAB without packing, and Meng et al. (2002) indicated the Bodenstein number was 42.6 for a porosity value of 0.963 as used in this study.

Considering oxygen mass transfer between the air and liquid phases, two partial differential equations can be written to predict oxygen concentrations over time and position in these phases:

$$\frac{\partial c}{\partial t} = D \frac{\partial^2 c}{\partial z^2} - U_{LR} \frac{\partial c}{\partial z} + K_L a (c^* - c) \tag{4.8}$$

$$\frac{\partial y}{\partial t} = -U_{GR} \frac{\partial y}{\partial z} - K_L a \frac{1-\theta_{GR}}{\theta_{GR}} (c^* - c) \tag{4.9}$$

There are some assumptions in writing these equations. Operating conditions such as gas flow rate and liquid volume are constant, therefore gas holdup, gas and liquid velocities, and liquid dispersion remain constant and can be determined by the hydrodynamic Equations 4.1 to 4.7. Flow and dispersion in the radial and angular directions are assumed to be negligible and the gas phase flows in a plug flow pattern. Also the variation of gas velocity as a result of oxygen mass transfer and hydrostatic pressure has been ignored, which is reasonable in a relatively small ELAB for low soluble oxygen. For oxygen transfer from air to water, the liquid phase limits the mass

transfer rate. The oxygen concentration in the liquid phase at the air interface (c^*) is related to the bulk air phase oxygen concentration according to Henry's law:

$$y = Hc^* \tag{4.10}$$

Equations 4.8 and 4.9 are linear partial differential equations and can be solved simultaneously by numerical finite differencing (Fraser et al., 1994). Because, at low aeration rates, there are no air bubbles in the downcomer, mass transfer only occurs in the riser section. The riser can be divided into N finite difference elements, and the downcomer is assumed to be a plug flow column for liquid, as shown in Figure 4.2.

Using forward differencing for time and central and backward differencing for the space dimension in Equations 4.8 and 4.9, respectively, and substitution of c^* from Equation 4.10 gives the following algebraic equations:

$$c_n^t = (A_L + B_L)c_{n-1}^{t-1} + (1 - 2A_L - E_L)c_n^{t-1} + (A_L - B_L)c_{n+1}^{t-1} + E_L y_n^{t-1}/H \tag{4.11}$$

$$y_n^t = 2B_G y_{n-1}^{t-1} + (1 - 2B_G - V_G/H)y_n^{t-1} + V_G c_n^{t-1} \tag{4.12}$$

where:

$$A_L = D\Delta t/(\Delta z)^2 \tag{4.13}$$

$$B_L = U_{LR}\Delta t/(2\Delta z) \tag{4.14}$$

$$B_G = U_{GR}\Delta t/\Delta z \tag{4.15}$$

$$E_L = K_L a\Delta t \tag{4.16}$$

$$V_G = K_L a\Delta t(1-\theta_{GR})/\theta_{GR} \tag{4.17}$$

These equations are applied from n = 1 to N over space, and from t = 0 to t_{Final} over time. Two boundary conditions for the liquid phase, one for the gas phase, and one initial condition for each phase are required. The boundary and initial conditions for the gas phase are simply:

$$y_0^t = y_{IN} \tag{4.18}$$

$$y_n^o = y_{IN} \tag{4.19}$$

The initial condition for the liquid phase is the dissolved oxygen concentration after dearation:

$$c_n^o = c_{\min} \tag{4.20}$$

The first boundary condition for the liquid occurs at the inlet of the riser, where it is mixed with the downcomer liquid. The concentration of oxygen in the downcomer is the same as the riser outlet after a time lag given by the residence time in the downcomer:

$$c_1^t = (A_L + B_L)c_{IN}^{t-1} + (1 - 2A_L - E_L)c_1^{t-1} + (A_L - B_L)c_2^{t-1} + E_L y_1^{t-1} / H \qquad (4.21)$$

where c_{IN} is the oxygen concentration in the outlet liquid from the downcomer:

$$c_{IN}^t = c_{\min} \qquad t<t_{Delay} \qquad (4.22)$$

$$c_{IN}^t = c_N^{t-t_{Delay}} \qquad t > t_{Delay} \qquad (4.23)$$

where:

$$t_{Delay} = H_D / J_{LD} \qquad (4.24)$$

$$J_{LD} = J_{LR} A_R / A_D \qquad (4.25)$$

The second boundary condition for liquid phase is at the top of the riser. Here there is no change in the oxygen concentration, as the liquid exits the riser:

$$c_N^t = (A_L + B_L)c_{N-1}^{t-1} + (1 - A_L - B_L - E_L)c_N^{t-1} + E_L y_N^{t-1} / H \qquad (4.26)$$

Equation 4.8 is a parabolic equation and for stability purposes, all coefficients in Equation 4.11 need to be equal to or greater than zero, which results in the following limit (Kreyszig, 1999; Carnahan et al., 1969):

$$\frac{D\Delta t}{\Delta z^2} \leq \frac{1}{2} \qquad (4.27)$$

Considering this stability limitation and choosing 0.1 m for Δz, Δt must be less than 2.73 s. Equations 4.11 and 4.12 were solved using Matlab®.

4.5 Results and Discussion

The hydrodynamic characteristics for the ELAB with and without the packed bed, predicted by Equations 4.1 to 4.7, are listed in Table 4.3. It can be seen that using a packed bed in the ELAB increases gas holdup by 37%, decreases liquid velocity by 53% and decreases dispersion by 49%. The lower velocity increases the residence time

(delay time) in the downcomer. Earlier, we reported that packing decreases the mean air bubble size (Meng et al., 2002). These factors combined to produce much higher air / liquid mass transfer rates in the packed bed ELAB compared to an unpacked ELAB. The increased frictional losses created by flow past the packing are reflected in the lower liquid circulation velocity. The energy needed to create the bubbles is due mostly to flow through the sparger orifices for small ELABs, and so there is no significant operating cost for the packed bed ELAB relative to an unpacked ELAB.

The mass transfer model (Equations 4.8 and 4.9) was best fit to experimental data to determine oxygen K_La values for absorption and desorption for both with and without packing in the ELAB. Figure 4.3a shows a typical best fit for oxygen absorption in water in the ELAB with and without packing. The presence of packing increased K_La values from 1.1×10^{-3} to 4.2×10-3 s^{-1} and are reported in Table 4.4 (with standard error equal to 1.85 percent of the mean value, determined by performing eight runs at each condition). It can be seen that using a small amount of woven mesh packing (with a high porosity equal to 96.3 percent) has increased the oxygen mass transfer coefficient in the ELAB 3.7 times. Robinson and Wilke (1974) reported oxygen K_La values in a well-mixed, stirred tank bioreactor at 5×10^{-3} s^{-1} at the same aeration conditions used in this study, however by increasing the impeller speed to a very high value of 2200 rpm, they were able to increase K_La to 3×10^{-2} s^{-1}. The addition of packing to the ELAB has therefore resulted in a K_La value similar to that found in well-mixed vessel, but only at reasonable impeller speeds.

Figure 4.3b shows the same oxygen data (and model) at early times and it is clear that there is a cyclical trend in the build up of oxygen in the bioreactor. This is due to the recirculation of the liquid. In the case of the packed ELAB the total recirculation time was 150 s, whereas the unpacked ELAB had a total recirculation time of 70 s. These different frequencies are visible both in the model and experimental results in Figure 4.3b.

The obtained oxygen mass transfer coefficient for this ELAB without packing is in acceptable agreement with the reported empirical relation of Rubio et al. (2001) and others (Fraser et al., 1994; Wang et al., 2003; Fernandez et al., 2001), who assumed the ELAB behaved like a well-mixed vessel. If the ELAB can be considered as a

completely stirred reactor, the slope of $Ln(c^*-c)/(c^*-c_0)$ vs. time can be used to evaluate K_La. It is also necessary to correct the obtained K_La by the ratio of the total volume to the riser volume (Fraser et al., 1994; Wang et al., 2003). However, decreasing the liquid circulation rate increases the error of the well-mixed calculation method, since the ELAB no longer resembles a well-mixed reactor. Eight times replication of oxygen mass transfer in the ELAB without packing (both absorption and desorption) revealed a standard error less than 1.85 percent of the mean value for the model developed in this work. Considering this ELAB as a stirred reactor for the same data yielded a standard error equal to 4.89 percent of the mean value, and also predicted K_La values 14.2 percent less due to the assumption of constant oxygen concentration in the air phase in the whole column instead of a variable oxygen concentration. Therefore, it seems necessary to consider the reactor as a distributed column, using Equations 4.8 and 4.9, and determine K_La by best fitting of experimental data, as we have done here. The advantage of this method will be very important for organic chemicals with high solubility (such as phenol), because there will be large variations in the gas phase concentration. Furthermore, Equations 4.8 and 4.9 are applied only to the riser section and give the correct K_La values without applying any volume ratio correction factor.

Figure 4.4a and 4.4b shows the theoretical oxygen concentrations over time and length in both the liquid and gas phases in the ELAB without packing predicted by the model over an early time range (0 to 40s). As seen in Figures 4.3b and 4.4a, at early times there is a wavy behaviour in the oxygen liquid concentration curve, which is due to the circulation of the deaerated liquid, but this behaviour damps out after a few circulations. Figures 4.4a shows the liquid concentration increasing with time and length of the ELAB, but these concentration gradients decrease in both time and position as the liquid becomes saturated, which in the case of the unpacked bioreactor takes almost 4000s due to the slow oxygen mass transfer rate. Figure 4.4b shows a very small decrease in air phase oxygen concentration (maximum value of 1.5 percent of initial oxygen concentration) which occurs between 10 and 40 s at the top of the bioreactor. This small decrease in oxygen concentration is due to the low oxygen solubility in water.

4.6 Conclusion

A mathematical model considering an ELAB as a distributed column with respect to both the liquid and gas phases was developed to predict mass transfer of oxygen with respect to both time and space. The model was found to fit experimental oxygen transfer data closely and it was shown that the distributed model is a much more accurate method to determine K_La for ELABs with low liquid circulation rates, as compared to a completely stirred reactor. The model correctly predicted wavy oxygen concentrations in the liquid phase and small oxygen losses in the air phase.

By fitting experimental data to the model, the oxygen mass transfer coefficients were found to be 3.7 times higher in a packed bed ELAB compared to the same vessel without a packed bed. The ELAB with a small amount of packing (96.3 percent porosity) is a novel bioreactor strategy with potential for much better mass transfer than the same ELAB without packing. This strategy shows great promise to enhance biomass growth and as a possible submerged culture vessel to handle the bioremediation of hydrophobic air pollutants.

4.7 Nomenclature

A_D downcomer cross-sectional area (m^2)

A_R Riser cross-sectional area (m^2)

Bo Bodenstein number (Equation 4.7)

c Dissolved oxygen concentration in the liquid phase (g/L)

c^* Equilibrium oxygen concentration (g/L)

c_{IN} Inlet liquid oxygen concentration to the riser section (g/L)

c_{min} The minimum oxygen concentration in the liquid (g/L)

C_F Friction loss variable (m/s, Equation 4.3)

D Axial dispersion coefficient (m^2/s)

E Gas holdup function (Equation 4.3)

h_P Packing height (m)

H Henry's law coefficient (Equation 4.10)

H_D Length of the downcomer, includes all horizontal connections and elbows (m)

J_{GR} Gas superficial velocity in the riser section (m/s)

J_{LD} Liquid superficial velocity in the downcomer section (m/s)

J_{LR} Liquid superficial velocity in the riser section (m/s)

K_La Overall volumetric mass transfer coefficient (s^{-1})

L Length of the circulation loop (m)

t Time (s)

t_{Delay} Delay time in the downcomer (s)

U_{GR} Gas velocity in the riser section (m/s)

U_{LR} Liquid velocity in the riser section (m/s)

y Oxygen concentration in the gas phase (g/L)

y_{IN} Inlet gas oxygen concentration to the riser section (g/L)

z Axial distance up the riser section (m)

Δt Time step (s)

Δz Length step (m)

ϕ_S Packing porosity

θ_{GR} Gas holdup

4.8 References

Bello, R. A.; Robinson, C. W.; Moo-Young, M. Gas Holdup and Overall Volumetric Oxygen Transfer Coefficent in Airlift Contactors. *Biotechnol. Bioeng*. **1985**, *27*, 369.

Bi, Y.; Hill, G. A.; Sumner, R. J. Enhancement of the Overall Volumetric Oxygen Transfer Coefficient in a Stirred Tank Bioreactor Using Ethanol. *Can. J. Chem. Eng*. **2001**, *79*, 463.

Carnahan, B.; Luther, H. A.; Wilkes, J. O. *Applied Numerical Methods*; John Wiley: New York, 1969.

City of Saskatoon website: **www.city.saskatoon.sk.ca/org/water_treatment**, 2006.

Dhaouadi, H.; Poncin, S.; Midoux, N.; Wild, G. Gas-Liquid Mass Transfer in an Airlift Reactor – Analytical Solution and Experimental Confirmation. *Chem. Eng. and Processing.* **2001**, *40*, 129.

Fernandez, F. G. A.; Sevilla, J. M. F.; Perez, J. A. C.; Grima, E. M.; Chisti, Y. Airlift-Driven External-Loop Tubular Photobioreactors for Outdoor Production of Microalgae: Assessment of Design and Performance. *Chem. Eng. Sci.* **2001**, *56*, 2721.

Fraser, R. D.; Hill, G. A. Hydrodynamic Characteristics of a Spinning Sparger, External Loop Airlift Bioreactor. *Can. J. Chem. Eng.* **1993**, *71*, 419.

Fraser, R. D.; Ritchie, B. J.; Hill, G. A. Dynamic Mixing and Oxygen Transfer in Small, Airlift Loop Bioreactors: Model and Experimental Verification. *Biotechnol. Prog.* **1994**, *10*, 543.

Freitas, C.; Fialova, M.; Zahradnik, J.; Teixeira, J. A. Hydrodynamics of a Three-Phase External-Loop Airlift Bioreactor. *Chem. Eng. Sci.* **2000**, *55*, 4961.

Godo, S.; Klein, J.; Polakovic, M.; Bales, V. Periodical Changes of Input Air Flowrate – A Posible Way for Improvement of Oxygen Transfer and Liquid Circulation in Airlift Bioreactors. *Chem. Eng. Sci.* **1999**, *54*, 4937.

Harding, R. C.; Hill, G. A.; Lin, Y.-H. Bioremediation of Toluene Contaminated Air Using an External Loop Airlift Bioreactor. *J. Chem. Technol. Biotechnol.* **2003**, *78*, 406.

Kreyszig E. *Advanced Engineering Mathematics*; John Wiley: New York, 1999.

Meng, A. X.; Hill, G. A.; Dalai, A. K. Hydrodynamic Characteristics in an External Loop Airlift Bioreactor Containing a Spinning Sparger and a Packed Bed. *Ind. Eng. Chem. Res.* **2002**, *41*, 2124.

Ritchie, B. J.; Hill, G. A. Biodegradation of Phenol Polluted Air Using an External Loop Airlift Bioreactor. *J. Chem. Technol. Biotechnol*. **1995**, *62*, 339.

Robinson, C. W.; Wilke, C. R. Simultaneous Measurement of Interfacial Area and Mass Transfer Coefficients for a Well-Mixed Gas Dispersion in Aqueous Electrolyte Solutions. *AIChE J*. **1974**, *20*, 285.

Rubio, F. C.; Garcia, J. L.; Molina, E.; Chisti, Y. Axial Inhomogeneities in Steady-State Dissolved Oxygen in Airlift Bioreactors: Predictive Models. *Chem. Eng. J*. **2001**, *84*, 43.

Su, X.; Heindel, T. J. Gas Holdup Behaviour in Nylon Fiber Suspensions. *Ind. Eng. Chem. Res*. **2004**, *43*, 2256.

Wang, S.; Arimatsu, Y.; Koumatsu, K.; Furumoto, K.; Yoshimoto, M.; Fukunaga,K.; Nakao, K. Gas Holdup, Liquid Circulating Velocity and Mass Transfer Properties in a Mini-Scale External Loop Airlift Bubble Column. *Chem. Eng. Sci.*. **2003**, *58*, 3353.

Wei, V. Q.; Hill, G. A.; Macdonald, D. G. Bioremediation of Contaminated Air Using an External-Loop Airlift Bioreactor. *Can. J. Chem. Eng.* **1999**, *77*, 955.

Xu, Y.; Liu, D.; Xie, D. Study on the Effects of Oscillating Period on Mass Transfer Characteristic in Airlift Loop Reactor. *J. Chem. Eng. of Chin. Univ.* **2002**, *16(1)*, 13.

Table 4.1 Specifications of the ELAB.

Riser section diameter, mm	89
Riser cross-sectional area (A_R), m^2	6.22×10^{-3}
Downcomer section diameter, mm	47
Downcomer cross-sectional area (A_D), m^2	1.74×10^{-3}
Liquid height above the sparger, m	1.45
Liquid volume, m^3	1.2×10^{-2}
Loop length, m	3.20
Downcomer length (H_D), m	1.81
Number of orifices in sparger	6
Orifice diameter, mm	1.6

Table 4.2 Analysis of inorganic constituents in tap water for the city of Saskatoon, SK (City of Saskatoon website, 2006).

Aluminum, mg Al/L	0.04
Barium, mg Ba/L	0.031
Boron, mg B/L	0.028
Calcium, mg Ca/L	26
M-Alkalinity, mg $CaCo_3$/L	87
P-Alkalinity, mg $CaCo_3$/L	6
Carbonate, mg $CaCo_3$/L	11
Bicarbonato, mg $CaCo_3$/L	76
Total Hardness, mg $CaCo_3$/L	136
Chloride, mg Cl/L	10
Chlorine Residual, mg Cl_2/L	1.6
Fluoride, mg F/L	0.68
Iron, mg Fe/L	0.01
Magnesium, mg Mg/L	18
Potassium, mg K/L	3.5
Sodium, mg Na/L	25
Sulfate, mg SO_4/L	66

Table 4.3 Hydrodynamic characteristics of ELAB with and without packed bed.

Parameter	Without packing	With packing	Change in Value, %
θ_{GR}	0.0110	0.0151	+37
U_{LR}, m/s	0.0269	0.0127	-53
D, m^2/s	0.00183	0.00094	-49
t_{Delay}, s	19.0	40.4	+112

Table 4.4 Best fit model values for oxygen mass transfer coefficients.

K_La, s^{-1}	Without packing	With packing
Absorption	0.0011	0.0040
Desorption	0.0011	0.0042

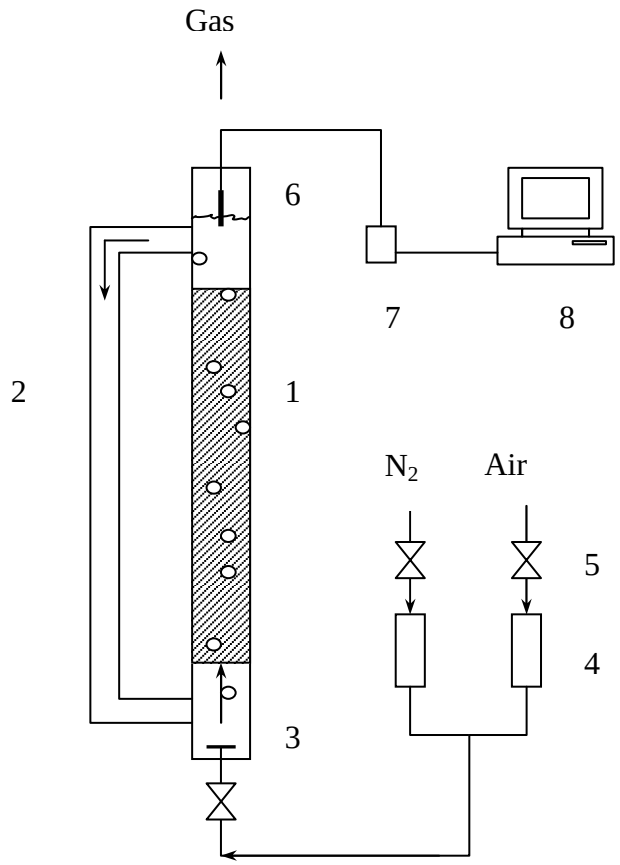

1- Riser section with packing
2- Downcomer section
3- Gas sparger
4- Flow meter
5- Adjusting valve
6- Oxygen probe
7- Dissolved oxygen meter
8- Computer for data acquisition

Figure 4.1 Schematic of the External Loop Airlift Bioreactor.

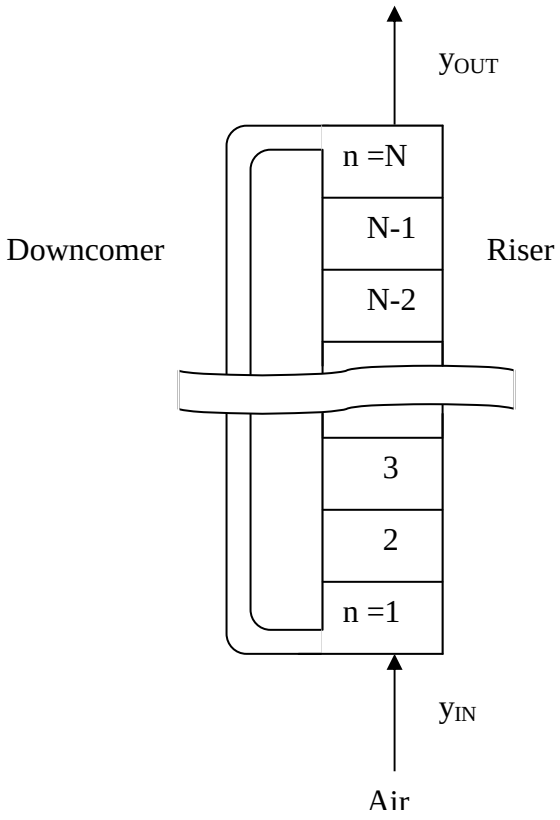

Figure 4.2 Schematic of the ELAB showing the finite difference sections.

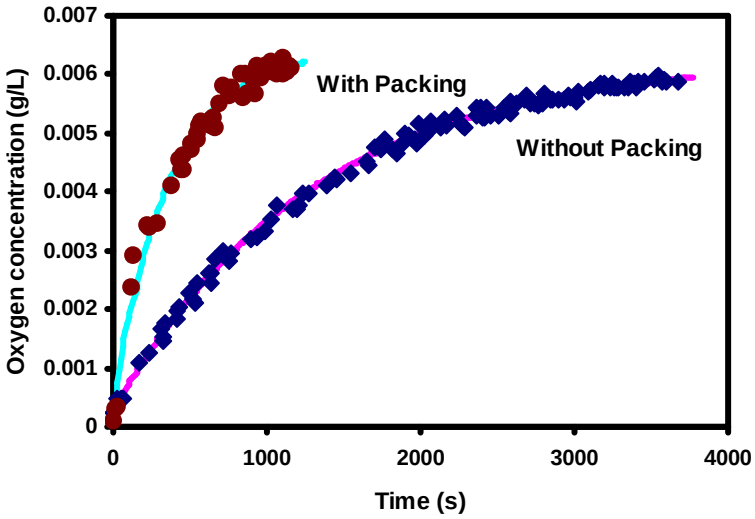

(a)

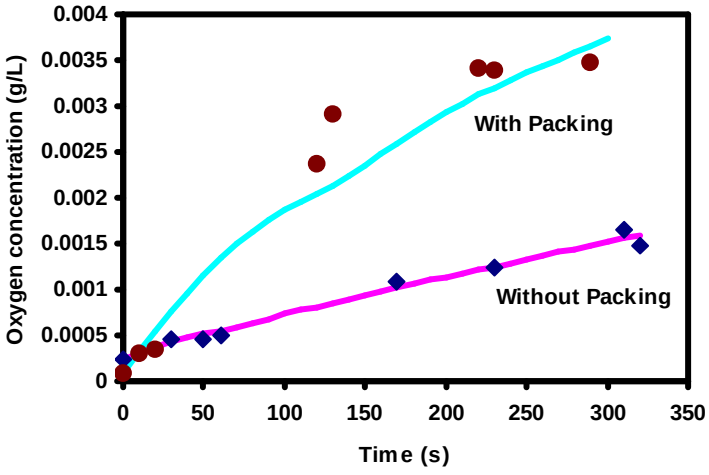

(b)

Figure 4.3 Comparison of mass transfer model in liquid phase (Equation 4.8) to experimental data of oxygen absorption in water in the ELAB with and without packing: (a) in 4000 s, (b) in first 300 seconds.

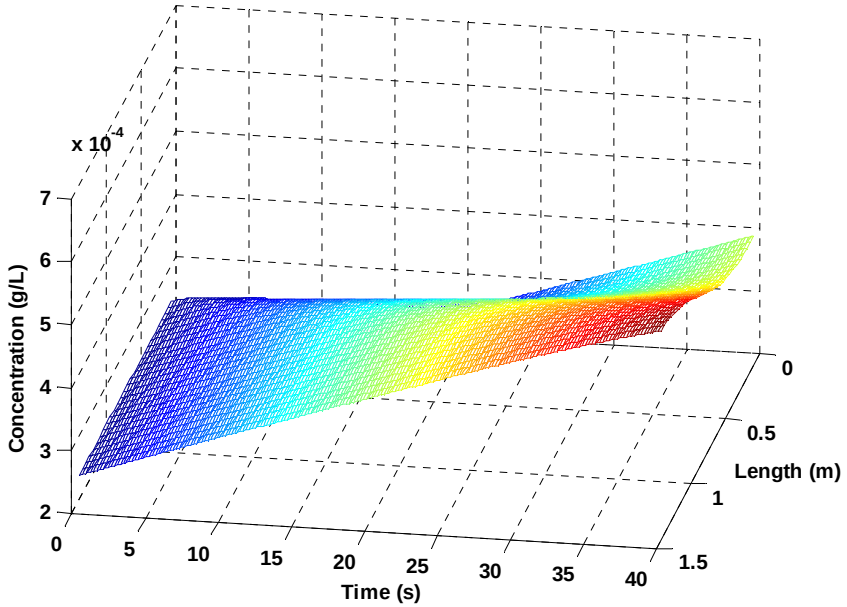

(a)

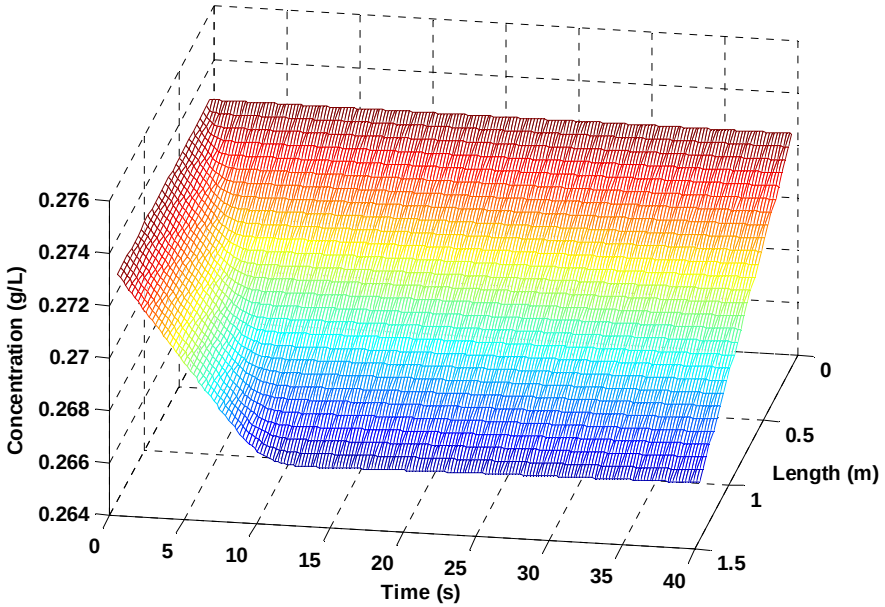

(b)

Figure 4.4 Oxygen mass transfer model in the ELAB without packing in first 40 seconds:
(a) in liquid phase (Equation 4.8), (b) in gas phase (Equation 4.9).

Chapter 5 - Hydrodynamic and Oxygen Mass Transfer in an External Loop Airlift Bioreactor with a Stainless Steel Packed Bed

A similar version of this chapter has been copyrighted and published in the **Biochemical Engineering Journal**:

Nikakhtari, H.; Hill, G. A. Hydrodynamic and Oxygen Mass Transfer in an External Loop Airlift Bioreactor with a Packed Bed. *Biochem. Eng. J.* **2005**, *27*, 138-145.

Contribution of the PhD candidate

A modification in the existing apparatus was designed by Hossein Nikakhtari and Gordon A. Hill, and parts were manufactured in the glass and machine shops of the University of Saskatchewan and Pegasus (Guelph, ON). Installation of the modified apparatus was performed by Hossein Nikakhtari. Experiments were planned by Hossein Nikakhtari and Gordon A. Hill, and were performed by Hossein Nikakhtari. Modeling and computer program development were by Hossein Nikakhtari with advice from Gordon A. Hill. All written text of the published paper was created by Hossein Nikakhtari with Gordon A. Hill providing editorial guidance.

Contribution of this chapter to the overall study

As mentioned earlier, the main idea of this project was inserting a packed bed in the riser section of an ELAB and the investigation of its three important enhancement effects: 1. Enhancement of oxygen mass transfer rate, 2. Enhancement of VOCs mass transfer rate, and 3. Enhancement of the bioremediation process. In the previous chapter, the enhancement of oxygen mass transfer rate using a nylon mesh packing in the riser section of the ELAB was studied. Since it was noticed that nylon packing releases some

organic additives that may interfere with VOC mass transfer studies, it was decided to replace the nylon mesh with stainless steel packing and also replace all plastic parts in the column with glass parts. These modifications changed all hydrodynamic equations. Therefore, in this chapter, the hydrodynamic conditions of the modified ELAB were studied and new equations were introduced. Then, using stainless steel packing, the enhancement of oxygen mass transfer rate was determined and using the new hydrodynamic equations, a mathematical model to predict the oxygen mass transfer coefficient was developed. Different airflow rates were also investigated and the dependence of the oxygen mass transfer coefficient on the air superficial velocity was determined.

Additional experimental details

The ELAB used in this chapter was made of glass. A schematic drawing of it is shown in Figure 5.1 and a photograph of it with the stainless steel packing in its riser section is shown in Figure 5.01. A photograph of the stainless steel mesh packing used in this chapter is shown in Figure 5.02.

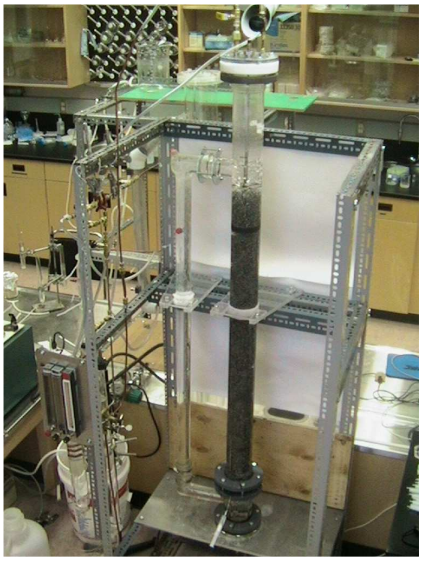

Figure 5.01 A photograph of the glass ELAB with the stainless steel packing in the riser section.

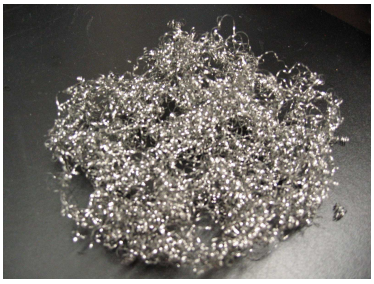

Figure 5.02 A photograph of the stainless steel mesh packing.

A schematic drawing of the stainless steel sparger in the bottom of the ELAB is shown in Figure 5.03. The sparger had a diameter of 78 mm and it had 6 orifices, each with a, diameter of 1.5 mm. The column base that is seen in the Figure sits on a frame, and the glass ELAB sits on that base.

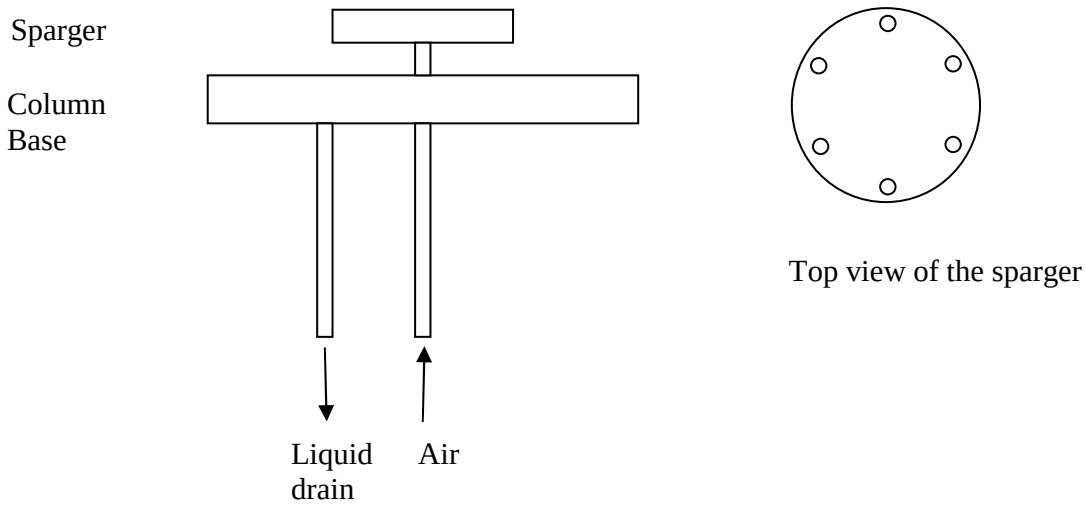

Figure 5.03 A schematic drawing of the stainless steel sparger in the bottom of the ELAB.

Figure 5.04 shows a schematic drawing of the stainless steel packing holder. The holder itself sits on a stainless steel stand which is shown in Figure 5.05. Packing is placed between two rings that can be seen in the Top view of the holder in Figure 5.04. The position of the upper ring was variable, which allows adjusting the height of the packed bed. In this work, this height was kept at the maximum possible value, 1.2 m. The lower ring distance from the bottom of the column can also be adjusted by varying

the location of the ring on the stand (Figure 5.05). In all experiments with a packed bed, this distance of the packed bed above the sparger was kept at 12 cm.

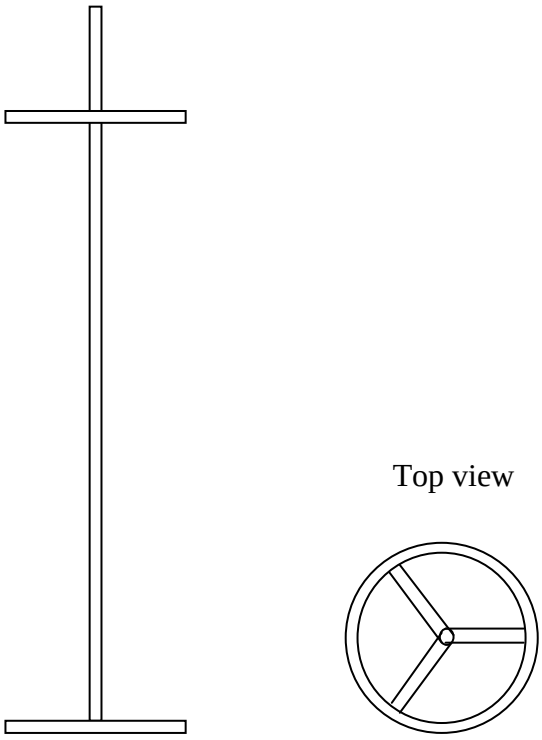

Figure 5.04 A schematic drawing of the packing holder with adjustable total packing height.

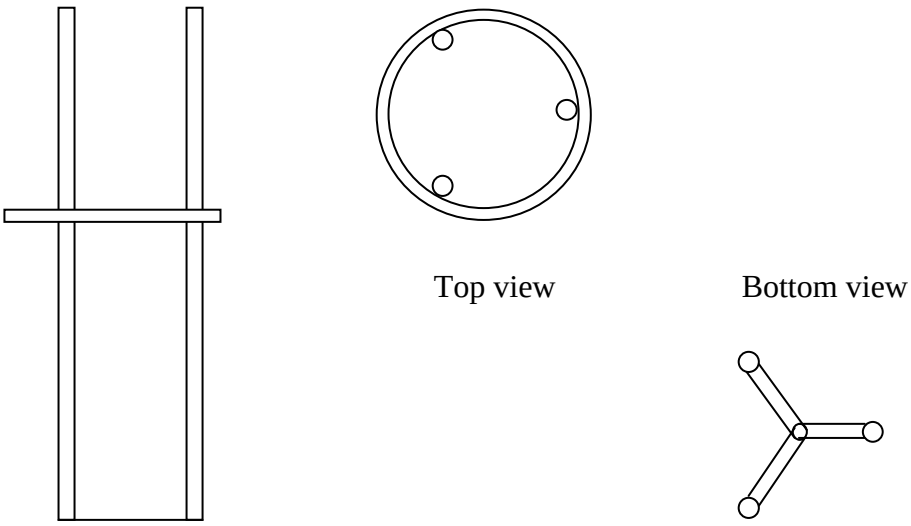

Figure 5.05 A schematic drawing of the stand for the packing holder.

5.1 Abstract

A stainless steel mesh packing with 99.0% porosity has been inserted in the riser section of an external loop airlift bioreactor (ELAB). The hydrodynamic characteristics and oxygen mass transfer rates of the ELAB, both with and without packing, were compared. The packing increased the overall volumetric oxygen mass transfer coefficient by an average factor of 2.45 compared to the unpacked column. The packing increased gas holdup, decreased bubble size, and decreased liquid circulation rates in the bioreactor, all of which contributed to the dramatic improvement in the oxygen mass transfer rates.

A dynamic, spatial model was used to predict the transient oxygen concentration distribution in the ELAB with and without a packed bed. This model was compared to simulating the ELAB as a completely stirred reactor and demonstrated improved prediction of the cyclical changes in liquid oxygen concentrations. The oxygen mass transfer coefficient was determined as a best fitting parameter of the model and at higher gas superficial velocities was found to increase to values approaching 0.021 s^{-1} using the small amount of packing. Finally, simplified correlations were developed to predict the oxygen mass transfer coefficient in the ELAB with and without the packed bed.

Key words: Hydrodynamics, Gas-Liquid Mass Transfer, Oxygen Transfer, Airlift Bioreactors, Packed Bed Bioreactors, Dynamic Modeling.

5.2 Introduction

Due to their simple design, without any moving parts but still providing sufficient mixing for microbial reactions, external loop airlift bioreactors (ELAB) have achieved increasing attention among biological researchers and equipment manufacturers. However, the oxygen mass transfer rate in the ELAB is smaller than that in well-mixed bioreactors and can limit the growth rate of cells, because oxygen is a

crucial element for aerobic cultures and it has low solubility in water. In this study, an ELAB has been modified by adding a packed bed to the riser section while maintaining the downcomer section to provide liquid circulation and mixing. The resulting design is a combination of a conventional ELAB and packed bed bioreactor. It has been reported for packed bed bioreactors that although mass transfer is higher than unpacked bioreactors, it can still limit the performance of the reactor and should be fully investigated (Sarti et al., 2001).

In gas-liquid packed bed columns, previous investigators have reported that the mass transfer coefficient is increased by increase in the liquid superficial velocity, but not as significantly by increase in the gas superficial velocity (Yuan et al., 2004; Deront et al., 1998). However, in the loop airlift column, the liquid superficial velocity is not independent from the gas superficial velocity because the gas upward movement is the driving force for the liquid movement. Both the liquid velocity and mass transfer coefficient will be increased by an increase in gas superficial velocity. The gas holdup, liquid velocity, and mass transfer coefficient can be modelled as functions of the gas superficial velocity. For instance, Guo et al. (1997) observed a linear increase of the gas holdup with the gas superficial velocity in a packed column at low values (gas superficial velocity less than 0.011 m/s) and a power function increase at higher values.

Doig et al. (2004) used microplates with porous frits installed in a special miniaturized bubble column bioreactor and reported oxygen mass transfer coefficients as high as 0.06 s^{-1} at a gas superficial velocity of 0.02 m/s. However, to generate the air flow through the frits, high air pressures were needed upstream of the bioreactor. Vychodilova et al. (2004) studied the mass transfer of oxygen into water in a co-current packed bed column with a height of 2.05 m, at different gas and liquid flow rates. They used glass spheres with a diameter of 0.01 m and a voidage of 0.4 as a packing and reported oxygen mass transfer coefficients as high as 0.05 s^{-1} at high gas and liquid flow rates.

Chisti et al. (1990) studied the enhancement of oxygen mass transfer in liquids with different viscosities in an ELAB using two separate blocks of static mixer elements in the riser section. They found the oxygen mass transfer coefficient to be a power function of the gas superficial velocity and found that it almost doubled due to the use of

static mixers. Chisti and Moo-Young (1993) have also studied liquid circulation velocity in an ELAB using spherical beads and Raschig rings in the riser section of the column. Using 1 m deep of 0.002 m diameter spherical beads at a low gas superficial velocity of 0.01 m/s, the liquid superficial velocity fell to a low value of 0.008 m/s which still provided adequate circulation for microbial cultures.

In this study, a stainless steel wire mesh packing in the riser of an ELAB has been used to improve the hydrodynamic and oxygen mass transfer characteristics over a range of superficial gas velocities. The packing had a very high voidage, 0.990, but still greatly improved the rate of oxygen transfer into the liquid medium compared to an unpacked ELAB. A mechanistic model is shown to accurately predict the experimental data.

5.3 Experimental Apparatus and Procedures

The same ELAB used in our earlier work (Nikakhtari and Hill, 2005) was used in this study except that woven stainless steel mesh with a fiber diameter of 4.6×10^{-4} m replaced the nylon mesh. Nylon mesh had been found to release organic chemicals into the aqueous media which interfered with cell cultivations. In this study, all parts of the bioreactor were made of glass or stainless steel. Meng et al. (2002) reported the best packing conditions for an ELAB with nylon mesh packing involved using a maximum packing height and maximum packing porosity. In this work, the maximum height of the packing between downcomer inlet and outlet branches, equal to 1.2 m, and the maximum possible porosity of the packing, equal to 99.0%, were used. High packing porosity produces the lowest flow resistance and hence a minimum increase in required aeration power. Furthermore, high porosity minimizes problems due to plugging during cell cultures whereas mesh packing provides high surface areas for cell immobilization.

The packing was fixed in place in the riser using a stainless steel holder with large openings at the bottom and top to provide negligible resistances to fluid flow and mass transfer rates. Figure 5.1 shows a schematic diagram of the ELAB with the packed

bed. The riser section diameter, liquid height above sparger and riser to downcomer cross-sectional area ratio (A_R/A_D) were 89 mm, 1.42 m and 3.57, respectively. The sparger had six, 1.6 mm diameter orifices equally spaced at a radial position of 37.5 mm.

A wide range of gas flow rates were used and operation at each flow rate was repeated from three to eight times, including both absorption and desorption, to calculate the standard error of the mass transfer coefficient at each flow rate. The highest gas flow rate was chosen such that no gas bubbles were observed in the downcomer section. The gas flow rate was measured by a calibrated rotameter. A dissolved oxygen meter (model 50175, Hach Co., Loveland) with a membrane probe (model 50180, Hach Co., Loveland) was used to measure the dissolved oxygen concentrations in water. The probe was placed 5 cm below the water surface at the top of the riser section. Using WinWedge® data acquisition software, oxygen concentrations were recorded every 10 s with ± 0.2 mg/l repeatability. Reverse osmosis water was used as the continuous phase and was de-aerated using nitrogen gas. Following de-aeration, air, as the dispersed phase, suddenly entered the ELAB through the sparger. This procedure was performed both with and without packing installed in the riser section of the ELAB. Gas pressure was measured using a pressure gauge with $\pm 0.03 \times 10^5$ Pa accuracy. Since an ordinary sparger was used in the ELAB with hole diameters equal to 1.6 mm, both the air and nitrogen gas inlet pressures were small, less than 0.48×10^5 Pa gauge for the maximum gas superficial velocity of 0.0157 m/s. All experiments were carried out at room temperature (23 ± 2 ºC) and pressure (mean value of 0.932×10^5 Pa). At the lowest gas superficial velocity (1.85×10^{-3} m/s), a hemispherical metal net with 1 mm hole diameters was positioned in front of the probe tip to prevent attachment of rising air bubbles to the probe membrane.

At all gas superficial velocities, gas holdup was measured within ± 5% error by measuring the increase in the liquid level after introducing air to the riser section. The liquid velocity was measured by injection of 0.1 ml water soluble ink into the top of the column and recording its travel time through the downcomer. Velocity measurements were made independently of the mass transfer measurements, so that the ink was not present during the mass transfer experiments.

5.4 Model

The experimentally measured gas volume in the riser section of the column was used to calculate the gas holdup at different gas flow rates according to:

$$\theta_{GR} = \frac{V_{GR}}{V_{GR} + V_{LR}} \tag{5.1}$$

Gas holdups were best fit to an empirical correlation similar to earlier work [11]:

$$\theta_{GR} = aJ_{GR}{}^{b} \tag{5.2}$$

To determine the liquid velocity in the riser section, the same correlations reported by Meng et al. (2002) were used:

$$U_{LR} = C_F E \tag{5.3}$$

where E is the gas holdup driving force for liquid circulation, given by:

$$E = \left[\frac{\theta_{GR}}{(1-\theta_{GR})^{-2} + (A_R / A_D)^2} \right]^{0.92} \tag{5.4}$$

and C_F is the friction resistance for liquid flow.

The axial mixing in the ELAB is evaluated using the Bodenstein number:

$$Bo = U_{LR} L / D \tag{5.5}$$

The Bodenstein number was reported by Fraser and Hill (1993) to be 47 in a similar ELAB without packing, and in presence of packing Meng et al. (2002) indicated that the Bodenstein number depends on packing porosity and is 45.5 for a porosity value of 0.990 as used in this study. The Bodenstein number is not very sensitive to the packing, so no further work was done to determine this coefficient with more accuracy.

Considering oxygen mass transfer between the gas and liquid phases, two partial differential equations to predict oxygen concentrations over time and position in these phases are (Nikakhtari and Hill, 2005; Fraser et al., 1994):

$$\frac{\partial c}{\partial t} = D \frac{\partial^2 c}{\partial z^2} - U_{LR} \frac{\partial c}{\partial z} + K_L a (c^* - c) \tag{5.6}$$

$$\frac{\partial y}{\partial t} = -U_{GR} \frac{\partial y}{\partial z} - K_L a \frac{1-\theta_{GR}}{\theta_{GR}} (c^* - c) \tag{5.7}$$

Hydrodynamic variables needed to solve these equations were calculated using Equations 5.1 to 5.5. Flow and dispersion in the radial and angular directions are assumed to be negligible and the gas phase is assumed to flow in a plug pattern. Also the variation of gas velocity as a result of oxygen mass transfer and hydrostatic pressure has been ignored which is reasonable in a relatively small ELAB and for low soluble oxygen. For oxygen transfer from air to water, the liquid phase limits the mass transfer rate. The oxygen concentration in the liquid phase at the air interface (c^*) is related to the bulk air phase oxygen concentration according to Henry's law:

$$y = Hc^* \tag{5.8}$$

Equations 5.6 and 5.7 are linear partial differential equations and were solved simultaneously by numerical finite differencing, using forward differencing for time and central and backward differencing for the space dimension, in Equations 5.6 and 5.7, respectively and the Matlab® software package. The solution procedure and equations were explained previously (Nikakhtari and Hill, 2005). The boundary condition for the gas phase is at the inlet of the riser section and is equal to the inlet air oxygen concentration. Before starting the experiment, no mass transfer occurs between gas and liquid phase, so the initial concentration of the gas phase in the bioreactor can be assumed to be in equilibrium with the liquid phase. The initial condition for the liquid phase is the dissolved oxygen concentration after de-aeration. Boundary conditions for the liquid occur at the inlet and outlet of the riser. Inlet liquid to the riser was assumed to have the same oxygen concentration as the outlet liquid from the riser but with a time delay, $t_{Delay,}$ because the downcomer acts as a time delay component. There are no air bubbles in the downcomer and therefore no mass transfer occurs there. The value of t_{Delay} is determined by:

$$t_{Delay} = H_D / J_{LD} \tag{5.9}$$

$$J_{LD} = J_{LR} A_R / A_D \tag{5.10}$$

5.5 Results and Discussion

Air inlet pressures, and therefore required power to force air through the fittings, sparger and into the ELAB were measured at different gas superficial velocities as shown in Figure 5.2. This data was correlated by (coefficient of determination of 0.9971):

$$P_G = 2.83E04 \times J_{JR}^2 - 186 \times J_{GR} + 0.445 \qquad (5.11)$$

With the packed bed inserted into the riser, no increase in inlet gas pressure was detectable within the accuracy of the pressure gauge. The extra required power for moving the air through the packing in the riser is small due to the high porosity of the packed bed which causes negligible pressure drop compared to the pressure drop across the sparger orifices.

Fitting Equation 5.2 to the experimental data for gas holdup for both cases of without and with packed bed is shown in Figure 5.3. Parameters in Equation 5.2 were determined to be:

$a = 3.228$; $b = 1.016$ .. without packed bed (5.12)

$a = 1.460$; $b = 0.784$ .. with packed bed (5.13)

The parameters for the packed bed column apply to a packing height and porosity of 1.2 m and 0.990, respectively. The coefficient of determinations of Equation 5.2 are 0.998 and 0.999 for without and with packed bed cases, respectively. A linear equation (Equation 5.2 with a = 2.998 and b = 1) was also found to fit the gas holdup data for the case of no packing with a coefficient of determination of 0.9998. Using a packed bed in the column, compared to the case without a packed bed, there was an increase in gas holdup from a minimum value of 20.1% to a maximum of 91.9% as the gas superficial velocities varied from 0.015 to 0.002 m/s. The gas holdup showed an average increase of 46.4% when the packed bed was used in the column compared to the unpacked ELAB. This increased holdup contributes to an increase in mass transfer area, consequently an increase in the volumetric mass transfer coefficient. Increased gas hold up is partially due to a drop in the interstitial velocity of the gas due to the resistance of the packing in the column and partially due to decrease in gas bubble sizes.

Fitting Equations 5.3 and 5.4 to the experimental data for liquid velocity in the riser is shown in Figure 5.4a. The values of the coefficient, C_F, were:

$$C_F = 48.9 \quad \text{.. without packed bed} \tag{5.14}$$

$$C_F = 10.8 \quad \text{.. with packed bed} \tag{5.15}$$

The coefficient for the packed bed case applies only to the packing height and porosity used in this study. The coefficient of determinations were 0.996 for both cases. Liquid velocity versus gas superficial velocity, as predicted by Equation 5.3, is shown in Figure 5.4b. Using the packed bed in the ELAB, in spite of the high porosity of the packing, resulted in a large decrease in liquid velocity from 60.5 to 72.6% over the examined gas superficial velocity range from 0.0025 to 0.011 m/s. This reduced liquid velocity contributes to higher gas holdups since the rising air bubbles would have less upward frictional drag being applied to their surfaces. Chisti and Moo-Young reported a non-linear relationship between liquid superficial velocity and gas superficial velocity at high aeration rates (up to 0.12 m/s). For the ELAB without a packed bed, the difference in measured liquid velocities between our work and that of Chisti and Moo-Young's (1993) is about 50% at low gas superficial velocities but reduces to 3.1% as the gas superficial velocity increases to 0.02 m/s. Liquid velocity is a sensitive factor of frictional energy losses as the fluid flows around the bioreactor loop, so it is not unexpected that different values will occur due to slight differences in the geometrical design of the ELAB. Chisti and Moo-Young (1993) also observed a dramatic reduction in the liquid velocity in the presence of packing (in their case, one meter deep bed of spheres with diameter of 0.01 m and porosity of 0.4), which was more than observed in this study likely due to the fact that we used a packing with much higher porosity, 0.99 instead of 0.4.

Figure 5.5a shows typical recorded oxygen concentrations in the ELAB with the packed bed during four replications of oxygen desorption and absorption experiments at a gas superficial velocity of 4.16×10^{-3} m/s. As the oxygen concentration approaches equilibrium, the recorded data points showed increased scatter which was a characteristic of the oxygen meter and probe used in this study. Figure 5.5b shows similar data for three replications at the high gas superficial velocity of 1.57×10^{-2} m/s which demonstrates more scatter when oxygen concentration approaches equilibrium.

The fluctuations in oxygen measurement were visually observed to be proportional to the frequency and intensity at which gas bubbles collided with the probe membrane, both of which increased as the aeration rate increased.

Figure 5.6a compares predictions using Equations 5.6 and 5.7 to measured oxygen concentrations during absorption experiments at the gas superficial velocity of 4.16×10^{-3} m/s for both with and without a packed bed. The model is able to accurately predict oxygen concentration changes at the top of the riser over time. Figure 5.6b shows the same results in the first 200 s. It can be seen that the model follows the cyclic changes of oxygen concentrations during early times which are caused by liquid recirculation through the downcomer. These oscillations damp out after a few circulations once the supply of unaerated liquid in the downcomer becomes homogeneous with the riser liquid. Both the model and data points demonstrate a significantly higher mass transfer rate in the column with a packed bed compared to that without the packing.

The best fit mass transfer model (Equations 5.6 and 5.7) was used to determine the oxygen mass transfer coefficient for each experiment. Figure 5.7 compares the mass transfer coefficients over a range of gas superficial velocities both with and without a packed bed. It is clear that the mass transfer coefficients measured with packing are much higher than those measured without packing. At the superficial velocity of 0.008 m/s, the value of $K_L a$ was 2.52 times higher when packing was used in the riser. Higher superficial velocities could not be studied without packing because air bubbles began to be carried through the downcomer. Eight replications of the experiments at the gas superficial velocity of 0.0032 m/s in the ELAB without a packed bed showed a very small standard error of the mass transfer coefficient, equal to 1.85% of the mean in this case. On the other hand, the standard error of the mass transfer coefficient in the ELAB with a packed bed starts from a small value of 3.7% of the mean at low gas superficial velocities and increased up to 22.6% of the mean at higher gas superficial velocities. This increase in the standard error is due to the large fluctuations in oxygen concentration measurements discussed earlier. Good agreements were observed between mass transfer coefficients of absorption and desorption experiments at the same operating conditions which was expected since the liquid phase is the significant

resistance against oxygen mass transfer and this resistance is the same for both absorption and desorption.

A common correlation for the mass transfer coefficient in stirred reactors is a power equation in which the mass transfer coefficient (K_La) is correlated with the gas power uptake per unit volume and the gas superficial velocity (Puthli et al., 2004). In the ELAB, the gas power uptake is not independent from the gas superficial velocity and K_La can be correlated with only the gas superficial velocity, which is also commonly done for bubble columns (Doig et al., 2004; Rubio et al., 2001). In the ELAB with packed bed used in this study, this correlation yields:

$$K_L a = 0.531 J_{GR}^{\ 0.762}; \qquad R^2 = 0.945 \tag{5.16}$$

If only low superficial gas velocities are considered (< 0.006 m/s), a simple first order equation can be used for both conditions:

$$K_L a = 2.530 J_{GR} - 0.003; \quad \text{with packing;} \qquad R^2 = 0.9918 \tag{5.17}$$

$$K_L a = 0.7369 J_{GR} - 0.00005; \quad \text{without packing;} \qquad R^2 = 0.9928 \tag{5.18}$$

The oxygen volumetric mass transfer coefficient observed in the column with a packed bed is always higher than the coefficient in the column without a packed bed. The improvement depends on the gas superficial velocity, and increased by a factor of 1.83 to 2.52 as the gas superficial velocity increased from 0.002 to 0.008 m/s. In an earlier study using nylon mesh packing, a 3.73 fold increase in oxygen mass transfer coefficient was observed but this was for a packing porosity of 96.3% (Nikakhtari and Hill, 2005). Therefore, increasing the packing porosity may decrease the oxygen mass transfer factor but provides other advantages such as less gas pressure drop and less column plugging potential. In this study, the oxygen mass transfer coefficient in the ELAB with a packed bed approached 0.021 s^{-1} at high gas superficial velocities which is comparable to the oxygen mass transfer coefficient in stirred reactors at similar aeration conditions and reasonable mixing rates (Puthli et al., 2004). This suggests that a packed ELAB could be expected to achieve similar cell culture densities as a well-mixed bioreactor but with much less capital and operating expenses.

The significant increase in the mass transfer coefficient when a small amount of mesh packing is added to the ELAB is due to the 46.4% increase in gas holdup and also

due to the decrease in the gas bubble size in the presence of packing. These factors contribute to increased mass transfer area and therefore increased volumetric mass transfer coefficients. The gas bubbles were not uniform in the column without a packed bed and their diameters reached 30 mm; however, in the column with a packed bed gas bubbles were visually observed to be more uniform and the maximum diameter never exceeded 9 mm. Meng et al. (2002) generated detailed bubble size data using nylon mesh packing in the riser and reported a mean bubble diameter decrease of 41.8%. Although the mean gas bubble sizes were not measured here, the stainless steel mesh packing seems to break down gas bubbles effectively similar to nylon mesh packing.

An investigation of simplifying the oxygen mass transfer model was finally undertaken. First, the model was simplified by setting the dispersion coefficient (D) equal to zero in Equation 5.6, since dispersion was only a small component of the hydrodynamics. This considers both the liquid and gas phases as flowing in plug flow patterns around the ELAB. This assumption resulted in a simplified solution process, and provided values of volumetric mass transfer coefficients for the ELAB with a packed bed that deviated only 2.0% from those achieved using the full model. The error of fit was also very good, with coefficient of determinations being nearly identical to the cases when the full model was used (0.970 in both cases). Larger deviations from the full model for the ELAB without a packed bed, equal to 4.9%, were observed due to a larger dispersion coefficient, which is in turn because of higher liquid velocities in the ELAB without a packed bed. The second simplification involved assuming the liquid was completely mixed in the ELAB and only considering spatial changes in the gas phase concentration. This well-mixed model cannot predict cyclic changes in the liquid concentrations and predicted mass transfer coefficients that averaged 27.2% less than the full model. The final model was to assume both the liquid and gas phases were completely well-mixed. This is a simple method that is frequently used to measure volumetric mass transfer coefficients in ELABs (Chisti et al., 1990; Fraser et al., 1994; Wang et al., 2003). This model is also not able to predict cyclic changes in the liquid phase concentration in early times, and it predicts volumetric mass transfer coefficients that averaged 29.4% less than the full model. Since the completely plug flow model provided reasonable accuracy and similar volumetric mass transfer coefficients as the

full model, it is concluded that it is a reasonable approximation of the hydrodynamic and mass transfer conditions in the ELAB. The assumptions of completely well-mixed conditions in either or both of the liquid or gas phases, on the other hand, is not able to accurately predict volumetric mass transfer coefficients.

Dhaouadi et al. (2001) used a distributed model for the liquid phase (similar to Equation 5.6) but simplified the model by neglecting the variation of the gas phase oxygen concentration. This method predicted mass transfer coefficients that averaged 2.5% less than the full model due to larger than real oxygen concentrations in the gas phase. The deviation is small because there is not a large change in oxygen concentration in the air phase during this oxygen mass transfer process. This can be seen in Figure 5.8 which shows the predicted variation in the oxygen concentration in the outlet air phase during an absorption experiment in the ELAB with a packed bed at a gas superficial velocity of 4.16×10^{-3} m/s. The maximum decrease in oxygen concentration is only 6.0% which occurs in the early seconds of the experiment. However, the assumption of constant gas phase concentrations will not be good for mass transfer of volatile organic chemicals that would have 100% gas phase concentration variations if they were completely absorbed into the water.

5.6 Conclusion

By fitting experimental data to a full, mechanistic model of an ELAB both with and without a packed bed in the riser, oxygen mass transfer coefficients were found over a wide range of gas flow rates and were correlated to empirical equations. Using a small amount of packing (99.0% porosity), the oxygen mass transfer coefficient was increased by an average factor of 2.45 in a packed bed ELAB compared to the same ELAB without a packed bed, reaching a value of 0.021 s^{-1} at a gas superficial velocity of 0.0157 m/s. The ELAB with a small amount of packing is a novel bioreactor with much higher mass transfer due to increased gas holdup and small bubble diameters. The packing surface area can also be used for cell immobilization, and therefore has potential to

greatly enhance gas-liquid fermentations and other gas-liquid biochemical operations. In that case, VOC mass transfer rates may be affected by the presence of bacteria and biofilm in the ELAB. Both a full, mechanistic mathematical model and a plug flow model were found to fit experimental oxygen transfer data closely and were shown to be an accurate method to determine K_La for ELABs with low liquid circulation rates, as compared to models assuming well-mixed conditions.

5.7 Nomenclature

A_D downcomer cross-sectional area (m^2)

A_R Riser cross-sectional area (m^2)

Bo Bodenstein number (Equation 5.5)

c Dissolved oxygen concentration in the liquid phase (g/l)

c^* Equilibrium oxygen concentration (g/l)

C_F Friction loss variable (m/s, Equation 5.3)

D Axial dispersion coefficient (m^2/s)

E Gas holdup function (Equation 5.4)

H Henry's law coefficient (Equation 5.8)

H_D Length of the downcomer, includes all horizontal connections and elbows (m)

J_{GR} Gas superficial velocity in the riser section (m/s)

J_{LD} Liquid superficial velocity in the downcomer section (m/s)

J_{LR} Liquid superficial velocity in the riser section (m/s)

K_La Overall volumetric mass transfer coefficient (s^{-1})

L Length of the circulation loop (m)

P_G Power (W)

t Time (s)

t_{Delay} Delay time in the downcomer (s)

U_{GR} Gas velocity in the riser section (m/s)

U_{LR} Liquid velocity in the riser section (m/s)

V_{GR} Gas volume in the riser section of the ELAB (m^3)

V_{LR} Liquid volume in the riser section of the ELAB (m^3)

y Oxygen concentration in the gas phase (g/l)

z Axial distance up the riser section (m)

Z Riser section height (m)

θ_{GR} Gas holdup

5.8 References

Chisti, Y.; Moo-Young, M. Airlift Bioreactors with Packed Beds of Immobilized Biocatalysts: Theoretical Evaluation of the Liquid Circulation Performance. *Food Bioprod. Process: Trans. I. Chem. E.* **1993**, *71C*, 209-214.

Chisti, Y.; Kasper, M.; Moo-Young, M. Mass Transfer in External-Loop Airlift Bioreactors Using Static Mixers. *Can. J. Chem. Eng.* **1990**, *68*, 45-50.

Deront, M.; Samb, F. M.; Adler, N.; Peringer, P. Volumetric Oxygen Mass Transfer Coefficient in an Upflow Cocurrent Packed-Bed Bioreactor. *Chem. Eng. Sci.* **1998**, *53*, 1321-1330.

Dhaouadi, H.; Poncin, S.; Midoux, N.; Wild, G. Gas-Liquid Mass Transfer in an Airlift Reactor – Analytical Solution and Experimental Confirmation. *Chem. Eng. and Processing.* **2001**, *40*, 129-133.

Doig, S. D.; Diep, A.; Baganz, F. Characterisation of a Novel miniaturized Bubble Column Bioreactor for High Throughput Cell Cultivation. *Biochem. Eng. J.* **2004**, *23*, 97-105.

Fraser, R. D.; Hill, G. A.; Hydrodynamic Characteristics of a Spinning Sparger, External Loop Airlift Bioreactor. *Can. J. Chem. Eng.* **1993**, *71*, 419-425.

Fraser, R. D.; Ritchie, B. J.; Hill, G. A. Dynamic Mixing and Oxygen Transfer in Small, Airlift Loop Bioreactors: Model and Experimental Verification. *Biotechnol. Prog.* **1994**, *10*, 543-547.

Guo, Y. X.; Rathor, M. N.; Ti, H. C. Hydrodynamics and Mass Transfer Studies in a Novel External Loop Airlift Reactor. *Chem. Eng. J.* **1997**, *67*, 205-214.

Meng, A. X.; Hill, G. A.; Dalai, A. K. Hydrodynamic Characteristics in an External Loop Airlift Bioreactor Containing a Spinning Sparger and a Packed Bed. *Ind. Eng. Chem. Res.* **2002**, *41*, 2124-2128.

Nikakhtari, H.; Hill, G. A. Enhanced Oxygen Mass Transfer in an External Loop Airlift Bioreactor Using a Packed Bed. *Ind. Eng. Chem. Res.* **2005**, *44*, 1067-1072.

Puthli, M. S.; Rathod, V. K.; Pandit, A. B. Gas-Liquid Mass Transfer Studies with Triple Impler System on a Laboratory Scale Bioreactor. *Biochem. Eng. J.* **2004**, *23*, 25-30.

Rubio, F. C.; Garcia, J. L.; Molina, E.; Chisti, Y. Axial Inhomogeneities in Steady-State Dissolved Oxygen in Airlift Bioreactors: Predictive Models. *Chem. Eng. J.* **2001**, *84*, 43-55.

Sarti, A.; Vieira, L. G. T.; Foresti, E.; Zaiat, M. Influence of the Liquid-Phase Mass Transfer on the Performance of a Packed-Bed Bioreactor for Wastewater Treatment. *Bioresource Technol.* **2001**, *78*, 231-238.

Vychodilova, H.; Jiricny, V.; Stanek, V. An Experimental Study of Absorption of Oxygen in Water in Co-Current Packed Bed Column by Transient Technique. *Chem. Biochem. Eng. Q.* **2004**, *18*, 129-136.

Wang, S.; Arimatsu, Y.; Koumatsu, K.; Furumoto, K.; Yoshimoto, M.; Fukunaga, K.; Nakao, K. Gas Holdup, Liquid Circulating Velocity and Mass Transfer Properties in a Mini-Scale External Loop Airlift Bubble Column. *Chem. Eng. Sci.* **2003**, *58*, 3353-3360.

Yuan, Y.; Han, M.; Wang, L.; Wang, D.; Jin, Y. Mass Transfer Coefficient for Two-Phase Countercurrent Flow in a Packed Column with a Novel Internal. *Chem. Eng. J.* **2004**, *99*, 273-277.

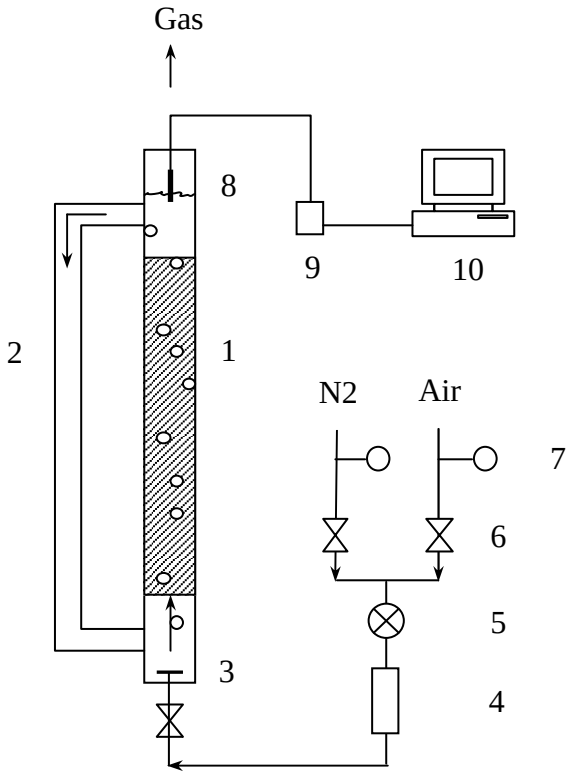

1- Riser section with packing
2- Downcomer section
3- Gas sparger
4- Flow meter
5- Two-way valve
6- Adjusting valve
7- Pressure gage
8- Oxygen probe
9- Dissolved oxygen meter
10- Computer for data acquisition

Figure 5.1 Schematic of the External Loop Airlift Bioreactor.

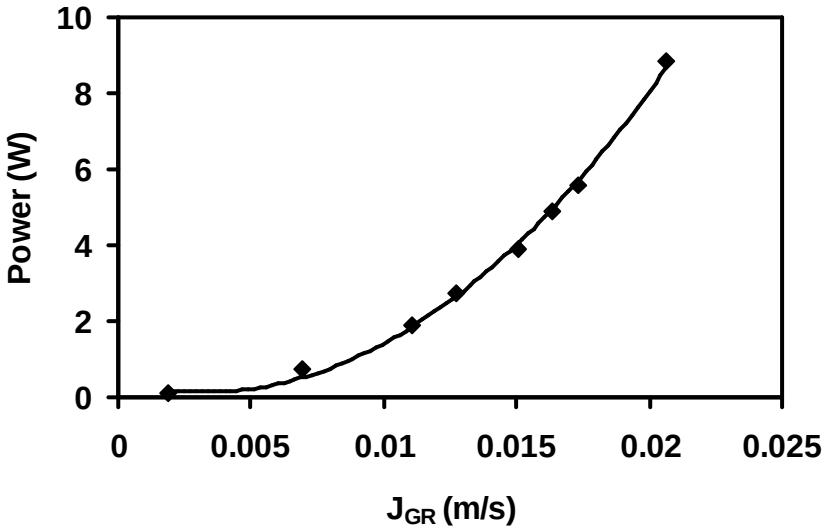

Figure 5.2 Measured power to run gas through the ELAB, (symbols= Data, Line= Equation 5.11).

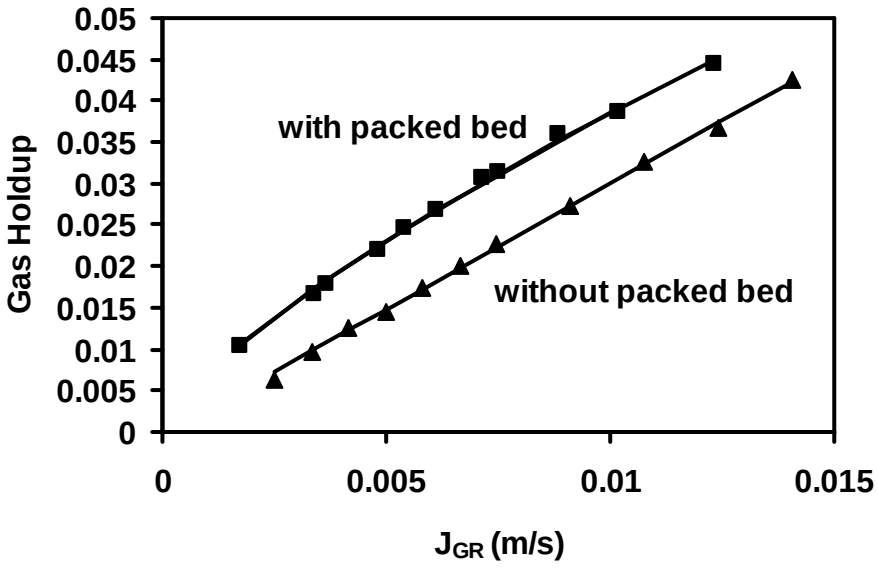

Figure 5.3 Effect of gas superficial velocities on the gas holdup in the ELAB with and without a packed bed, (symbols= Data, Lines= Equation 5.2).

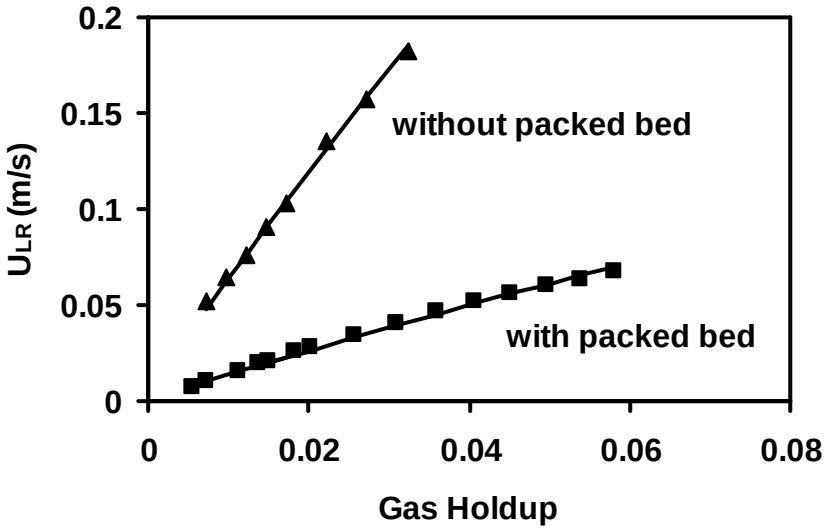

(a)

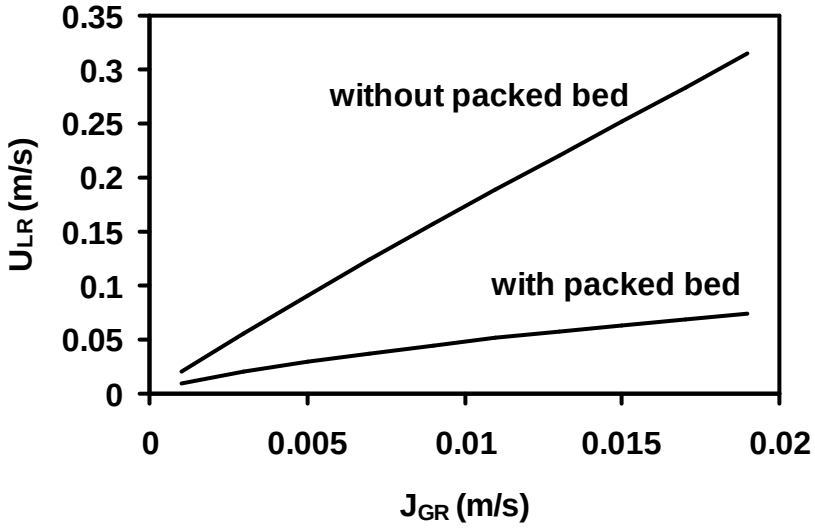

(b)

Figure 5.4 Effect of gas holdup (a, data and model) and gas superficial velocities (b, model) on the liquid riser velocity in the ELAB with and without a packed bed.

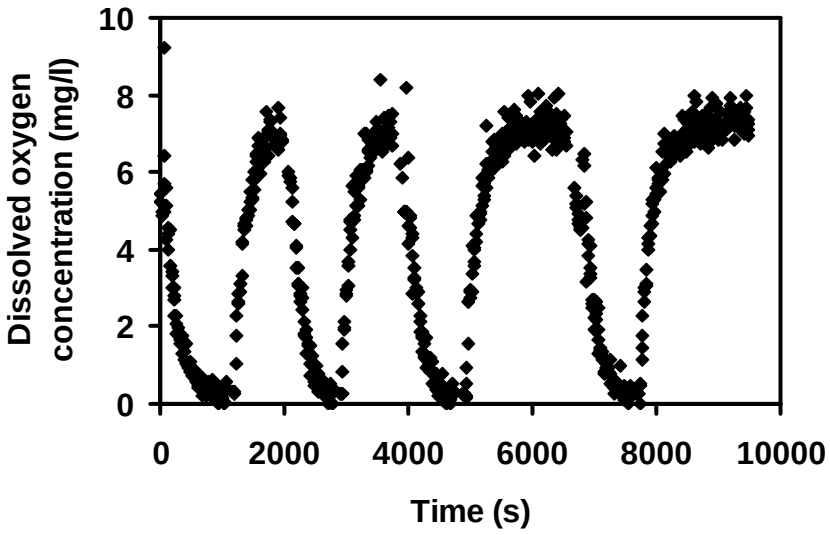

(a)

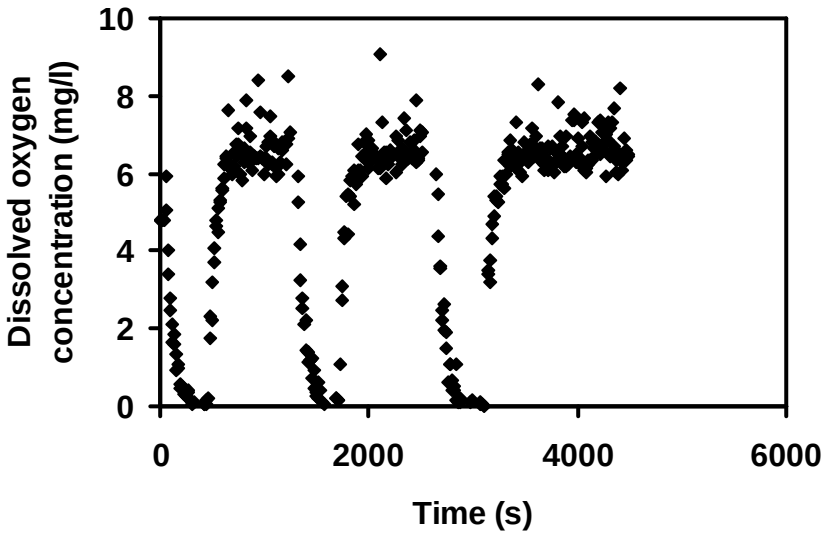

(b)

Figure 5.5 Transient oxygen concentrations in the ELAB with a packed bed at a gas superficial velocity of (a) 4.16×10^{-3} m/s and (b) 1.57×10^{-2} m/s.

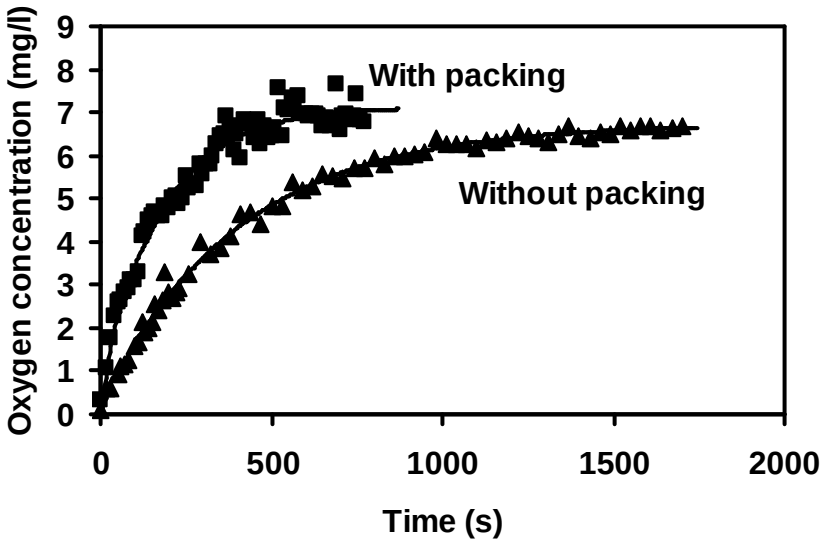

(a)

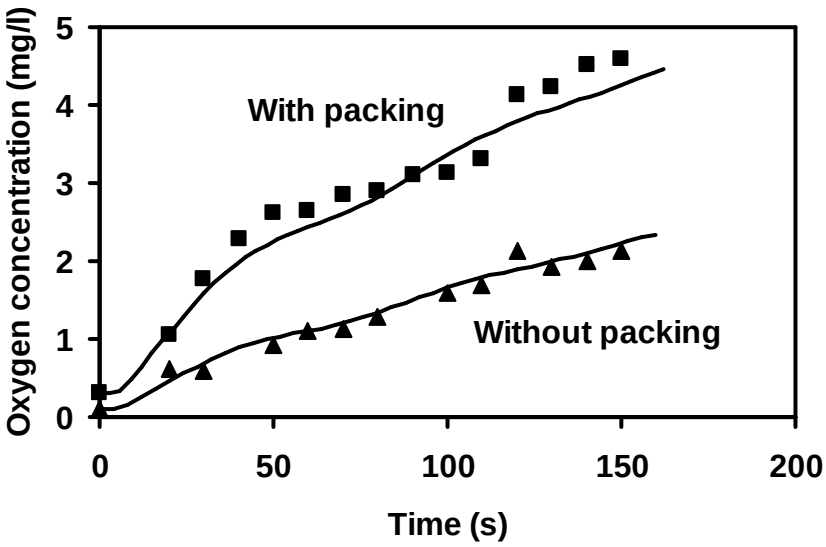

(b)

Figure 5.6 Comparison of the mechanistic mass transfer model (Equations 5.6 and 5.7) to experimental data of oxygen absorption in water in the ELAB with and without packing at the gas superficial velocity of 4.16×10^{-3} m/s: (a) in first 2000 s, (b) in first 200 seconds.

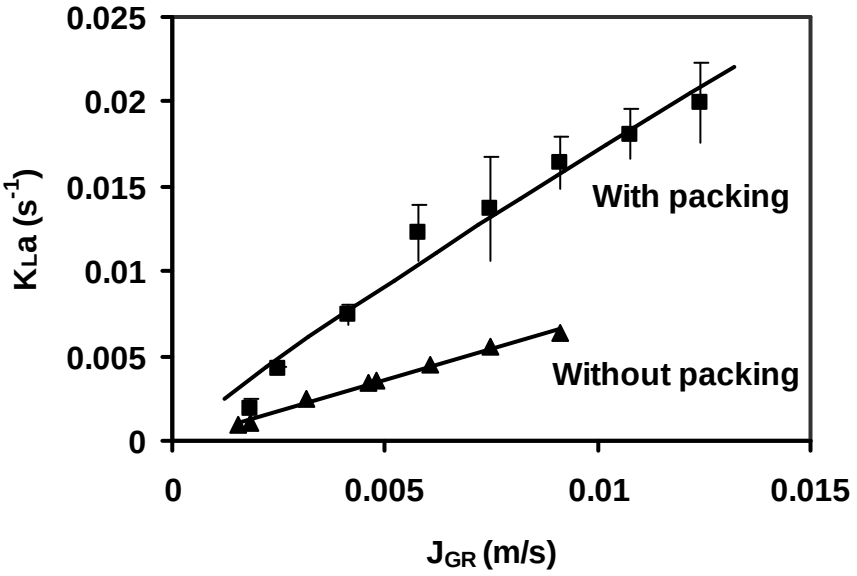

Figure 5.7 Volumetric oxygen mass transfer coefficients in the ELAB with and without a packed bed at various superficial gas velocities.

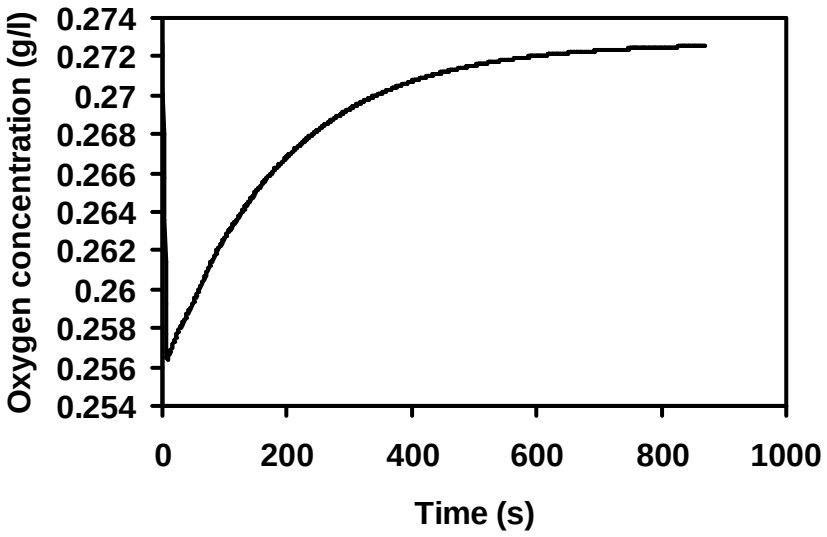

Figure 5.8 Predicted variations (Equation 5.7) of the oxygen concentration in outlet air phase during absorption in the ELAB with a packed bed at a gas superficial velocity of 4.16×10^{-3} m/s.

Chapter 6 - Volatile Organic Chemical Mass Transfer in an External Loop Airlift Bioreactor with a Packed Bed

A similar version of this chapter has been copyrighted and published in the journal of **Industrial and Engineering Chemistry Research**:

Nikakhtari, H.; Hill, G. A. Volatile Organic Chemical Mass Transfer in an External Loop Airlift Bioreactor with a Packed Bed. *Ind. Eng. Chem. Res.* **2005**, *44*, 9299-9306.

Contribution of the PhD candidate

Experiments were planned by Hossein Nikakhtari and Gordon A. Hill, and were performed by Hossein Nikakhtari. Modeling and computer program development were performed by Hossein Nikakhtari with advice from Gordon A. Hill. All written text of the published paper was created by Hossein Nikakhtari with Gordon A. Hill providing editorial guidance.

Contribution of this chapter to the overall study

In the previous two chapters, enhancements of oxygen mass transfer rate were studied. In this chapter, enhancement of VOCs (toluene, benzene, and phenol) mass transfer rates are studied. As mentioned earlier, for mass transfer studies of VOCs, nylon mesh packing interfered with measurements due to the release of some organic compounds. Therefore, in this chapter the modified ELAB with the stainless steel packing was used. The effect of the presence of VOCs on hydrodynamic conditions was determined. Some new hydrodynamic equations were introduced and used in the modeling study. Then using the stainless steel packing, the enhancement of VOCs absorption and desorption mass transfer rates were determined and using the new

hydrodynamic equations, a mathematical model was developed to predict the mass transfer coefficients.

Additional experimental details

The same ELAB with stainless steel packing as the previous chapter was used in this chapter. A gasifier was used in this chapter to produce an air stream saturated with a VOC. Three bubblers in series were used to measure the concentration of VOCs in the outlet air stream from the gasifier or the ELAB. A schematic drawing of the ELAB with the gasifier and bubblers is shown in Figure 6.1. A photograph of the gasifier and three bubblers is shown in Figure 6.01.

Figure 6.01 A photograph of the gasifier (in the pail) and three sampling bubblers in series.

6.1 Abstract

A stainless steel mesh packing with 99.0% porosity was installed in the riser section of an External Loop Airlift Bioreactor (ELAB) to develop a new bioreactor, which is a combination of a traditional ELAB and a packed bed bioreactor. The gas holdup and mass transfer rates of Volatile Organic Chemicals (VOCs) were studied in this ELAB, both with and without the packing. By using the packing, the overall volumetric VOC mass transfer coefficient increased to values of 0.005 and 0.004 s^{-1}, an average of 65.1% and 33.4% for toluene and benzene, respectively. The packing increased gas holdup and decreased bubble size in the bioreactor, both contributing to the improvements in the mass transfer rates. A difference was observed between absorption and desorption rates of VOCs, which was justified by the change in gas bubble sizes in the presence of VOCs.

A dynamic, spatial model was used to predict the transient, concentration distribution in the ELAB with and without a packed bed. The mass transfer coefficient was determined as a best fitting parameter of the model. This dynamic model was compared to simulating the ELAB as a completely stirred reactor, and the dynamic, spatial model demonstrated greater accuracy for prediction of the mass transfer rates at all operating conditions.

6.2 Introduction

Application of the circulating loop airlift bioreactor as a treatment technology for contaminated air effluents has achieved a great deal of attention in recent years. The External Loop Airlift Bioreactor, ELAB, provides a well-mixed environment appropriate for biological processes without the need for an impeller. We have already demonstrated

the successful use of the ELAB for bioremediation of both hydrophilic (Ritchie and Hill, 1995; Wei et al., 1999) and hydrophobic (Harding et al., 2003) air pollutants. Bioremediation rates of volatile organic chemicals (VOCs) as air pollutants is limited by the mass transfer rates of oxygen as well as the poorly water-soluble VOCs into the water phase. We reported the enhancement of oxygen mass transfer rate (by an average factor of 2.45) in the ELAB using a small amount of woven packing (99.0% porosity) in the riser section (Nikakhtari and Hill, 2005b). In the present work, we have used the same technique to study the enhancement of three VOCs (toluene, benzene, and phenol) mass transfer rates in the same ELAB. The bioreactor used for this work is a combination of a conventional ELAB and a packed bed bioreactor. Although in packed bed bioreactors the liquid-phase mass transfer is higher than unpacked bioreactors, mass transfer can still limit the performance of the reactor and therefore needs to be fully studied (Sarti et al., 2001).

Chao et al. (1998) have investigated the mass transfer coefficient of some organic chemicals, including toluene, during desorption in a packed column using different sizes of sand as packing. They reported toluene mass transfer coefficient from 0.0006 to 0.001 s^{-1} when the air flow rate increased from 1.5 to 3.5 L/min. Fang and Lin (1986) have compared mass transfer coefficients from their and other work for benzene desorption in a beaker at different air flow rates. They reported an average benzene desorption mass transfer coefficient equal to 0.0021 s^{-1} at an air flow rate per reactor volume equal to 0.0074 s^{-1}. Lo and Hwang (2004) suggested using oxygen mass transfer coefficients and penetration theory to calculate VOC mass transfer coefficients. According to penetration theory, the mass transfer coefficient ratio is equal to square root of the diffusion coefficient ratio. This will be discussed more later. Cesario et al. (1997) have reported enhancement of oxygen and toluene mass transfer rates into water by dispersing a water-immiscible organic solvent, a perfluorocarbon (CF40). They used a stirred reactor and found an increase in the mass transfer coefficient equal to 2.2-fold for oxygen and 1.15-fold for toluene at the highest solvent volume fraction (15% v/v).

In this study, a stainless steel, mesh packing was used in the riser section of an ELAB to investigate the improvement in VOC mass transfer rates at a variety of superficial gas velocities. The packing had a very high voidage, 0.990, but still

improved the rate of VOC transfer into the liquid phase compared to an unpacked ELAB. A mechanistic model is shown to accurately predict the experimental data.

6.3 Experimental Apparatus and Procedures

The same ELAB that was used in earlier work for oxygen mass transfer (Nikakhtari and Hill, 2005b) was used in this study. The nylon mesh that had been used in the earlier study was found to absorb and release organic chemicals into the aqueous media which interfered with VOC mass transfer experiments (Nikakhtari and Hill, 2005a), therefore the nylon mesh was replaced with a woven stainless steel mesh so that all parts of the bioreactor were made of glass or stainless steel. The maximum height of the packing between downcomer inlet and outlet branches, equal to 1.2 m, and the maximum possible porosity of the packing, equal to 99.0%, were used in this study as recommended by Meng et al. (2002) High packing porosity has advantages of lower frictional pressure drop and also minimizes problems due to plugging during cell cultures, whereas the fine mesh packing still provides high surface areas for cell immobilization.

Figure 6.1 shows a schematic diagram of the ELAB with the packed bed. Specifications of the experimental ELAB and the stainless steel packing are listed in Table 6.1. Gas flow rate was manipulated over a wide range and was measured by rotameters calibrated for each gas stream. The concentration of chemicals in the liquid phase was measured by sampling from a port on the downcomer section of the ELAB and analyzing samples using a spectrophotometer (model Mandel 1240, Shimadzu, Kyoto, Japan) at an optimum wave length for each chemical (see Table 6.2). Optical density was converted to concentration using previously prepared calibration curves for each chemical. The concentration of chemicals in the inlet or outlet gas phase was measured by introducing a small portion (2.14×10^{-6} m^3/s) of the gas stream through fritted spargers located in a series of three bubblers (0.5 m height and 0.05 m diameter, each containing 0.7 litres of water), where the chemicals were absorbed. As long as the

last bubbler showed zero concentration of the chemical being analyzed, accumulated concentrations in the previous bubblers were used to calculate the chemical concentration in the air phase. This method was checked by measurement of VOC concentration in the air phase using a 100 μL gastight syringe for sampling and a pre-calibrated gas chromatograph (Hewlett Packard 5890 Series II, GMI, Inc., Ramsey, Minnesota). These two methods for the measurement of VOC concentration in the air phase showed less than 7% difference.

Reverse osmosis water was used as the continuous phase in the ELAB. Air at a controlled, measured flow rate was introduced through a fritted sparger into a bubbler with a height of 0.69 m and a diameter of 0.055 m, containing 1 liter of pure VOC (except for phenol which was slurried with water similar to Ritchie et al. (1995)). Outlet air, which was saturated with that organic chemical, was introduced to the ELAB through a sparger located in the base of the riser. When the water in the ELAB was saturated with the VOC, the gas stream was switched to pure air, and the desorption part of the experiment was started. This procedure was performed both with and without the packing installed in the riser section of the ELAB. Since a stationary, ordinary sparger was used in the ELAB with hole diameters equal to 1.6 mm, air inlet pressures were small, less than 0.48×10^5 Pa gauge for the maximum gas superficial velocity of 0.0116 m/s. All experiments were carried out at room temperature (23 ± 2 ºC) and pressure (mean value of 0.932×10^5 Pa).

At all gas superficial velocities, gas holdup was measured within ± 5% by measuring the increase in the liquid level in the riser section of the ELAB after introducing the air to the column. The liquid surface tension was measured using the capillary tube method. A capillary tube with 2 mm inside diameter and a traveling telescope were used for this purpose. Using pure water as a standard fluid with known surface tension (72 dynes/cm), the method demonstrated ± 2% error.

6.4 Model

Hydrodynamic equations previously achieved for the same ELAB (Nikakhtari and Hill, 2005b) were used in this study.

Gas holdups:

$$\theta_{GR} = aJ_{GR}^{\ b} \tag{6.1}$$

$$a = 3.229 \quad ; \quad b = 1.016 \quad \text{.. without packed bed} \tag{6.2}$$

$$a = 1.180 \quad ; \quad b = 0.743 \quad \text{.. with packed bed} \tag{6.3}$$

To determine the liquid velocity in the riser section:

$$U_{LR} = C_F E \tag{6.4}$$

where E is the gas holdup driving force for liquid circulation, given by:

$$E = \left(\frac{\theta_{GR}}{(1-\theta_{GR})^{-2} + (A_R / A_D)^2}\right)^{0.92} \tag{6.5}$$

and C_F is the friction resistance for liquid flow:

$$C_F = 48.9 \quad \text{.. without packed bed} \tag{6.6}$$

$$C_F = 10.8 \quad \text{.. with packed bed} \tag{6.7}$$

The axial mixing in the ELAB is evaluated using the Bodenstein number:

$$Bo = U_{LR} L / D \tag{6.8}$$

The Bodenstein number was reported by Fraser and Hill (1994) to be 47 in a similar ELAB without a packing. In the presence of packing, Meng et al. (2002) indicated that the Bodenstein number depends on packing porosity and is 45.5 for a porosity value of 0.990 as used in this study.

Two partial differential equations can be written to predict VOC concentration over time and position in the gas and liquid phases during mass transfer between these two phases:

$$\frac{\partial c}{\partial t} = D\frac{\partial^2 c}{\partial z^2} - U_{LR}\frac{\partial c}{\partial z} + K_L a(c^* - c) \tag{6.9}$$

$$\frac{\partial y}{\partial t} = -U_{GR}\frac{\partial y}{\partial z} - K_L a\frac{1-\theta_{GR}}{\theta_{GR}}(c^* - c) \tag{6.10}$$

The reason for using overall mass transfer coefficients in these equations is that the mass transfer coefficient of VOCs in the air is much higher than their mass transfer coefficient in water, and the liquid phase is the controlling step for the whole mass transfer process. Hydrodynamic variables needed to solve Equations 6.9 and 6.10 were calculated using Equations 6.1 to 6.8. Flow and dispersion in the radial and angular directions are assumed to be negligible and the gas phase is assumed to flow in a plug pattern. The VOC concentration in the liquid phase at the air interface (c^*) is related to the bulk air phase VOC concentration according to Henry's law:

$$y = Hc^* \tag{6.11}$$

Equations 6.9 and 6.10 are linear partial differential equations and were solved simultaneously using Matlab® by numerical finite differencing (forward differencing for time and central and backward differencing for the space dimension in Equations 6.9 and 6.10, respectively). The finite difference solving procedure and equations were similar to those used for oxygen and have been explained previously (Nikakhtari and Hill, 2005a and b). The boundary condition for the gas phase is at the inlet of the riser section and is equal to inlet air concentration which was experimentally measured and therefore known. Before starting the experiment, no mass transfer occurs between the gas and liquid phases, so the initial concentration of the gas phase in the bioreactor can be assumed to be in equilibrium with the liquid phase. Pure water was used at the beginning, so the initial concentration of VOCs in the liquid phase is zero. Boundary conditions for the liquid occur at the inlet and outlet of the riser. Inlet liquid to the riser was assumed to have the same VOC concentration as the outlet liquid from the riser but with a time delay, $t_{Delay,}$ because the downcomer acts as a time delay component. There are no air bubbles in the downcomer, and therefore no mass transfer occurs there. The value of t_{Delay} is determined by:

$$t_{Delay} = H_D / J_{LD} \tag{6.12}$$

$$J_{LD} = J_{LR} A_R / A_D \tag{6.13}$$

6.5 Results and Discussion

The concentrations of toluene, benzene, and phenol in the inlet air to the ELAB were measured at air superficial velocities from 0.0075 to 0.0106 m/s. In this velocity range, the concentrations of all VOCs in the inlet gas were found to be independent of the gas superficial velocity and equal to the VOCs saturated concentration in the air at room temperature. These concentrations and some other specifications of VOCs are shown in Table 6.2.

Figure 6.2a compares the model (Equation 6.9) to experimental data for liquid phase VOC concentration versus time from one of the absorption experiments of benzene at a gas superficial velocity of 7.13×10^{-3} m/s in the ELAB with a packed bed. This typical figure shows that the model is able to accurately predict concentration changes at the top of the riser section over time. Figure 6.2b shows the same results in the first 150 s. It can be seen that the model follows the cyclic changes of benzene concentrations during early times, which are caused by liquid recirculation through the downcomer. These oscillations damp out after a few circulations, once the supply of unaerated liquid in the downcomer becomes homogeneous with the riser liquid. Benzene concentrations in the air phase leaving the ELAB were measured for some of the experiments, one of which is shown in Figure 6.3 for the desorption experiment at the gas superficial velocity of 7.13×10^{-3} m/s in the ELAB with a packed bed. It is seen that model (Equation 6.10) is also able to predict the dynamic change of benzene concentrations in the air phase leaving the ELAB.

The mass transfer model (Equations 6.9 and 6.10) was fit to the experimental data to determine the mass transfer coefficient for each experiment. Figure 6.4 compares the mass transfer coefficients over a range of gas superficial velocities both with and without a packed bed. Four complete replications of the toluene absorption experiment in the ELAB without a packed bed at the gas superficial velocity of 0.0084 m/s resulted in a mean $K_L a$ of 0.0030 s^{-1} with a standard error of ±0.0002. By adding a packed bed, the mean $K_L a$ increased to 0.0044 s^{-1} with a standard error of ±0.0004. Based on the t-test with 95% confidence interval, the mean values can be considered significantly different. In convective mass transfer, the overall mass transfer coefficient is correlated

with the velocity by a power function (Chao et al., 1998; Fang and Lin, 1986; Welty et al., 2001):

$$K_L a = a J_{GR}^{\ b} \tag{6.14}$$

Parameters (a and b) and coefficient of determinations of this equation are reported in Table 6.3 for all conditions. The best fit lines are shown in Figure 6.4. It is noticeable that the mass transfer coefficients of both toluene and benzene were higher during their absorption than their desorption experiments. The reason for this is discussed later in the mechanism section.

Figure 6.4 shows that the mass transfer coefficients measured with packing were higher than those measured without packing for both absorption and desorption processes in the range of gas superficial velocities investigated. By inserting a small amount of woven packing (99.0% porosity) in the riser section of the ELAB, the gas holdup was increased and the gas bubble size was decreased. These factors contributed to increased mass transfer area, and therefore an increase in the volumetric mass transfer coefficients. The toluene volumetric mass transfer coefficient increased on average 60% for absorption and 71% for desorption processes. Similarly, the benzene volumetric mass transfer coefficients increased on average 24% for absorption and 43% for desorption processes. These percentages are less than reported earlier for the increase in oxygen mass transfer coefficient in the same ELAB with the same packed bed, which was 245% (Nikakhtari and Hill, 2005b). However, this still represents significant increases in the mass transfer coefficients when a small amount of mesh packing is added to the ELAB.

Figure 6.4 demonstrates that in most of the cases (toluene desorption and benzene absorption and desorption) adding packing to the ELAB enhances mass transfer coefficient more effectively at the higher than lower gas superficial velocities, which is similar to what was observed for oxygen mass transfer (Nikakhtari and Hill, 2005b). Mass transfer coefficients showed an average increase of 24.2% at J_{GR} = 0.002 m/s, whereas 54.0% at J_{GR} = 0.010 m/s for benzene absorption and desorption and toluene desorption cases. It has been reported that an increase in gas flow rate (or gas superficial velocity) increases the number of produced bubbles, but does not affect bubble diameters (Perry and Green, 1999). However, there are more chances for bubbles to

coalesce during flow in the column when there are more bubbles. Therefore, at the higher gas superficial velocities there are larger bubbles in the column, a fact experimentally observed and reported by others (Tuteja et al., 1992). The reason for greater mass transfer improvements at higher gas superficial velocities when packing is added is that it breaks down these larger coalesced gas bubbles. The benefits of adding packing are better realized at higher rather than lower gas superficial velocities.

The results for benzene desorption mass transfer coefficient is in reasonable agreement with those found by others in a stirred tank reactor (Fang and Lin, 1986). Chao et al. (1998) have reported mass transfer coefficients for toluene desorption in a packed column with 0.406 m height and 0.095 m inside diameter, using different sizes of sand packing (coarse sand, 1.709 mm; medium sand, 0.398 mm; fine sand, 0.278 mm). Figure 6.5 compares their reported toluene mass transfer coefficients using fine sand packing with our achieved mass transfer coefficients for toluene desorption in the ELAB with a packed bed over a range of gas superficial velocities. A small amount of woven packing (99.0% porosity) has increased the mass transfer coefficient the same as the fine sand bed with presumably far less resistance to flow due to the much higher porosity.

6.5.1 Mechanism

In a previous work, we reported differences in the formation of air bubbles in the ELAB with and without a packed bed. Without packing, air bubbles were non-uniform and reached a maximum diameter of 30 mm. In the ELAB with a packed bed, the air bubbles were more uniform in size, and reached a maximum diameter of 9 mm (Nikakhtari and Hill, 2005b). In this work, we report that the diameter of air bubbles observed in pure water were larger than those observed in water saturated with benzene or toluene. Without packing, bubbles in the water saturated with benzene or toluene reached a maximum diameter of 17 mm. Figure 6.6 shows photographs of air bubbles at the air superficial velocity of 0.004 m/s in the ELAB with and without a packed bed, and in the ELAB without a packed bed but with saturated benzene solution. It is clear that the packing causes a large decrease in bubble size, but the benzene saturated water also contributes to decreased bubble sizes. Grund et al. (1992) have also reported a decrease of bubble sizes and increase of interfacial area in the presence of organic chemicals such

as toluene in the water phase. This decrease in the bubble size is due to decrease of the water surface tension in the presence of these organic chemicals. Surface tension of saturated toluene and benzene solutions were measured to be 0.0402 and 0.0394 N/m respectively (the surface tension of pure water is 0.072 N/m). The surface tensions of saturated toluene and benzene solutions are almost the same, so they result in similar decrease in bubble sizes. Direct dependence of gas bubble diameter with liquid surface tension has been reported to be a power function with an exponent of 0.33 for a single bubble-single orifice system (Perry and Green, 1999) and 0.4 (practical) to 0.6 (theoretical) for an agitated vessel with non-viscous liquids (Hu et al., 2003).

This decrease in bubble size in the saturated solutions causes an increase in the gas holdup due to the slower rising velocity for smaller gas bubbles. Lower rising velocities for smaller bubbles and increased gas holdup in organic chemical solutions, like toluene, in bubble columns has already been reported (Grund et al., 1992). Gas holdups in the saturated toluene solution in the ELAB with and without a packed bed were measured over a wide range of gas superficial velocities, and are shown in Figure 6.7. Gas holdups in the ELAB with and without a packed bed are also shown in this figure (Nikakhtari and Hill, 2005b). Using a packing in the riser section of the ELAB causes an average increase of 46.4% in the gas holdup (Nikakhtari and Hill, 2005b), and saturation of the water with toluene causes an average increase of 27.1% in the gas holdup, which is less than the effect of the packed bed. The effect of inserting packing in the ELAB in a saturated toluene solution is not as effective as in water. In a saturated toluene solution, the packing causes an 18.3% increase in the gas holdup. The saturated benzene solution had identical gas holdups as that observed with saturated toluene. Power functions that were used earlier for gas holdup in the ELAB can be used to correlate the gas holdup in the saturated toluene solution:

$$\theta_{GR} = 2.14 J_{GR}^{0.886} \quad ; \quad R^2 = 0.998 \quad \text{without packing} \qquad (6.15)$$

$$\theta_{GR} = 1.43 J_{GR}^{0.745} \quad ; \quad R^2 = 0.999 \quad \text{with packing} \qquad (6.16)$$

The trend in bubble sizes during absorption and desorption experiments are shown schematically in Figure 6.8. The change in surface tension means that during absorption, air bubble diameters decrease over the experiment, as the water phase gets saturated with the organic chemical. In contrast, during a desorption experiment, air

bubble diameters increase over the experiment, as the water phase gets stripped of the organic chemical. As a result, in an absorption experiment, there are smaller bubbles with higher gas holdups towards the end of the process when the driving force for mass transfer (concentration difference) is low. These two effects compensate each other and the overall mass transfer rate stays high. However, in a desorption experiment, there are larger bubbles with less gas holdup towards the end of the experiment when the driving force for mass transfer is low. These two effects amplify each other and the mass transfer rate decreases.

Inserting packing in the ELAB caused a significant decrease in the bubble sizes in the case of oxygen experiments. However, in toluene or benzene experiments, bubble sizes have already been decreased due to presence of these organic chemicals in the water. The magnitude of reduction in bubble size caused by inserting packing in the ELAB is less than that realized in the pure water (oxygen) case. Burns and Zhang (2001) also noted that a reduction in bubble size due to decrease in interfacial tension dominated the effect of packing (silica beads in their case). In our study, the effect of packing is higher for desorption than absorption in both toluene and benzene experiments, but was still significant even in the saturated solutions.

According to Lo and Hwang, mass transfer coefficients of VOCs can be predicted by knowing the mass transfer coefficient of oxygen and using penetration theory (Lo and Hwang, 2004):

$$\frac{k_{Li}}{k_{Lo}} = \sqrt{\frac{D_{Li}}{D_{Lo}}} \tag{6.17}$$

However, they have assumed equal mass transfer area and exposure time for oxygen and VOCs under the same hydrodynamic conditions. Here, we showed that the mass transfer area and exposure time cannot be assumed the same for different species due to different bubble sizes and gas holdups in the presence of different species. Comparing mass transfer coefficients of toluene or benzene with oxygen using penetration theory did not give reasonable results. However, comparing the mass transfer coefficients of toluene with benzene did due to similar surface tensions. In this case, the average ratio of benzene K_La to toluene K_La has only 7.5% deviation from penetration theory:

Penetration theory: $\frac{K_{L,Benzene}a}{K_{L,toluene}a} = 1.06$

Experimental ratio found in this work: $\frac{K_{L,Benzene}a}{K_{L,toluene}a} = 1.14$

The average mass transfer coefficient ratio of oxygen to toluene was found to be 3.11, which does not match with the result from the penetration theory (1.58), but is close to 3.33 that has been reported by Cesario et al. for the same mass transfers into pure water in a stirred reactor (Cesario et al., 1997). Lau et al. (2004) have also mentioned the influence of liquid properties, such as viscosity and surface tension, on the k_L part of the volumetric mass transfer coefficient.

6.5.2 Comparison of the model with simpler models

Assumptions of $D = 0$, and $U_{LR} = 0$ in Equation 6.9; and the assumption of constant concentration for the gas phase equal to the inlet gas concentration converts the transient, spatial model to that of a completely mixed reactor. As noted earlier during a study on the oxygen mass transfer (Nikakhtari and Hill, 2005b), the assumption of the ELAB as a completely mixed reactor causes an underestimation of the mass transfer coefficient equal to 64.5% of that determined using Equations 6.9 and 6.10. The low mass transfer coefficients determined using well-mixed theory is due to significant changes in the gas phase concentration which can be seen in Figure 6.9. The benzene concentration in the air phase in the ELAB with a packed bed during an absorption experiment at a gas superficial velocity of 7.13×10^{-3} m/s drops 86.0%, which shows up in the outlet air stream in the early seconds after starting the experiment. The assumption of a distributed liquid phase concentration (Equation 6.9) alongside a constant gas phase concentration, equal to the inlet gas concentration, caused a 43.9% underestimation in the mass transfer coefficient. The assumption of an axial dispersion coefficient (D) equal to zero resulted in a 34.6% underestimation in the mass transfer coefficient. These two latter assumptions had given acceptable results in the oxygen mass transfer study (Nikakhtari and Hill, 2005b), which was due to the negligible changes in gas phase oxygen concentrations. It is interesting that considering the ELAB as a mixed reactor (a common assumption to predict mass transfer coefficients in the ELAB) or other

simplifying assumptions that were reasonable for the oxygen mass transfer study can not be used for VOCs mass transfer studies in the ELAB. Only the full distributed model (Equation 6.9 and 6.10) gives accurate results for determining the volumetric mass transfer coefficients of VOCs.

6.5.3 Phenol experiments

Phenol has a small Henry's coefficient, low air phase saturated concentration (see Table 6.2), and is highly soluble in water (80.19 g/L at 25 ^{o}C (Yaws, 1999)). Therefore, its absorption or desorption occurs very fast in the lower section of the column. The finite differencing simulation required very small space and time steps to be stable in this case. In order to achieve a solution, space steps started with a very small value and were gradually increased to reduce computer time to a reasonable value. Even then, fitting the model to the experimental data was found to be insensitive to the mass transfer coefficient.

Figure 6.10a shows the absorption process of phenol in the ELAB predicted by the full distributed model. It can be seen that mass transfer of organic chemicals with a very low Henry's coefficient (like phenol) occur right after their entrance to the column, and in the rest of the column their concentration stays constant. This can be compared with absorption of benzene over the same time period in Figure 6.10b. For benzene there is a concentration distribution over the full height of the column, which depends on the mass transfer coefficient. On the other hand, for phenol, the bulk liquid concentration increases over time due to accumulation of all the phenol in the liquid phase during the absorption process. Mass transfer is not the controlling step in this process, and the model fits the experimental data with many chosen values of the volumetric mass transfer coefficient. Assuming the ELAB as a completely stirred reactor gives completely wrong and very small values for phenol mass transfer coefficients.

6.6 Conclusion

By fitting experimental data to a full, mechanistic model in an ELAB both with and without a packed bed in the riser section, the mass transfer coefficients of toluene and benzene were found over a wide range of gas superficial velocities. Using a small amount of packing (99.0% porosity), VOC mass transfer coefficients were increased by an average of 65.1% for toluene and 33.8% for benzene. Desorption of VOCs was slower than absorption due to variation of bubble sizes caused by surface tension changes during the mass transfer experiments. The ELAB with a small amount of packing is a novel bioreactor with much higher mass transfer rates due to increased gas holdup and small bubble diameters. The packing surface area can also be used for cell immobilization, and therefore has potential to greatly enhance gas-liquid fermentations and other gas-liquid biochemical operations. In that case, VOC mass transfer rate may be affected by the presence of bacteria and biofilm in the ELAB. It was shown that only the full, mechanistic mathematical model is an accurate method to determine K_La for VOC absorption in ELABs with low liquid circulation rates, as compared to models assuming well-mixed conditions.

6.7 Nomenclature

A_D Downcomer cross-sectional area (m^2)

A_R Riser cross-sectional area (m^2)

Bo Bodenstein number

c VOC concentration in the liquid phase (g/L)

c^* Equilibrium VOC concentration (g/L)

C_F Friction loss variable (m/s, Equation 6.4)

D Axial dispersion coefficient (m^2/s)

D_L Liquid phase diffusivity (m^2/s)

E Gas holdup function (Equation 6.5)

H Dimensionless Henry's law coefficient

H_D Length of the downcomer, includes all horizontal connections and elbows (m)

J_{GR} Gas superficial velocity in the riser section (m/s)

J_{LD} Liquid superficial velocity in the downcomer section (m/s)

J_{LR} Liquid superficial velocity in the riser section (m/s)

K_La Overall volumetric mass transfer coefficient (s^{-1})

k_L Mass transfer coefficient

L Length of the circulation loop (m)

t Time (s)

t_{Delay} Delay time in the downcomer (s)

U_{GR} Gas velocity in the riser section (m/s)

U_{LR} Liquid velocity in the riser section (m/s)

V Bioreactor volume (m^3)

y VOC concentration in the gas phase (g/L)

z Axial distance up the riser section (m)

θ_{GR} Gas holdup

6.8 References

Burns, S. E.; Zhang, M. Effect of System Parameters on the Physical Characteristics of Bubbles Produced Through Air Sparging. *Environ. Sci. Technol.* **2001**, *35*, 204.

Cesario, M. T.; de Wit, H. L.; Tramper, J.; Beeftink, H. H. Dispersed Organic Solvent to Enhance the Overall Gas/Water Mass Transfer Coefficient of Apolar Compounds in the biological Waste-Gas Treatment. Modeling and Evaluation. *Biotechnol. Prog.* **1997**, *13*, 399.

Chao, K. P.; Ong, S. K.; Protopapas, A. Water-to-Air Transfer of VOCs: Laboratory-Scale Air Sparging System. *J. Environ. Eng.* **1998**, *124*, 1054.

Fang, C. S.; Lin, J. H. Mass Transfer of Benzene in Air Stripping and Aeration. *AIChE National Meeting, New Orleans, LA.* **1986**, 1.

Fraser, R. D.; Ritchie, B. J.; Hill, G. A. Dynamic Mixing and Oxygen Transfer in Small, Airlift Loop Bioreactors: Model and Experimental Verification. *Biotechnol. Prog.* **1994**, *10*, 543.

Grund, G.; Schumpe, A.; Deckwer, W. D. Gas-Liquid Mass Transfer in a Bubble Column with Organic Liquids. *Chem. Eng. Sci.* **1992**, *47*, 3509.

Harding, R. C.; Hill, G. A.; Lin, Y.-H. Bioremediation of Toluene Contaminated Air Using an External Loop Airlift Bioreactor. *J. Chem. Technol. Biotechnol.* **2003**, *78*, 406.

Hu, B.; Nienow, A. W.; Pacek, A. W. The Effect of Sodium Caseinate Concentration and Processing Conditions on Bubble Sizes and Their Break-up and Coalescence in Turbulent, Batch Air/Aqueous Dispersions at Atmospheric and Elevated Pressures. *Colloids Surf., B.* **2003**, *31*, 3.

Lau, R.; Peng, W.; Velazquez-Vargas, L. G.; Yang, G. Q.; Fan, L.-S. Gas-Liquid Mass Transfer in High-Pressure Bubble Columns. *Ind. Eng. Chem. Res.* **2004**, *43*, 1302.

Lo, C.-S.; Hwang, S.-J. Dynamic behavior of an Internal-Loop Airlift Bioreactor for Degradation of Waste Gas Containing Toluene. *Chem. Eng. Sci.* **2004**, *59*, 4517.

Meng, A. X.; Hill, G. A.; Dalai, A. K. Hydrodynamic Characteristics in an External Loop Airlift Bioreactor Containing a Spinning Sparger and a Packed Bed. *Ind. Eng. Chem. Res.* **2002**, *41*, 2124.

Nikakhtari, H.; Hill G. A. Enhanced Oxygen Mass Transfer in an External Loop Airlift Bioreactor Using a Packed Bed. *Ind. Eng. Chem. Res.* **2005a**, *44*, 1067.

Nikakhtari, H.; Hill G. A. Hydrodynamic and Oxygen Mass Transfer in an External Loop Airlift Bioreactor with a Packed Bed. *Biochem. Eng. J.* **2005b**, *27*, 138.

Perry, R.H.; Green, D.W. Perry's Chemical Engineer's Handbook; McGraw-Hill: New York 1999.

Ritchie, B. J.; Hill, G. A. Biodegradation of Phenol Polluted Air Using an External Loop Airlift Bioreactor. *J. Chem. Technol. Biotechnol*. **1995**, *62*, 339.

Sarti, A.; Vieira, L.G.T.; Foresti, E.; Zaiat, M. Influence of the Liquid-Phase Mass Transfer on the Performance of a Packed-Bed Bioreactor for Wastewater Treatment, *Bioresource Technol.* **2001**, *78*, 231.

Tuteja, R. K.; Liu, Q.; Siefken, T. C.; Misra, V. N. Bubble Size Measurement in a Flotation Column. *Extractive Metallurgy of Gold and Base Metals Confrence*. **1992**, 231.

Wei, V. Q.; Hill, G. A.; Macdonald, D. G. Bioremediation of Contaminated Air Using an External-Loop Airlift Bioreactor. *Can. J. Chem. Eng.* **1999**, *77*, 955.

Welty, J. R.; Wicks, C. E.; Wilson, R. E. Fundamentals of momentum, heat, and mass transfer; John Wiley: New York, 2001, pp 576 - 579.

Yaws, C. L. Chemical Properties Handbook; McGraw-Hill: New York, 1999.

Table 6.1 Specifications of the ELAB and packing.

Riser section diameter, mm	89
Riser cross-sectional area (A_R), m^2	6.22×10^{-3}
Downcomer section diameter, mm	47
Downcomer cross-sectional area (A_D), m^2	1.74×10^{-3}
Liquid height above the sparger, m	1.42
Liquid volume, m^3	1.2×10^{-2}
Loop length, m	3.20
Downcomer length, including elbows (H_D), m	1.61
Number of orifices in sparger	6
Orifice diameter, mm	1.6
Packing metal	Stainless Steel
Packing density, kg/m^3	5139.3
Packing fiber diameter, m	4.6×10^{-4}
Packing weight, kg	0.399
Packing height, m	1.2
Packing porosity, %	98.96

Table 6.2 Properties of VOCs and Oxygen.

VOC or Oxygen	Concentration in the inlet gas	Diffusion coefficient in water, Wilke Chang correlation (Welty et al., 2001)	Henry's coefficient at 25 ^{o}C (Yaws, 1999)	Spectrophotometer wave length
	(g/L)	(D_L, m^2/s)	(H, $atm \cdot m^3/mol$)	(nm)
Toluene	0.150	9.6×10^{-10}	6.3522×10^{-3}	214
Benzene	0.350	1.1×10^{-9}	5.5486×10^{-3}	253
Phenol	0.0008	1.0×10^{-9}	7.5958×10^{-7}	273
Oxygen	0.273	2.4×10^{-9}	0.874	___

Table 6.3 Parameters and coefficient of determinations of Equation 6.14 for different operating conditions.

Organic Chemical	ELAB	Process	a	b	R^2
Toluene	without a packed bed	absorption	0.108	0.746	0.973
		desorption	0.075	0.970	0.999
	with a packed bed	absorption	0.060	0.542	0.998
		desorption	0.182	1.038	0.997
Benzene	without a packed bed	absorption	0.235	0.919	0.979
		desorption	0.091	0.912	0.983
	with a packed bed	absorption	0.722	1.101	0.986
		desorption	0.311	1.088	0.964

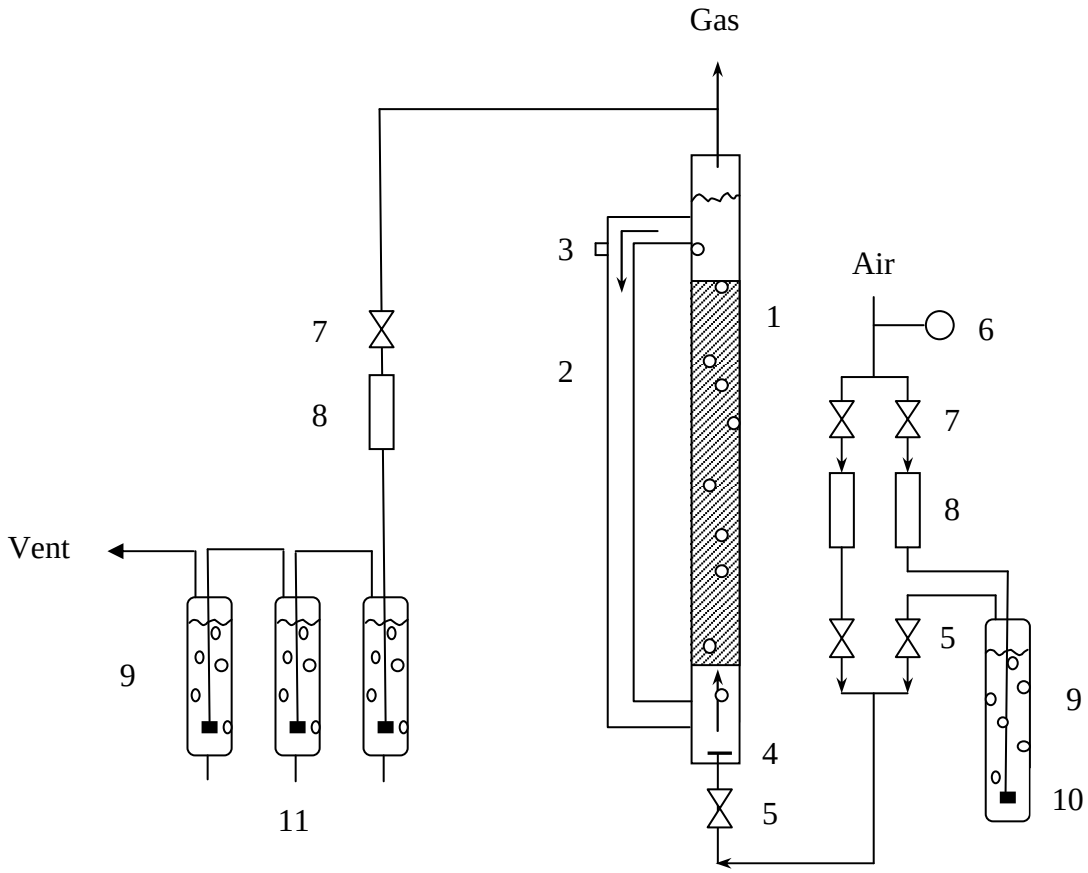

1- Riser section with packing
2- Downcomer section
3- Sampling port
4- Gas sparger
5- Two-way valve
6- Pressure gage
7- Adjusting valve
8- Flow meter
9- Bubbler
10- Sparger
11- Sampling valve

Figure 6.1 Schematic of the External Loop Airlift Bioreactor.

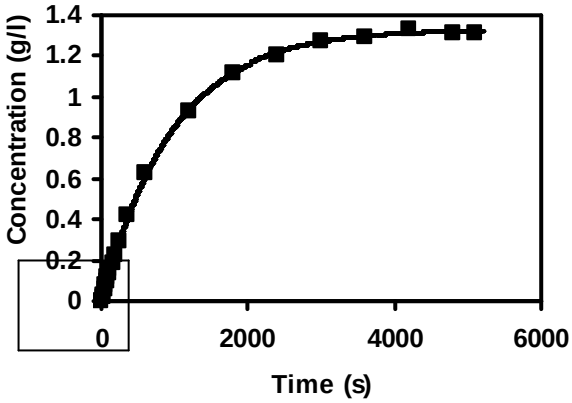

(a)

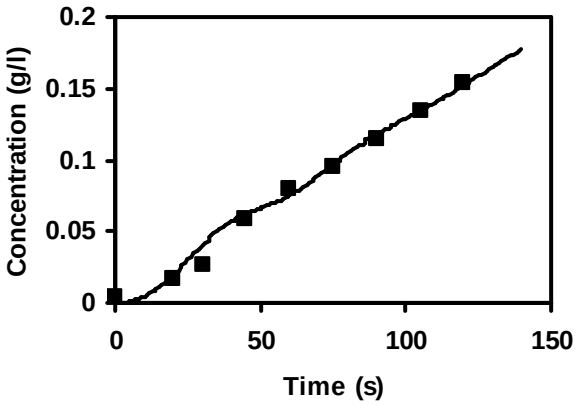

(b)

Figure 6.2 Comparison of the mechanistic mass transfer model (Equation 6.9) to experimental data of benzene absorption in water in the ELAB with packing at the gas superficial velocity of 7.13×10^{-3} m/s: (a) in first 6000 s, (b) in first 150 seconds.

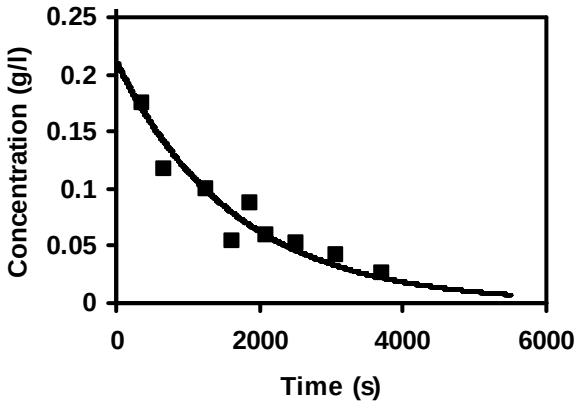

Figure 6.3 Comparison of the mechanistic mass transfer model (Equation 6.10) to experimental data of the gas phase concentrations during benzene desorption in the ELAB with packing at the gas superficial velocity of 7.13×10^{-3} m/s.

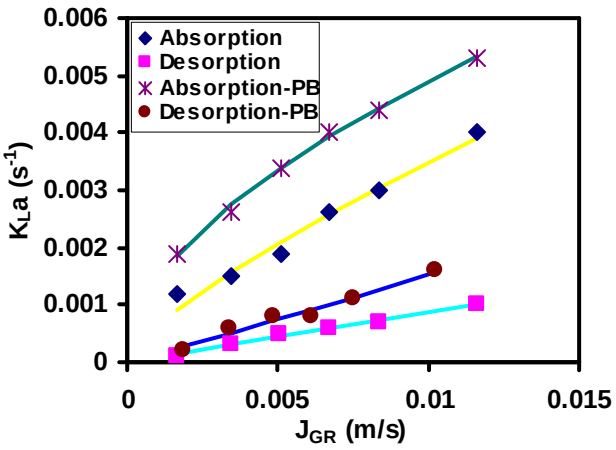

(a)

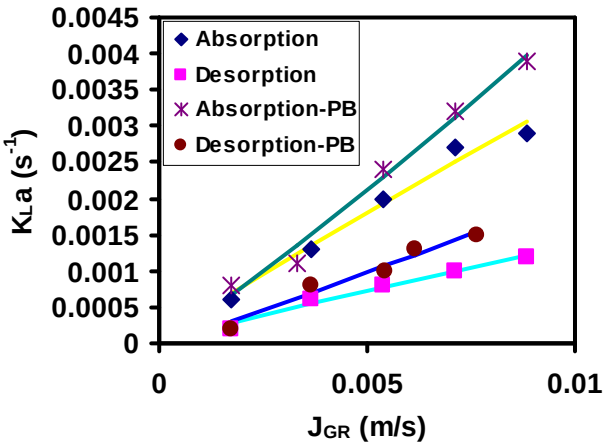

(b)

Figure 6.4 Volumetric mass transfer coefficients for absorption and desorption processes in the ELAB with and without a packed bed at various superficial gas velocities: (a) toluene, (b) benzene (Solid lines represent the model according to Table 6.3).

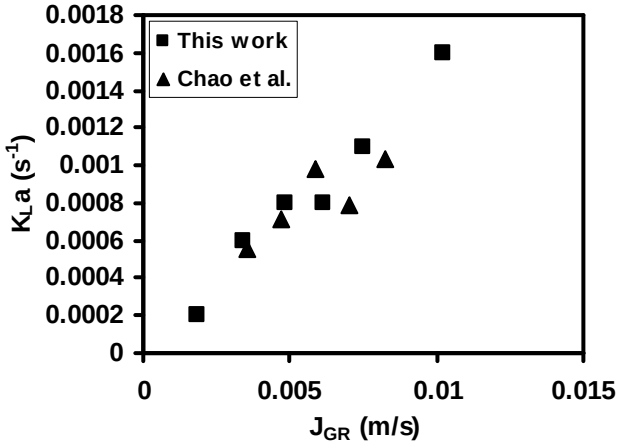

Figure 6.5 Comparison of Chao et al. (1998)'s results with results of this work for toluene desorption from water to air.

(a)

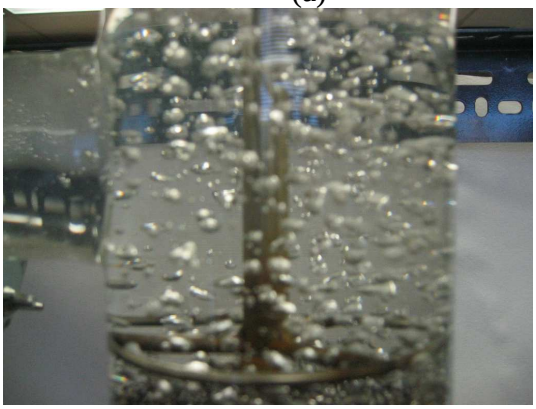

(b)

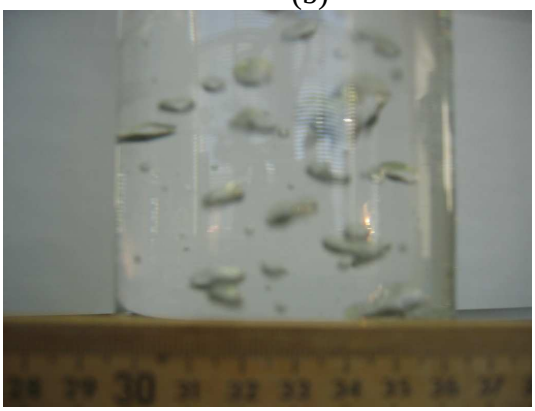

(c)

Figure 6.6 Photographs of air bubbles in the top of the ELAB at a gas superficial velocity of 0.004 m/s, (a) without packing, (b) with packing, (c) without packing through saturated benzene solution.

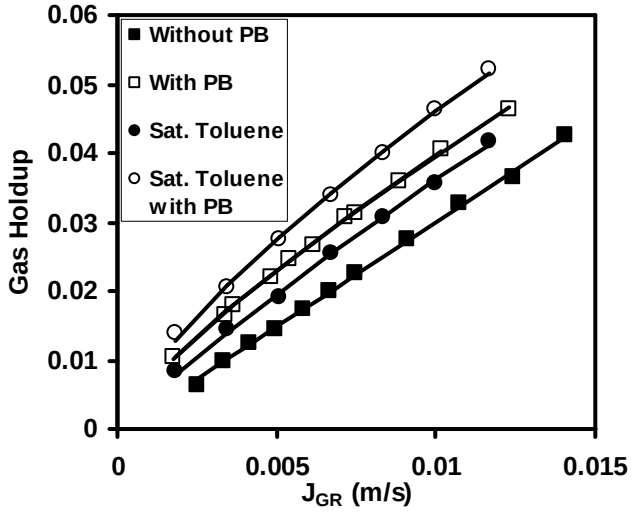

Figure 6.7 Effect of gas superficial velocities and toluene saturation on the gas holdup in the ELAB with and without a packed bed (Solid lines represent equations that were fit for each case: Equations 6.2, 6.3, 6.15, and 6.16).

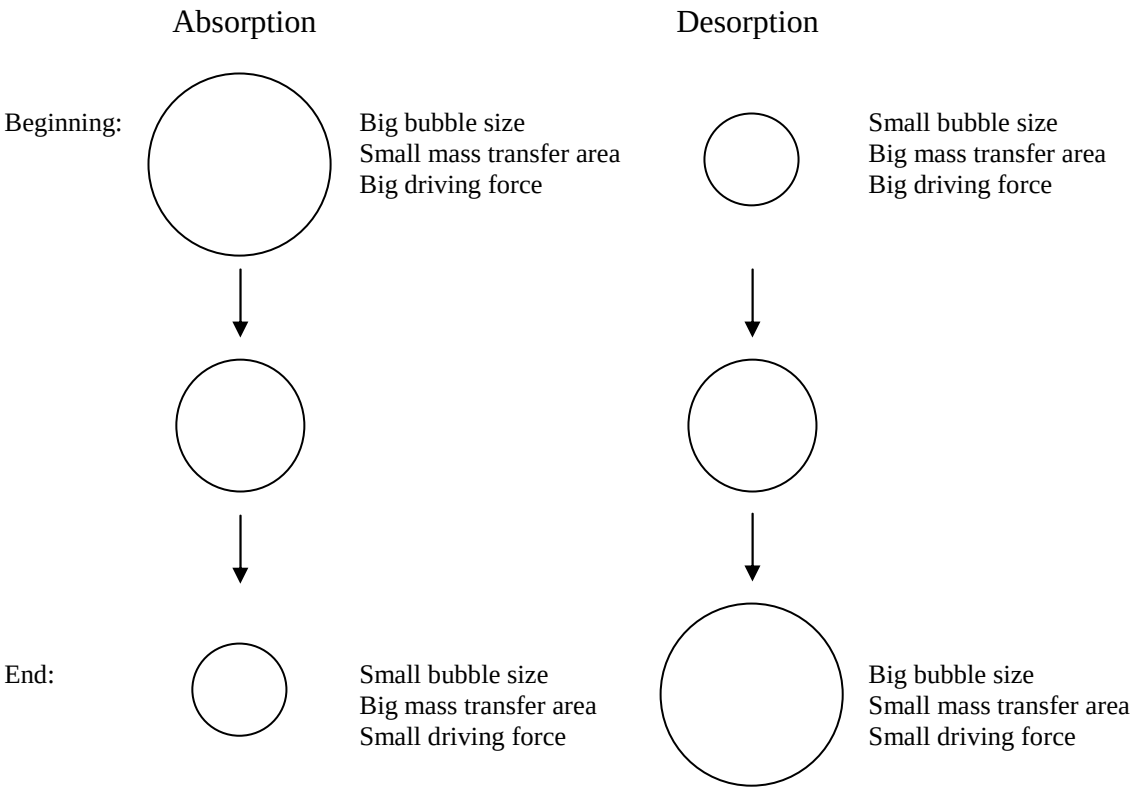

Figure 6.8 Schematic drawing of variation of bubble size during absorption or desorption.

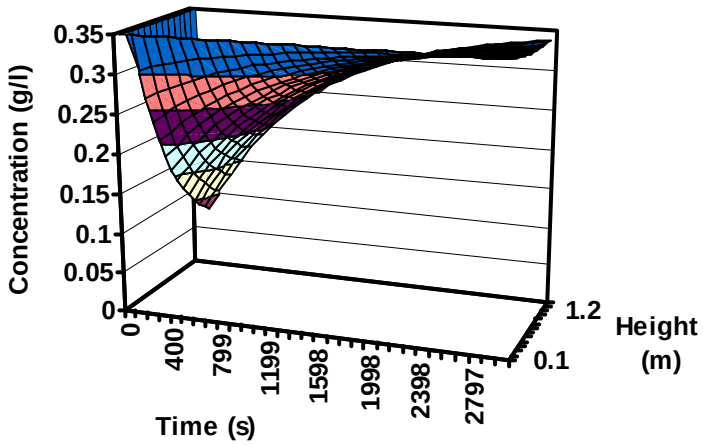

Figure 6.9 Variation of the benzene concentration in the air phase over time and height, during absorption in the ELAB with a packed bed at a gas superficial velocity of 7.13 × 10^{-3} m/s.

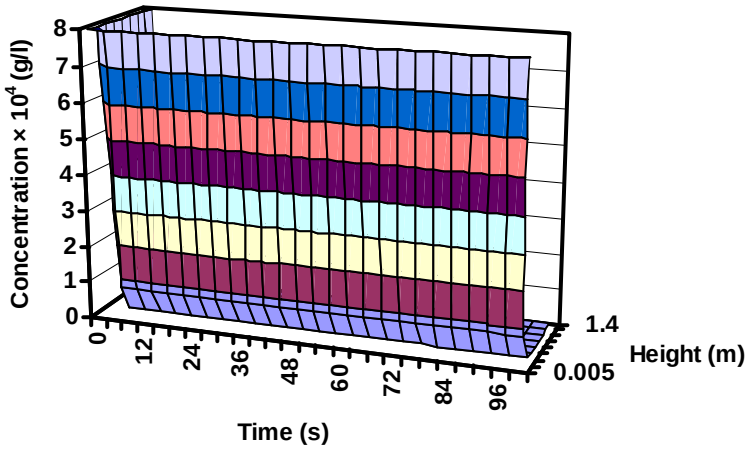

(a)

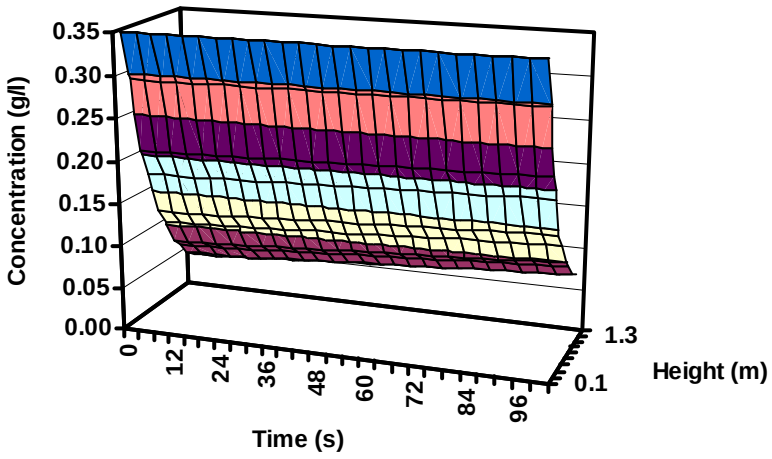

(b)

Figure 6.10 Concentration variation in the gas phase in the ELAB without packing during an absorption process, (a) phenol, (b) benzene.

Chapter 7 - Continuous Bioremediation of Phenol Polluted Air in an External Loop Airlift Bioreactor with a Packed Bed

A brief version of this chapter has been published in the proceedings of the **Congress on Biotechniques for Air Pollution Control**, and a similar version to the present chapter has been copyrighted and accepted for publication in the **Journal of Chemical Technology and Biotechnology**:

Nikakhtari, H.; Hill, G. A. Continuous Bioremediation of Phenol Polluted Air in an External Loop Airlift Bioreactor with a Packed Bed. Proceedings of the Congress on Biotechniques for Air Pollution Control, La Coruna, Spain, 2005.

Nikakhtari, H.; Hill, G. A. Continuous Bioremediation of Phenol Polluted Air in an External Loop Airlift Bioreactor with a Packed Bed. *J. Chem. Technol. Biotechnol.* Accepted in Nov. 2005.

Contribution of the PhD candidate

Experiments were planned by Hossein Nikakhtari and Gordon A. Hill, and were performed by Hossein Nikakhtari. Modeling and computer program development were by Hossein Nikakhtari with advice from Gordon A. Hill. All written text of the submitted paper was created by Hossein Nikakhtari with Gordon Hill providing editorial guidance.

Contribution of this chapter to the overall study

As mentioned, the idea of this project was inserting a packed bed in the riser section of an ELAB and studying the enhancement of oxygen and VOCs mass transfer rates and the enhancement of the bioremediation process. In the previous chapters, effects of using a packed bed in the riser section of the ELAB on enhancement of oxygen and VOCs mass transfer rates were studied. In this chapter, the last and main

part of this project was accomplished: enhancement of phenol bioremediation using this new ELAB with a packed bed. The same modified ELAB with the stainless steel packing as described in the previous two chapters was used. The same hydrodynamic equations, introduced in the two previous chapters, were used in the modeling part of this chapter. An immobilized biofilm was developed on the stainless steel packing and was used for bioremediation of phenol from an artificially polluted air stream. It was shown that this new bioreactor increased the phenol bioremediation load to the highest reported value in the literature. A mathematical model to predict VOC concentrations in the ELAB was also developed.

Additional experimental details

The same ELAB with stainless steel packing as described in the previous two chapters was used in this chapter. A 50 L feed tank with a pump was used to feed medium to the ELAB continuously. The top of the column was sealed to be able to collect and analyze outlet air. A schematic drawing of the set up is shown in Figure 7.1. A photograph of the ELAB and feed pumps is shown in Figure 7.01a. Figure 7.01b shows a close up of the top part of the ELAB which was sealed. A photograph of the 50 L sterilized medium tank is shown in Figure 7.02. It was placed on top of a magnetic mixer to mix its contents continuously.

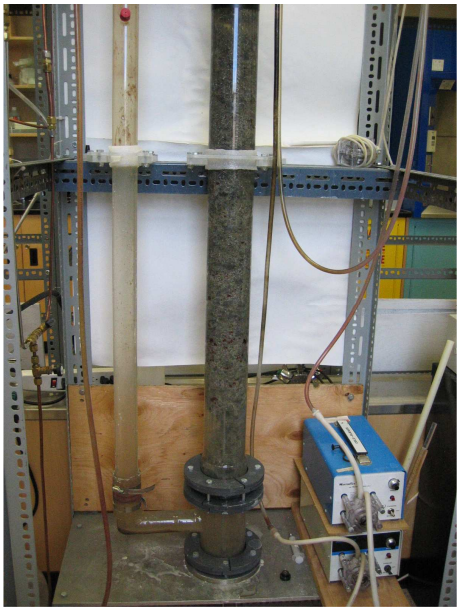

(a)

(b)

Figure 7.01 A photograph of (a) the ELAB and feed pumps, and (b) top of the ELAB.

Figure 7.02 A photograph of sterilized medium tank.

7.1 Abstract

An External Loop Airlift Bioreactor with a small amount (99% porosity) of stainless steel mesh packing inserted in the riser section was used for bioremediation of a phenol polluted air stream. The packing enhanced VOC and oxygen mass transfer rates and provided a large surface area for cell immobilization. Using a pure strain of *Pseudomonas putida*, fed-batch and continuous runs at three different dilution rates were completed with phenol in the polluted air as the only source of growth substrate. 100% phenol removal was achieved at phenol loading rates up to 33120 mg/h·m^3 using only one third of the column, superior to any previously reported biodegradation rates of phenol polluted air with 100% efficiency. A mathematical model has been developed and is shown to accurately predict the transient and steady state data.

Key words: Bioremediation, Phenol, Loop Bioreactor, Packed Bed Bioreactor, Biofilm, Air Pollution.

7.2 Introduction

For the past three decades, circulating loop airlift bioreactors have achieved increasing attention for treatment of contaminated air effluents. Applications have been reported for biodegradation of several air pollutants such as hexane (Oliveira and De Franca, 2005), ethyl acetate (Jianping et al., 2005), toluene (Loand and Hwang, 2004), and aromatic hydrocarbons (Edwards and Nirmalakhandan, 1999). The External Loop Airlift Bioreactor (ELAB) has a simple design, without any moving parts, and it provides sufficient mixing for slow microbial reactions. In the ELAB, a specific volatile organic chemical (VOC) may be completely degraded by a microorganism at normal temperature and pressure without producing a second polluted byproduct. We have

reported the use of the ELAB for bioremediation of hydrophilic (Ritchie and Hill, 1995; Wei et al., 1999) and hydrophobic (Harding et al., 2003) air pollutants. Ritchie and Hill (1995) reported on the bioremediation of phenol polluted air in an ELAB with a maximum phenol loading rate of 16200 mg/h·m^3. Biofilters, columns with packed beds of immobilized bacteria, are also widely used for air pollution treatments (Spigno et al., 2003; Delhomenie et al., 2003; Lim, 2001). Zilli et al. (1993) used a laboratory biofilter (total volume of 0.98 L) inoculated with two strains of *Pseudomonas putida* to continuously remove phenol from waste gases. They used an external pump for recirculation of liquid in the column and reported a maximum phenol elimination load of 124000 mg/h·m^3 with 93.1% efficiency. Zilli et al. (1996) later reported up to 730000 mg/h·m^3 phenol elimination load in a similar biofilter by using a high gas superficial velocity (0.128 m/s) but at the cost of a dramatic decrease in efficiency (24.58%). Remaining below the olfactory threshold phenol concentration in the outlet air (0.0002 mg/L), they achieved up to 42900 mg/h·m^3 elimination load.

In this work, we report on a novel improvement to the ELAB for bioremediation of phenol polluted air, the incorporation of a small quantity of packed bed in the riser section. A biofilm was fixed to the packing and greatly enhanced the biodegradation rate of phenol polluted air. The experimental data has been accurately modeled using a set of mechanistic, quasi-steady state equations.

7.3 Experimental

7.3.1 Microorganism and Media

Pseudomonas putida (ATCC 17484) was used for all microbial growth experiments. It was maintained on nutrient broth agar and stored at 4 °C. The growth media consisted of (mg in 1 L reverse osmosis water; analytical reagent grade chemicals, BDH, Toronto): K_2HPO_4, 750; KH_2PO_4, 840; $(NH_4)_2SO_4$, 474; NaCl, 60; $CaCl_2$, 60; $MgSO_4$, 60; $Fe(NH_4)SO_4$, 20; and 1 mL of trace mineral solution. The trace

mineral solution consisted of (mg in 1 L reverse osmosis water): $ZnSO_4.7H_2O$, 200; $MnCl_2$, 60; H_3BO_3, 600; $CoCl_2$, 400; $CuCl_2$, 20; $NiCl_2$, 40; Na_2MoO_4, 60. The pH of the media solution was 7.

7.3.2 Bioremediation procedure

The same ELAB that was used in earlier work for oxygen and VOC mass transfer studies (without any bioremediation experiments) was used in this study (Nikakhtari and Hill, 2005a and b). A schematic diagram of the ELAB with the packed bed is shown in Figure 7.1, and specifications of the ELAB and the stainless steel mesh packing are listed in Tables 7.1 and 7.2 respectively. Air was first passed through a gasifier with a height of 0.69 m and a diameter of 0.055 m, containing 1 liter of a saturated phenol solution containing phenol particles (130 g/L). The concentration of phenol in air exiting the gasifier was measured by introducing the stream to a series of two bubblers (0.5 m height and 0.05 m diameter, containing 0.7 L of water in each). As long as the second bubbler showed zero concentration of phenol, the accumulated concentration in the first bubbler was used to determine the phenol concentration in the air phase. Using this method, the phenol concentration in the air stream leaving the gasifier was found to remain at the saturated concentration at room temperature and pressure (0.80 ± 0.01 mg/L at 23 ºC and 0.932×10^5 Pa) over all the air flow rates used in this study. The outlet air from the gasifier was introduced to the ELAB through a sparger. For bioremediation experiments, the air flow rate was maintained by a calibrated rotameter at one of two flowrates, 9.23×10^{-5} and 1.38×10^{-4} m^3/s, which provided gas superficial velocities of 0.0148 and 0.0221 m/s in the riser section of the ELAB. The physical limitation of the gasifier limited the maximum air flow rate that could be used in this study. Fresh sterilized medium was pumped into the ELAB at the top and liquid was drained out of the bottom of the ELAB riser section to maintain a constant working liquid volume of 12 litres in the bioreactor. All experiments were carried out at room temperature (23 ± 2 ºC) and pressure (mean value of 0.932×10^5 Pa).

Several batch, shake flask cultures were performed to characterize the growth kinetics of the microorganism. Then one fed-batch run and three continuous runs at different dilution rates (0.05, 0.20, and 0.50 h^{-1}) were performed in the packed bed

ELAB. The conditions used for the lowest dilution rate were repeated for an extended duration to test the stability of the bioreactor. Finally an experiment at the highest possible gas flow rate was carried out to study the ability of the ELAB with a packed bed to remove a high phenol loading.

7.3.3 Biofilm development

A biofilm was first developed on the stainless steel mesh packing using a procedure developed by Wall and using 0.2% v/v polyethylenimine in water as a cross-linking agent (Wall, 1993). The biofilm was developed in three stages:

1- The ELAB was filled with a 0.2% polyethylenimine solution in reverse osmosis water for four hours. Then the ELAB was drained and rinsed with a 500 mg/L phenol solution in reverse osmosis water and air dried for two days.

2- The bioreactor was filled with medium containing 300 mg/L phenol and inoculated with 200 mL of fresh inoculum. The air superficial velocity was adjusted to 1.680×10^{-3} m/s. A 3.5 mL/min aqueous stream of nutrient media containing 500 mg/L phenol was pumped into the bioreactor and a similar flow of effluent occurred to provide for continuous growth of bacteria. This was maintained for 20 days.

3- The ELAB was drained and a feed of fresh medium with 250 mg/L phenol was pumped into the empty ELAB at a rate of 110 mL/min and the same air superficial velocity. After a further 20 days, a biofilm had formed on the mesh packing and the bioreactor was filled with fresh medium (without phenol) in order to commence batch and continuous culture experiments.

7.3.4 Analysis

A syringe was used to take samples from one of two ports (in the riser 10 cm above the downcomer outlet or in the downcomer 20 cm below the downcomer inlet). Biomass concentrations were measured at 620 nm wavelength using a spectrophotometer (model Mandel 1240, Shimadzu, Kyoto, Japan). Optical density was converted to cell dry weight using a previously prepared calibration curve. For measurement of phenol, samples were filtered and analyzed immediately using the same

spectrophotometer at 247 nm. Then absorbance was converted to phenol concentration using a prepared calibration curve.

A micro plate bioreactor (Jitterbug 130000, Boekel Scientific, Feasterville, PA) and a spectrophotometer (Automated Microplate Reader ELx808, BIO-TEK Instruments, Inc., Winooski, VT) with KC4 software and Thomas' formula was used to determine the cell count in biofilm samples (Thomas, 1942). A particle size analyzer (Mastersizer 2000, Malvern Instruments, Malvern, UK) was used to measure bacteria and detached biofilm particle size distributions. For scanning electron microscopy (SEM) of the biofilm, samples of biofilm were dehydrated, placed on a sample plate, gold plated, and observed with a Philips Holland, model 505 scanning electron microscope.

7.4 Model

There are three non-linear differential equations governing concentration distributions in the ELAB with a packed bed during the continuous steady state biodegradation process, which are similar to equations used by Quail and Hill (1991).

Substrate in the liquid phase (S):

$$D\frac{d^2S}{dz^2} - U_{LR}\frac{dS}{dz} + K_L a(S^* - S) - \frac{\mu X_T}{Y_{XS}} = 0 \qquad (7.1)$$

Free biomass in the liquid phase (X):

$$D\frac{d^2X}{dz^2} - U_{LR}\frac{dX}{dz} + \mu X_T = 0 \qquad (7.2)$$

Substrate in the air phase (y):

$$-U_{GR}\frac{dy}{dz} - K_L a\frac{1-\theta_{GR}}{\theta_{GR}}(S^* - S) = 0 \qquad (7.3)$$

The specific growth rate is defined by substrate inhibition kinetics:

$$\mu = \frac{\mu_{\max} S}{K_S + S + S^2 / K_I} \tag{7.4}$$

In earlier work we showed importance of using an axially distributed model including dispersion coefficient for mass transfer of VOCs (Nikakhtari and Hill, 2005a). The main assumption in these equations is that the process reaches a steady state condition after a short time. Dispersion in the radial and angular directions is assumed to be negligible and the gas phase flows in a plug flow pattern. Also oxygen does not limit growth. Hydrodynamic parameters in these equations have already been determined for the same ELAB and packing (Nikakhtari and Hill, 2005b):

$$\theta_{GR} = 1.460 \times J_{GR}^{\ 0.784} \tag{7.5}$$

$$U_{LR} = 10.8 \times E \tag{7.6}$$

$$E = \left(\frac{\theta_{GR}}{(1-\theta_{GR})^{-2} + (A_R / A_D)^2}\right)^{0.92} \tag{7.7}$$

The axial mixing in the ELAB is evaluated using the Bodenstein number:

$$Bo = U_{LR} \times L / D \tag{7.8}$$

Meng et al. (2002) indicated that the Bodenstein number depends on packing porosity and is 45.5 for a porosity value of 0.990 as used for the stainless steel packing in this work.

The substrate concentration in the liquid phase at the air interface (S^*) is calculated by Henry's law:

$$S^* = y / H \tag{7.9}$$

The total biomass concentration is the sum of the active biomass concentration in the biofilm and the concentration of the free biomass in the liquid phase (Quail and Hill, 1991):

$$X_T = X_{biof} + X \tag{7.10}$$

$$X_{biof} = 4 \times 10^3 W_P \delta \rho_{biof} \alpha / (V_R \rho_P D_P) \tag{7.11}$$

For calculation of X_{biof}, it is assumed that the packing is uniformly covered by a layer of biofilm. Equation 7.11 is simply the packing surface area multiplied by the biofilm thickness (δ), the biofilm density (ρ_{biof}), and a correction factor (α) to allow for the EPS material surrounding the bacteria. Liquid volume in the riser section of the

ELAB (V_R) is 8.83×10^{-3} m^3. The K_La for phenol was estimated using penetration theory (Welty et al., 2001) and assuming equal mass transfer areas for both oxygen and phenol:

$$\frac{K_L a_{phenol}}{K_L a_{oxygen}} = \sqrt{\frac{D_{L-phenol}}{D_{L-oxygen}}} \tag{7.12}$$

There are five boundary conditions at the inlet of the ELAB for the above differential equations:

$$X_{IN} = 0 \tag{7.13}$$

$$(dX/dz)_{IN} = 0 \tag{7.14}$$

$$S_{IN} = 0 \tag{7.15}$$

$$(dS/dz)_{IN} = 0 \tag{7.16}$$

$$y_{IN} = 0.80 \quad mg/L \text{ (saturated concentration)} \tag{7.17}$$

At the start of continuous operation, a quasi-steady state situation is assumed to govern the build up of free biomass in the bioreactor. After each liquid circulation in the ELAB, inlet concentrations of free biomass and phenol are the same as those concentrations at the top of the riser section corrected for liquid hold up in the downcomer. This change in inlet boundary conditions for free biomass and phenol takes a time equal to the liquid travel time in the downcomer, which is a constant for any specific air flowrate. For instance, this delay time is 8 s for the gas superficial velocity of 0.0148 m/s (Nikakhtari and Hill, 2005b). If F_0 is the replaced liquid rate in the ELAB, after each circulation, two of the boundary conditions are changed:

$$X_{IN} = X_{OUT}\frac{F}{F+F_0} \tag{7.18}$$

$$S_{IN} = S_{OUT}\frac{F}{F+F_0} \tag{7.19}$$

where:

$$F = U_{LR}(1-\theta_{GR})A_R \tag{7.20}$$

Considering the value of of liquid travel time in the downcomer, these equations can be used to predict variation of biomass and substrate concentrations over the quasi-steady state part of the process, as well as over the column height at any time. Equations 7.1, 7.2 and 6.3 were solved simultaneously using Matlab®.

7.5 Results and Discussion

Using the Wilke Chang correlation (Welty et al., 2001), the diffusion coefficients for phenol and oxygen in water were calculated to be 1.04×10^{-9} and 2.4×10^{-9} m^2/s respectively, and the oxygen volumetric mass transfer coefficient for this condition was earlier determined to be 0.021 s^{-1} (Nikakhtari and Hill, 2005b). Applying Equation 7.12, the phenol volumetric mass transfer coefficient was calculated to be 0.0138 s^{-1}. This mass transfer coefficient was used in the simulation, however both the model and experiments revealed that all phenol is absorbed in the water phase at all operating conditions. This means that the effluent air phase is completely cleansed of phenol, and therefore, the phenol concentration in the water phase does not depend on the phenol mass transfer coefficient. Using a mass transfer coefficient value 1000 times smaller than 0.0138 s^{-1} still predicts total phenol absorption. This is because phenol has a very small Henry's coefficient equal to 7.596×10^{-7} atm/mol·m^3 (Yaws, 1999), very low air phase saturated concentration (0.80 mg/L), and high water solubility (80 g/L). Thus, at all conditions studied in this work, the outlet air from the ELAB does not have any phenol due to the simple absorption process of this hydrophilic chemical.

The developed biofilm on the stainless steel packing and a micro-photograph of detached biofilm are shown in Figure 7.2a and b. The released biofilm particles were generally of the size and shape shown in Figure 7.2b, about 25 microns long by 5 microns wide. It is clear that an active layer of biofilm is present in the bioreactor and is released from time to time into the flowing, turbulent two phase air-water flow in the riser section of the ELAB. Figure 7.2c and d show scanning electron microscope photographs of biofilm from the bottom and top of the riser section of the ELAB, with a magnification of 1.1×10^5. These photographs show a difference in texture of bottom and top biofilm due to adequate phenol as a substrate at the bottom of the ELAB but in the top of the ELAB the biofilm was starved of adequate supplies of phenol. The top biofilm demonstated a loose, stringy texture while that at the bottom of the ELAB was very matted. Polysaccharides are thought to be the most abundant compound in dry biofilms, but the amount and types strongly depend on the bacteria and environmental conditions

(Ghannoum and OToole, 2004). In this study, using anthrone reagent (Clegg, 1956), the total amount of sugar and starch (carbohydrates) in the dry biofilm was measured to be 6.3 ± 0.1 % by weight.

Preliminary shake flask cultures were carried out under non-oxygen limiting conditions (Nikakhtari and Hill, 2005c) to determine the growth characteristics of *Pseudomonas putida* (ATCC 17484). The volume of the shake flask and liquid medium were 500 and 200 mL respectively, and the phenol initial concentration was 300 mg/L. The maximum specific growth rate (μ_{max}) and substrate yield factor (Y_{XS}) were determined to be 0.170 ± 0.004 h^{-1} and 0.37 ± 0.026 mg/mg respectively. Nine similar experiments were then carried out in shake flasks with attached biofilm and packing or with detached biofilm as the inoculum. Using the t-test with a 95% confidence interval, a significant difference was found between mean Y_{XS} values when biofilm was or was not presented in the solution. However, no difference was found between μ_{max} or Y_{XS} values when biofilm was in attached or detached form. In the presence of attached or detached biofilm, Y_{XS} was decreased by 76.5% to the value of 0.088 ± 0.016 mg/mg. This can be explained by the fact that in the presence of biofilm, bacteria are constantly producing more biofilm which includes both attached bacteria and extra-cellular polymer substances and this greatly reduces the amount of phenol that can be converted to suspended cells (Robinson et al., 1984).

Variation of phenol and free biomass concentrations during a fed-batch run are shown in Figure 7.3. Fed-batch run variations are similar to those reported by Ritchie and Hill (1995) without a packed bed, except they used lower air superficial velocities (maximum of 0.0118 m/s) and achieved slower biodegradation rates. They achieved a maximum phenol loading rate of 16200 mg/h·m^3. In Figure 7.3, the experimental phenol loading rate was 22160 mg/h·m^3 (30% improvement in bioremediation rate). In Ritchie and Hill's work (1995), the phenol concentration reached a negligible value after 14 hours of operation but in the present experimental work negligible phenol concentrations were achieved after only 6 hours in spite of the higher loading rate. This reveals that the ELAB with biofilm is able to handle a higher shock loading 2.3 times faster than an ELAB utilizing only suspended biomass, which is one of the best features of the ELAB

with biofilm. Stability of biofilms against high shocks is a known characteristic of these types of microbial cultures.

In Figure 7.3, the suspended biomass concentration shows an increase right after starting the air flow because some of the biofilm is released from the steel mesh when the turbulent fluid flow commences. This suspended biomass concentration shows some fluctuation with time, but appears to remain fairly constant at 60 mg/L. Ritchie and Hill (1995) reported a steadily increasing suspended biomass concentration, however in this study it is believed the bulk of the phenol consumption goes into maintaining and increasing the biofilm which was not present in the work of Ritchie and Hill. After about 40 hours, the medium ran out of nutrients (when a total of 886 mg/L of phenol had been metabolized) and the phenol concentration started to increase. This demonstrates that continuous feeding of nutrients is necessary to operate the bioreactor over extended periods of time in spite of the negligible build up of suspended biomass.

The results of three continuous runs at different dilution rates (0.05, 0.20, and 0.50 h^{-1}) are shown in Figure 7.4. The liquid flow rates are 0.6, 2.4, and 6 L/h resulting in residence times of 20, 5, and 2 h, respectively. Experiments were continued at each flowrate until steady concentrations were achieved, which resulted in durations over four residence times in each case. As observed in the fed-batch run, right after start-up of the air flowrate an increase in suspended biomass concentration was observed due to the biomass being released from the biofilm. After that the suspended biomass declines rapidly because loss in the effluent and re-entrapment in the biofilm is higher than its production rate due to growth. It is seen that steady state is reached in 40, 5, and 2 h for dilution rates of 0.05, 0.20 and 0.50 h^{-1}, respectively. Phenol concentrations increase during the early transient phases and then fall to low concentrations (below measurement accuracy) prior to achieving the steady state conditions. The maximum transient phenol concentrations reached were 14.9, 13.6, and 5.4 mg/L for dilution rates of 0.05, 0.20, and 0.50 h^{-1}, respectively. The dilution rate of 0.20 h^{-1} is just above maximum growth rate of the bacteria (0.17 h^{-1}) and 0.50 h^{-1} is three times higher than maximum growth rate of the bacteria. For both of these cases washout of the suspended bacteria occurs but a steady state condition is still achieved due to the growth activity of

the biomass in the biofilm. In general, the biofilm biomass dominated the consumption of phenol and in washout cases, essentially 100% of phenol was removed by the biofilm.

A replication of the 0.05 h^{-1} dilution rate was undertaken for an extended period of time to study the stability of the steady state condition in the column. For this dilution rate the residence time is 20 h. One residence time results in the consumption of 443.2 mg/L of phenol. As shown in the fed-batch experiment, over this time period, nutrients in the medium are sufficient for this phenol concentration so the dilution rate of 0.05 h^{-1} provides adequate nutrients for bacteria growth. Figure 7.5 shows that this run was continued for 17 residence times, a total of 340 h. It can be seen that, similar to Figure 7.4, the phenol concentration stays below 10 mg/L, but the free biomass concentration is high and demonstrates significant scatter. This is due to sporadic biofilm detachment and its removal through the liquid effluent. The procedure used to measure free biomass concentration in the liquid is not able to recognize free biomass from detached biofilm. Filtration of samples with Whatman 40 filter eliminated the detached biofilm and some of the free biomass and shows an average concentration of free biomass equal to 2.5 mg/L, close to the values observed in Figure 7.4 when the biofilm was not fully developed and not being detached from the packed bed. Size distribution analysis showed a surface-volume mean diameter of 594.3×10^{-6} and 1.86×10^{-6} m for solid particles in the ELAB solution and bacteria grown in a shake flask, respectively. Obviously, particles in the ELAB solution are mostly detached biofilm not bacteria. The results of size distribution analysis are shown in Figure 7.6.

Phenol concentrations in the long term experiment (Figure 7.5) were low at early times and then showed a slight increase after about 60 hours but stayed below 10 mg/L for the entire experiment. The slight increase in the phenol concentration after its depletion was also observed in all 12 batch, shake flask experiments discussed earlier. It seems that at low phenol concentrations (below 10 mg/L), the optical density measurement technique is distorted by metabolites excreted by *P. putida*, a condition reported earlier by Allsop et al (1993).

Finally an experiment was performed at a high air superficial velocity of 0.0221 m/s (maximum that could be passed through the gasifier) and the minimum dilution rate of 0.05 h^{-1} to show the ability of the ELAB with a packed bed to remove a high loading

of phenol from a contaminated air stream. The results of this experiment are shown in Figure 7.7. It is seen that, similar to previous experiments, the phenol concentration increases at the beginning of the experiment and then falls rapidly and stays below 10 mg/L. The concentration of the free biomass also stayed low during the experiment. This value of air flow rate provided a phenol loading rate of 33120 mg/h·m^3. Consistent with the negligible amount of phenol in the water phase, which remains constant over a long period of time, no measurable amounts of phenol occur in the effluent air phase, and the polluted air problem has been completely removed. It seems that this novel packed bed ELAB is capable of long term steady state operation with biofilm removal due to sporadic detachment caused by the turbulent two phase flow through the packing and then continuous removal of detached biofilm in the bioreactor effluent.

7.5.1 Model Verification

Using Equations 7.5 to 7.8, the value of hydrodynamic parameters were calculated to be: θ_{GR} = 0.0537, U_{LR} = 0.0651 m/s and D = 0.0046 m^2/s for the case of gas superficial velocity of J_{GR} = 0.0148 m/s, and θ_{GR} = 0.0737, U_{LR} = 0.0869 m/s and D = 0.0058 m^2/s for the case of gas superficial velocity of J_{GR} = 0.0221 m/s.

For modeling purposes, the biofilm value of Y_{XS} (0.088 mg/mg) was used since in the ELAB the majority of phenol consumption was carried out inside the biofilm. K_S and K_I in Equation 7.4 were set at 1 and 470 mg/L, respectively, as determined earlier for the same bacteria and substrate (Ritchie and Hill, 1995). The moisture content of the biofilm was measured to be 95%. Cell count experiments on biofilm samples showed a total number of 3.12×10^7 cells/mg dry weight of biofilm. The main portion of each cell is water such that cell density can be assumed to be 1 Kg/L (Bailey and Ollis, 1986). Considering the cell diameter equal to 1.86×10^{-6} m (Figure 7.6), it can be calculated that 11.2% of the biofilm dry weight is active bacteria and therefore the correction factor of Equation 7.11 (α) is 0.112. Taking samples of the packing with biofilm and weighing them wet, drying for several hours at 65 ^{o}C and 0.132×10^5 Pa, weighing again, washing, drying and weighing once more, the biofilm thickness (δ) was determined to be 150 μm which is in a good agreement with the previously reported value for the same bacteria

(Quail and Hill, 1991). Biofilm density (ρ_{biof}) was measured to be 1200 kg/m^3. Dry weight of the biofilm per unit wet biofilm volume was 38.5 mg/mL, which is in the range of previously reported values (10-50 mg/mL) (Characklis and Cooksey, 1983).

Variation of the experimentally measured free biomass concentration and the model prediction during the quasi-steady state period (Equations 7.1 to 7.4) are shown in Figure 7.8 for the dilution rate of 0.5 h^{-1}. It can be seen that there is a good fit of the quasi-steady state model to the experimental data. Figure 7.9 shows predictions of air and liquid phase substrate concentrations over the height of the column after it reaches the steady state condition. At these conditions, the free biomass reaches a constant concentration of 4.14 mg/L. These results match the measurements in continuous runs. Differences between predicted phenol concentrations at the top and bottom of the column were less than the sensitivity of the measurements. In this study, all samples taken at the same time from the top and bottom of the column always demonstrated identical phenol concentrations. Using the model, the assumption of plug flow for the liquid phase as well as the gas phase in the riser section (D = 0) was theoretically investigated. This assumption did not affect the concentration predictions for the quasi-steady state part of the operation significantly (Figure 7.8), but it affected the concentration distributions over the height of the column during steady state conditions, which is shown in Figure 7.9b. Plug flow conditions were not able to accurately predict substrate concentration distributions over the height of the column.

Changing the value of the biomass thickness (δ) in the simulation changes the position that substrate is depleted in the column. The model results (Figure 7.9) show that phenol is depleted approximately one third of the height of the column. This agrees with visual observations where the white biofilm only coated the bottom one third of the packing in continuous experiments (due to the depletion of phenol at that point). The biofilm at the bottom part of the packing differs from the biofilm at the top part not only in the color but in the texture as well, as discussed earlier (Figure 7.2c and d). The loading rate of 33120 mg/h·m^3 of phenol with 100% removal efficiency is achieved in one third of the column, and it can be estimated that using total height of the column a maximum loading rate of 100000 mg/h·m^3 could be achieved with 100% phenol

removal. This high capacity using a high porosity, packed bed ELAB will also be very beneficial for removal of more hydrophobic VOC pollutants.

7.6 Conclusion

A novel, high porosity packed bed ELAB has been shown to readily remove phenol from polluted air in both fed-batch and continuous flow operation modes, even when bioreactor dilution rates exceeded the maximum growth rate of the microorganism. This novel bioreactor was found to be able to continuously handle over 33120 mg/h·m^3 loading rate of phenol with 100% removal efficiency using only one third of the column height and reached steady state conditions in less than six hours. A mathematical model was developed that accurately predicted both transient and steady state concentrations in the ELAB. The model was used to show that the active biofilm thickness was 150 μm and that only one third of the packed bed height was needed to continuously remove phenol at the highest loading rate used in this study.

7.7 Nomenclature

A_D	Downcomer cross-sectional area (m^2)
A_R	Riser cross-sectional area (m^2)
Bo	Bodenstein number (Equation 7.8)
D	axial dispersion coefficient (m^2/s)
D_L	diffusivity in the liquid phase (m^2/s)
D_p	packing diameter (m)
E	Gas holdup function in Equation 7.6
F	Liquid flow rate in the ELAB (m^3/s)
F_0	Liquid make up, coming in or going out of the ELAB (m^3/s)

H	Henry's law coefficient (mg/mg)
J_{GR}	Gas superficial velocity in the riser section (m/s)
K_La	overall volumetric mass transfer coefficient (h^{-1})
K_I, K_S	constants in Equation 7.4 (mg/L)
S	substrate concentration (mg/L)
S_{IN}	substrate concentration in the inlet liquid to the Riser section
S_{OUT}	substrate concentration in the outlet liquid of the Riser section
S^*	substrate concentration at interface
U_{GR}	gas velocity in the riser section (m/s)
U_{LR}	liquid velocity in the riser section (m/s)
V_R	riser section volume (m^3)
W_p	packing weight (kg)
X	free biomass concentration (mg/L)
X_{biof}	biomass concentration in the biofilm (mg/L)
X_{IN}	biomass concentration in the inlet liquid to the riser section
X_{OUT}	biomass concentration in the outlet liquid of the riser section
X_T	total biomass concentration (mg/L)
y	substrate concentration in the gas phase (mg/L)
y_{IN}	substrate concentration in the inlet gas to the riser section
Y_{XS}	substrate yield factor (mg cell/ mg substrate)
z	axial distance up the riser section (m)

Greek Symbols

α	correction factor in Equation 7.11
δ	biofilm thickness (m)
μ	specific growth rate (h^{-1})
μ_{max}	maximum specific growth rate (h^{-1})
ρ_{biof}	biofilm density (kg of wet biofilm/m3 of wet biofilm)
ρ_p	packing density (kg/m3)
θ_{GR}	gas holdup in the Riser section

7.8 References

Allsop, P. J.; Chisti, Y.; Moo-Young, M.; Sullivan, G. R. Dynamics of Phenol Degradation by *Pseudomonas putida*. *Biotechnol. Bioeng.* **1993**, *41*, 572-580.

Bailey, J. E.; Ollis, D. F. Biochemical Engineering Fundamentals. 2nd ed.; McGraw-Hill: New York, 1986, pp 5.

Characklis, W. G.; Cooksey, K. E. Biofilms and Microbial Fouling. *Adv. Appl. Microbiol.* **1983,** *29*, 93-138.

Clegg, K. M. The Application of the Anthrone Reagent to the Estimation of Starch in Cereals. *J. Sci. Food. Agric.* **1956**, *7*, 40-44.

Delhomenie, M. C.; Bibeau, L.; Gendron, J.; Brzezinski, R.; Heitz, M. A Study of Clogging in a Biofilter Treating Toluene Vapors. *Chem. Eng. J.* **2003**, *94*, 211-222.

Edwards, F. G.; Nirmalakhandan, N. Modeling an Airlift Bioscrubber for Removal of Airphase BTEX. *J. Environ. Eng.* **1999**, 1062-1070.

Ghannoum, M.; OToole, G. A. Microbial Biofilms; American Society for Microbiology: Washington, 2004, pp 174-181.

Harding, R. C.; Hill, G. A.; Lin, Y-H. Bioremediation of Toluene Contaminated Air Using an External Loop Airlift Bioreactor. *J. Chem. Technol. Biotechnol.* **2003**, *78*, 1-6.

Jianping, W.; Yu, C.; Dongyan, C.; Xiaoqiang, J. Removal of Ethyl Acetate in Air Streams Using a Gas-Liquid-Solid Three Phase Flow Airlift Loop Bioreactor. *Biochem. Eng. J.* **2005**, *24*, 135-139.

Lim, K. H. Waste Air Treatment with a Biofilter: For the Case of Excess Adsorption Capacity. *J. Chem. Eng. Jpn.* **2001**, *34*, 766-775.

Lo, C-S.; Hwang, S-J. Dynamic behavior of an Internal-Loop Airlift Bioreactor for Degradation of Waste Gas Containing Toluene. *Chem. Eng. Sci.* **2004**, *59*, 4517-4530.

Meng, A. X.; Hill, G. A.; Dalai, A. K. Hydrodynamic Characteristics in an External Loop Airlift Bioreactor Containing a Spinning Sparger and a Packed Bed. *Ind. Eng. Chem. Res.* **2002**, *41*, 2124-2128.

Nikakhtari, H.; Hill, G. A. Hydrodynamic and Oxygen Mass Transfer in an External Loop Airlift Bioreactor with a Packed Bed. *Biochem. Eng. J.* **2005b**, *27*, 138-145.

Nikakhtari, H.; Hill, G. A. Modelling Oxygen Transfer and Aerobic Growth in Shake Flasks and Well-Mixed Bioreactors. *Can. J. Chem. Eng.* **2005c**, *83***,** 493-499.

Nikakhtari, H.; Hill, G. A. Volatile Organic Chemicals Mass Transfer in an External Loop Airlift Bioreactor with a Packed Bed. *Ind. Eng. Chem. Res.* **2005a**, *44*, 9299-9306.

Oliveira, F. J. S.; De Franca, F. P. Performance of an Internal-Loop Airlift Bioreactor for Treatment of Hexane-Contaminated Air. *Appl. Biochem. Biotechnol.* **2005**, *121-124*, 581-592.

Quail, B. E.; Hill, G. A. A Packed-Column Bioreactor for Phenol Degradation: Model and Experimental Verification. *J. Chem. Technol. Biotechnol.* **1991**, *52*, 545-557.

Ritchie, B. J.; Hill, G. A. Biodegradation of Phenol Polluted Air Using an External Loop Airlift Bioreactor. *J. Chem. Technol. Biotechnol.* **1995**, *62*, 339-344.

Robinson, J. A.; Trulear, M. G.; Characklis, W. G. Cellular Reproduction and Extracellular Polymer Formation by *Pseudomonas aeruginosa* in Continuous Culture. *Biotechnol. Bioeng.* **1984**, *26*, 1409-1417.

Spigno, G.; Pagella, C.; Fumi, M. D.; Molteni, R.; De Faveri, D. M. VOCs Removal from Waste Gases: Gas-Phase Bioreactor for the Abatement of Hexane by *Aspergillus niger*. *Chem. Eng. Sci.* **2003**, *58*, 739-746.

Thomas, H. A. Bacterial Densities from Fermentation Tube Tests. *J. Am. Water Works Assoc.* **1942**, *34*, 572-576.

Wall, J. B. Operational Effects on Phenol Degradation by *Pseudomonas putida* in a Co/Countercurrent Packed Bed Bioreactor. MSc Thesis: University of Saskatchewan, 1993.

Wei, V. Q.; Hill, G. A.; Macdonald, D. G. Bioremediation of Contaminated Air Using an External-Loop Airlift Bioreactor. *Can. J. Chem. Eng.* **1999**, *77*, 955-962.

Welty, J. R.; Wicks, C. E.; Wilson, R. E. Fundamentals of momentum, heat, and mass transfer; John Wiley: New York, 2001.

Yaws, C. L. Chemical Properties Handbook; McGraw-Hill: New York, 1999.

Zilli, M.; Converti, A.; Lodi, A.; Borghi, M. D.; Ferraiolo, G. Phenol Removal from Waste Gases with a biological Filter by *Pseudomonas putida*. *Biotechnol. Bioeng.* **1993**, *41*, 693-699.

Zilli, M.; Fabiano, B.; Ferraiolo, A.; Converti, A. Macro_Kinetic Investigation on Phenol Uptake from Air by Biofiltration: Influence of Superficial Gas Flow Rate and Inlet Pollutant Concentration. *Biotechnol. Bioeng.* **1996**, *49*, 391-398.

Table 7.1 Specifications of the ELAB.

Riser section diameter, mm	89
Riser cross-sectional area (A_R), m^2	6.22×10^{-3}
Downcomer section diameter, mm	47
Downcomer cross-sectional area (A_D), m^2	1.74×10^{-3}
Liquid height above the sparger, m	1.42
Liquid volume, m^3	1.2×10^{-2}
Number of orifices in sparger	6
Orifice diameter, mm	1.6

Table 7.2 Specifications of the stainless steel packing.

Metal	Stainless Steel
Diameter (D_p), m	4.6×10^{-4}
Density (ρ_p), kg/m^3	5139.3
Weight (W_p), kg	0.399
Height in the column, m	1.2
Porosity, %	98.96

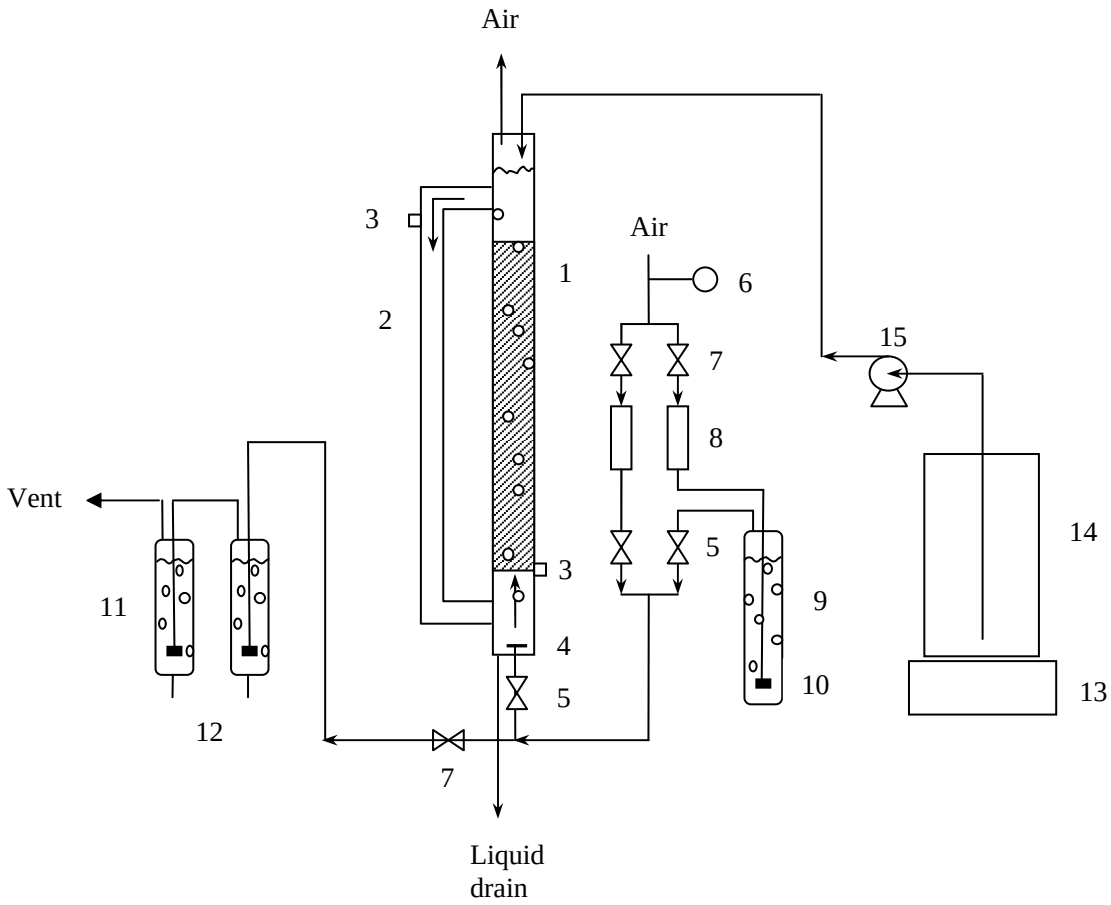

1- Riser section with packing
2- Downcomer section
3- Sampling port
4- Gas sparger
5- Two-way valve
6- Pressure gage
7- Adjusting valve
8- Flow meter
9- Gasifier
10- Sparger
11- Bubbler
12- Sampling valve
13 - Mixer
14- Medium tank
15- Adjustable pump

Figure 7.1 Schematic of the External Loop Airlift Bioreactor.

(a)

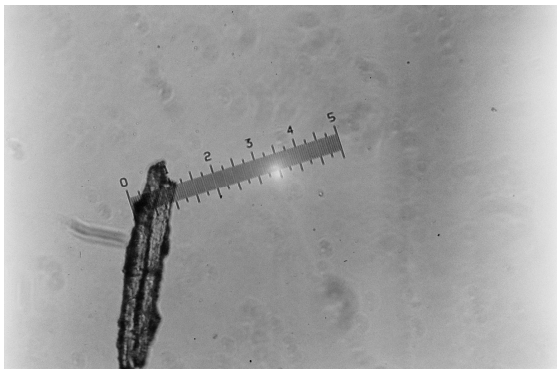

(b)

(c)

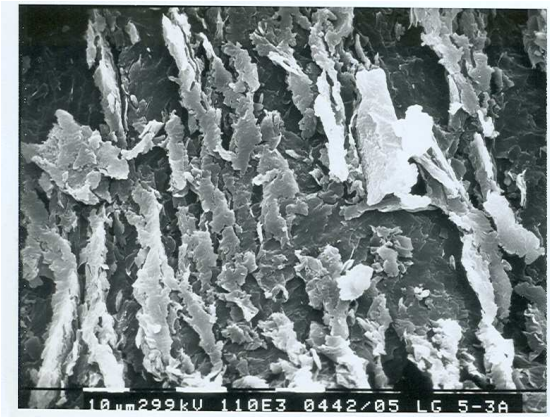

(d)

Figure 7.2 (a) Developed biofilm on the stainless steel packing, (b) Micro-photograph of detached biofilm, (c) SEM photograph of developed biofilm in the bottom of the riser (magnification:1.1×10^5), (d) SEM photograph of developed biofilm in top of the riser (magnification:1.1×10^5).

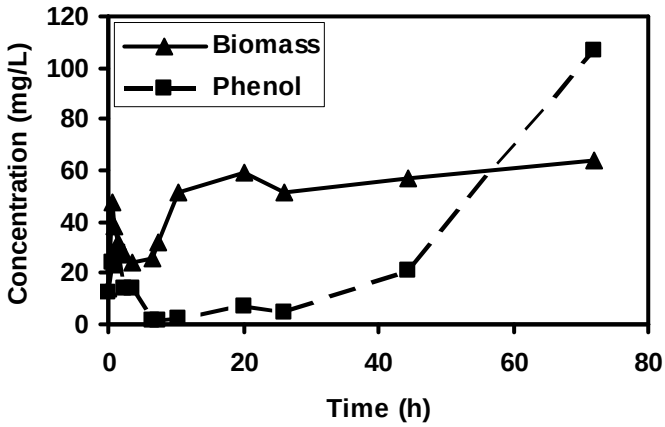

Figure 7.3 Phenol degradation during a fed-batch run, at an air superficial velocity of 0.0148 m/s.

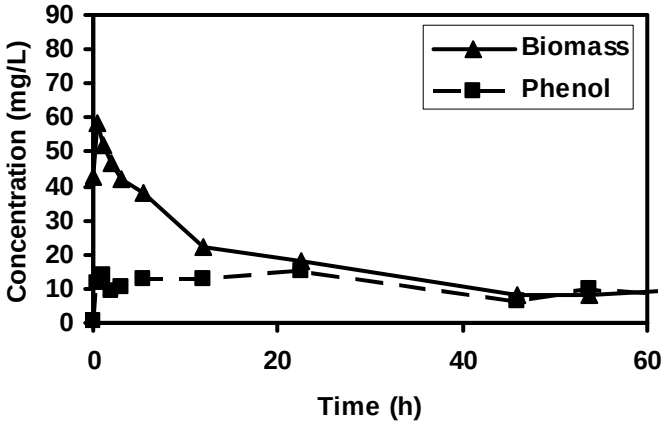

(a)

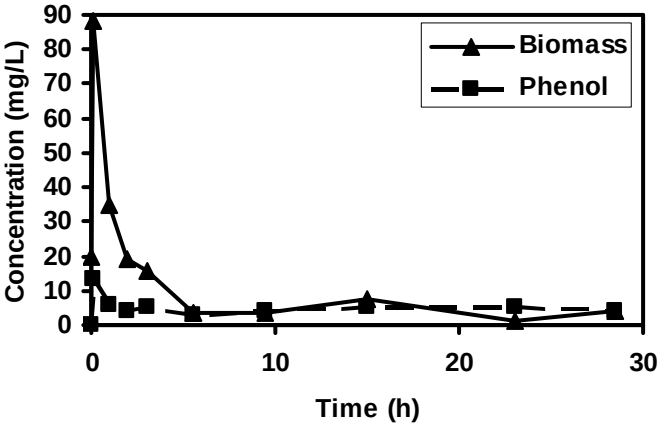

(b)

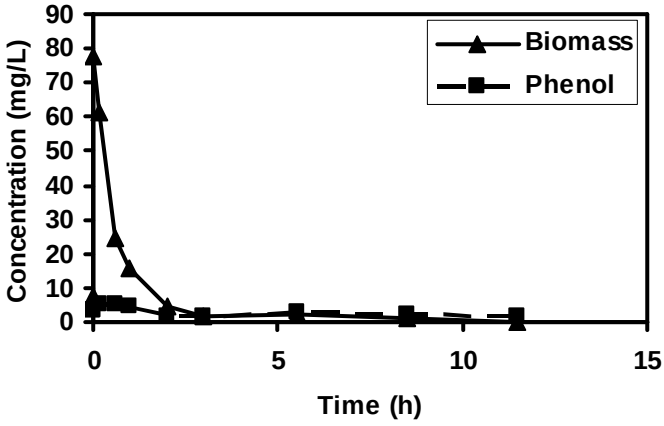

(c)

Figure 7.4 Continuous runs at an air superficial velocity of 0.0148 m/s and dilution rates of (a) 0.05 h^{-1} (liquid flow rate of 0.6 L/h), (b) 0.20 h^{-1} (liquid flow rate of 2.4 L/h), and (c) 0.50 h^{-1} (liquid flow rate of 6 L/h).

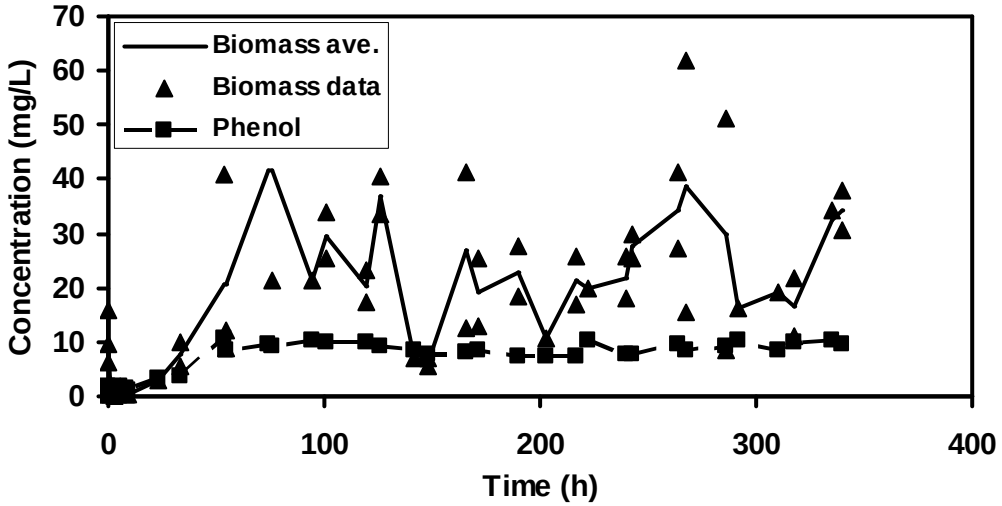

Figure 7.5 Extended continuous run at an air superficial velocity of 0.0148 m/s and a dilution rate of 0.05 h^{-1} (liquid flow rate of 0.6 L/h).

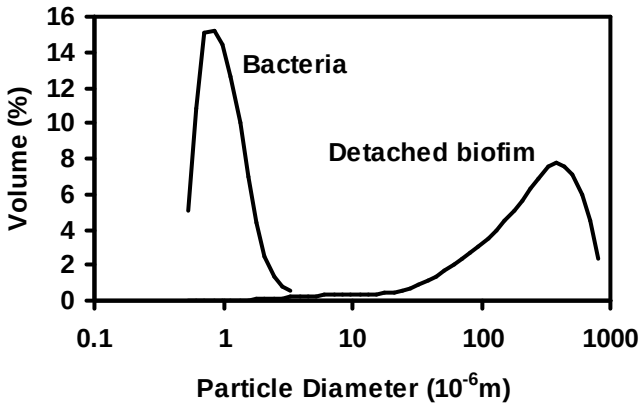

Figure 7.6 Size distribution of bacteria and detached biofilm.

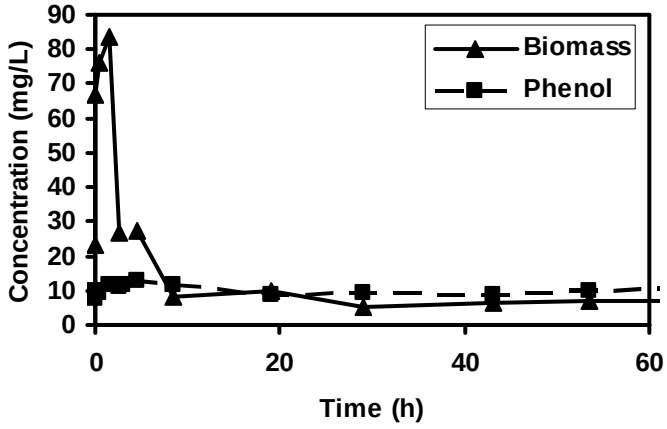

Figure 7.7 A continuous run at an air superficial velocity of 0.0221 m/s and a dilution rate of 0.05 h^{-1} (liquid flow rate of 0.6 L/h).

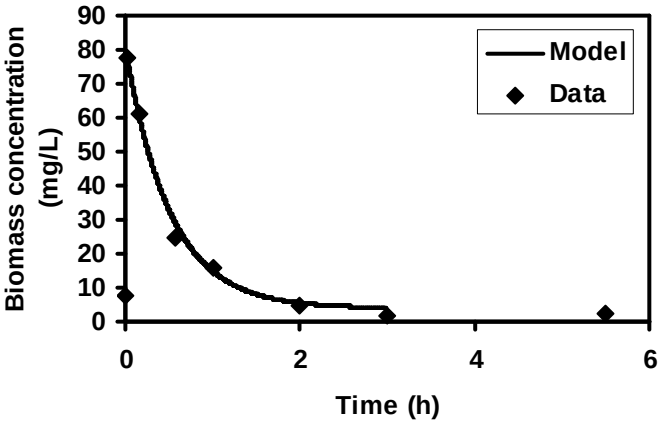

Figure 7.8 Model prediction and experimental data of free biomass concentration over the transient period of the bioremediation experiment at a dilution rate of 0.50 h^{-1}.

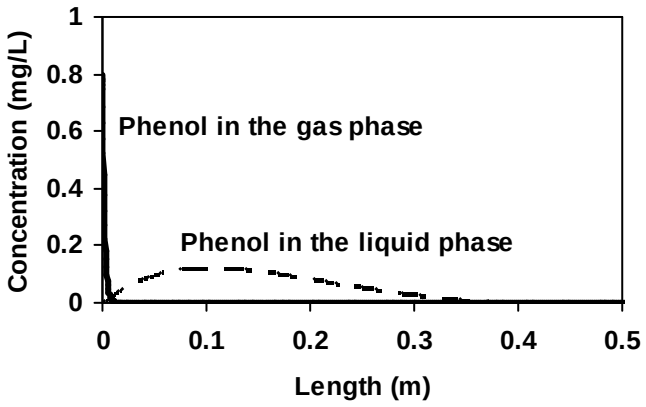

(a)

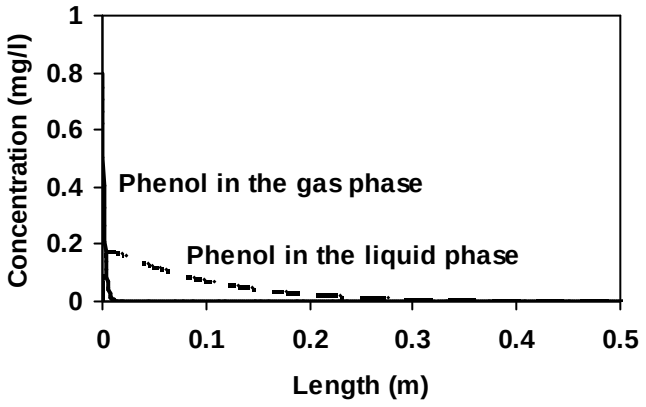

(b)

Figure 7.9 Biomass and phenol distribution in the bottom one third of the riser of the packed bed ELAB after reaching steady state conditions: (a) Full model, (b) Plug flow model.

Chapter 8 – Conclusions and Recommendations

8.1 Conclusions

Bioremediation and mass transfer experiments were completed first in shake flasks and a well-mixed bioreactor and then in the ELAB. In shake flasks, it was found that oxygen mass transfer rates could be comparable to those achieved in a well-mixed bioreactor when both high flask to liquid volume ratios and shaking turbulence were used. New predictive models for the oxygen transfer rates in both liquid and gas phases of shake flasks were introduced. The combined model for oxygen transfer and cell growth accurately predicted the transient concentrations of cell mass, substrate and oxygen in both shake flasks and a well-mixed bioreactor over a wide range of operating conditions. Then this model was improved by considering gas phase oxygen mass transfer resistances. Shake flask closures were found to have significant effects on the determination of oxygen yield factors when there is oxygen depletion during a growth experiment. It was shown that the improved model introduced in this work is able to fit experimental oxygen concentrations and predict oxygen yield factors with improved accuracy compared to models employed earlier in the literature.

A mathematical model considering an ELAB as a distributed column with respect to both the liquid and gas phases was developed to predict mass transfer of oxygen and VOCs with respect to both time and space. The model was found to fit experimental data closely and it was shown that the distributed model is a much more accurate method to determine $K_L a$ for ELABs with low liquid circulation rates, as compared to a completely stirred reactor. The model correctly predicted oscillating concentrations in the liquid phase and small losses in the air phase.

By fitting experimental data to a full, mechanistic model of an ELAB both with and without a packed bed in the riser, oxygen mass transfer coefficients were found over

a wide range of gas flow rates and were correlated to empirical equations. Using a small amount of packing (99.0% porosity), the oxygen mass transfer coefficient was increased by an average factor of 2.45 in a packed bed ELAB compared to the same ELAB without a packed bed, reaching a value of 0.021 s^{-1} at a gas superficial velocity of 0.0157 m/s. The oxygen mass transfer coefficient increase factor was as high as 3.7 for the ELAB with a nylon mesh packing and 96.3 percent porosity. Using the smaller amount of packing (99.0% porosity), VOC mass transfer coefficients were increased by an average of 65.1% for toluene and 33.8% for benzene. Desorption of VOCs was slower than absorption due to variation of bubble sizes caused by surface tension changes during the mass transfer experiments. It was shown that only the full, mechanistic mathematical model is an accurate method to determine $K_L a$ for VOC absorption in ELABs with low liquid circulation rates, as compared to models assuming well-mixed conditions. The ELAB with a small amount of packing is a novel bioreactor with much higher mass transfer due to increased gas holdup and small bubble diameters. The packing surface area can also be used for cell immobilization, and therefore has potential to greatly enhance gas-liquid fermentations and other gas-liquid biochemical operations.

The ELAB with a high porosity packed bed has been shown to readily remove phenol from polluted air in both fed-batch and continuous flow operation modes, even when the bioreactor dilution rates exceeded the maximum growth rate of the microorganism. This novel bioreactor was found to be able to continuously handle over 33120 $mg/h \cdot m^3$ loading rate of phenol with 100% removal efficiency using only one third of the column height and reached steady state conditions in less than six hours. A mathematical model was developed that accurately predicted both transient and steady state concentrations in the ELAB. The model was used to show that the active biofilm thickness was 150 μm and that only one third of the packed bed height was needed to continuously remove phenol at the highest loading rate used in this study, agreeing with the experimental observations.

8.2 Recommendations

Using the improved model developed in Chapter 3, batch biogrowth experiments in shake flasks can be done for different bacteria and different substrates to get correct oxygen yield factors for each situation. These oxygen yield factors can be analyzed stoichiometrically and then related to other growth parameters such as other yield factors.

There is little information about VOCs mass transfer into water, and the difference between their absorption and desorption rates was reported in this work for the first time. Even though this phenomenon was explained by varying bubble sizes during mass transfer experiments, it seems there is a large room for further investigations on this issue.

The presence of VOCs in the liquid phase or mass transfer of VOCs from air into liquid can affect the mass transfer rates of oxygen into the liquid phase. This issue will be important during bioremediation experiments when there is a considerable value of VOC in the liquid phase, or VOC mass transfer into the liquid phase. Therefore, a study of oxygen mass transfer rates in the presence of VOCs or at the same time as mass transfer of VOCs is strongly recommended.

The ELAB with a high porosity packed bed removed a high load of phenol from air in only one third of the bioreactor, and then it was limited by the maximum phenol polluted air flow that the gasifier was able to produce. In the next step, a gasifier with a larger capacity can be provided to determine the maximum phenol load that can be removed with 100% efficiency in this ELAB. The removal efficiency for higher loads can also be investigated.

Since the ELAB with a packed bed handled a high load of phenol in only one third of the bioreactor, this ELAB seems to have a high potential for bioremediation of more hydrophobic VOCs than phenol with higher loads. The next step of this work should involve using this ELAB for bioremediation of more hydrophobic VOCs such as toluene, vinyl chloride, and methylene chloride from a polluted air stream. Toluene is more toxic than phenol and it is harder to find a bacterium that is able to assimilate toluene at a high rate as phenol. For bioremediation of toluene, a mixed culture is

recommended, probably taken from industrially contaminated sites. This approach is easier compared to the selection of an efficient, pure bacterium. Species which are able to assimilate toluene can be identified at a later time.

Appendix A: Calibration curves

A.1 Biomass calibration curves

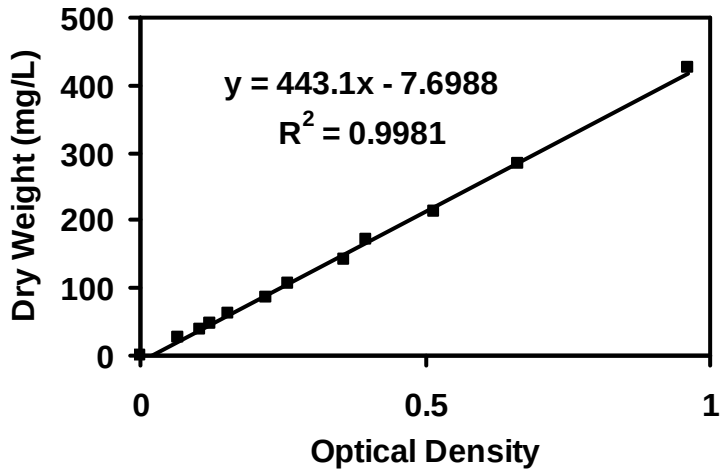

Figure A.1 Spectrophotometer calibration curve for detection of biomass (*Pseudomonas putida*, ATCC 23973) in the liquid phase at the wavelength of 620 nm.
The equation is accurate for biomass concentrations above 25 mg/L:

y: Dry biomass concentration (mg/L)

x: Optical density (absorbance)

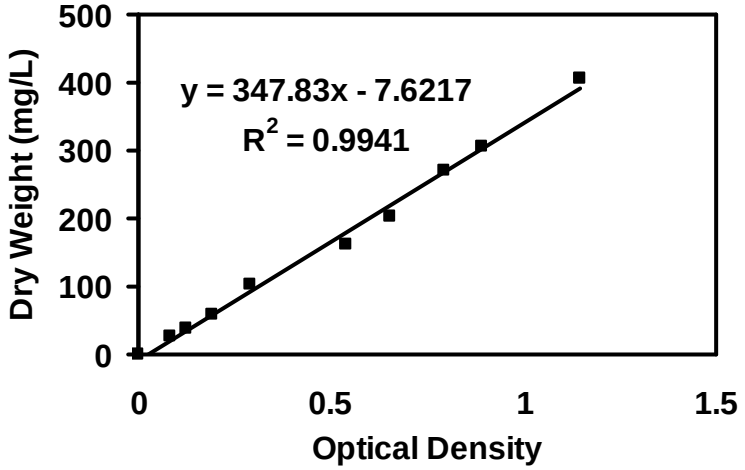

Figure A.2 Spectrophotometer calibration curve for detection of biomass (*Pseudomonas putida*, ATCC 17484) in the liquid phase at the wavelength of 620 nm.
The equation is accurate for biomass concentrations above 25 mg/L:

y: Dry biomass concentration (mg/L)

x: Optical density (absorbance)

A.2 Spectrophotometer calibration curves

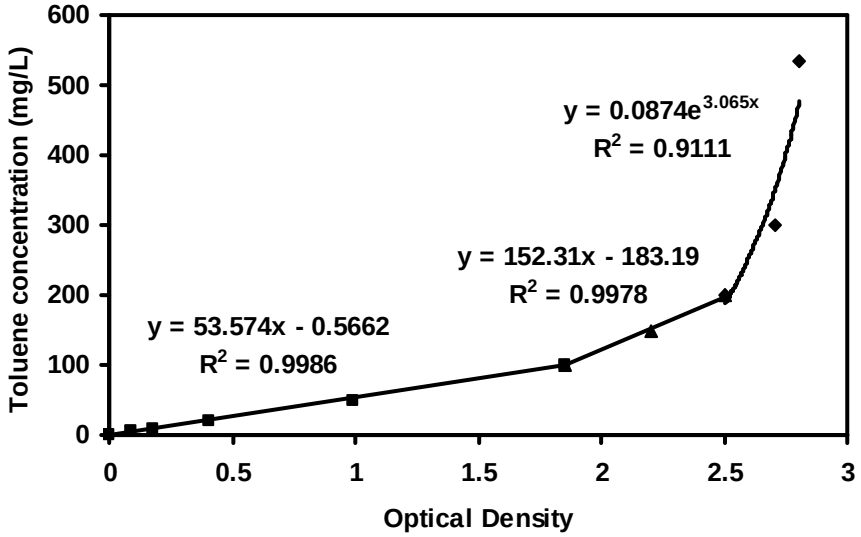

Figure A.3 Spectrophotometer calibration curve for detection of toluene in water at the wavelength of 214 nm.

y: Toluene concentration (mg/L)

x: Optical density (absorbance)

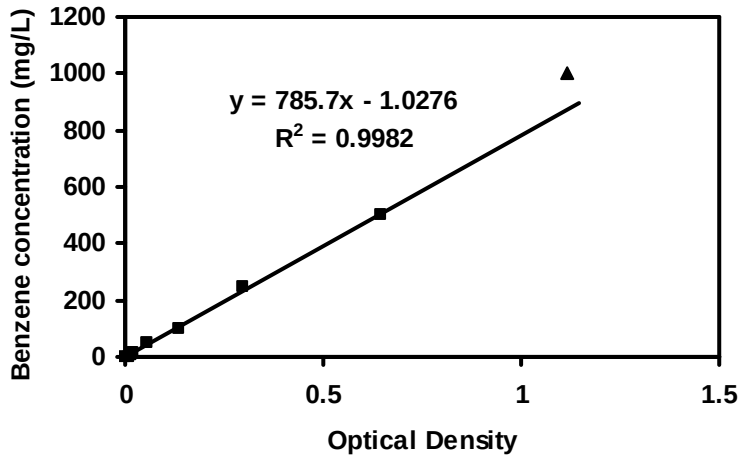

Figure A.4 Spectrophotometer calibration curve for detection of benzene in water at the wavelength of 253 nm, it is accurate up to the concentration of about 600 mg/L.

y: Benzene concentration (mg/L)

x: Optical density (absorbance)

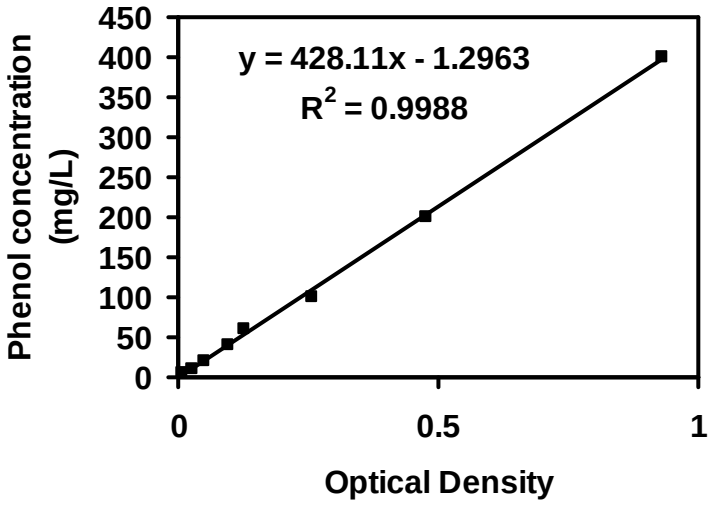

Figure A.5 Spectrophotometer calibration curve for detection of phenol in the liquid phase at the wavelength of 247 nm.

y: Phenol concentration (mg/L)

x: Optical density (absorbance)

A.3 Gas flow meter calibration curves

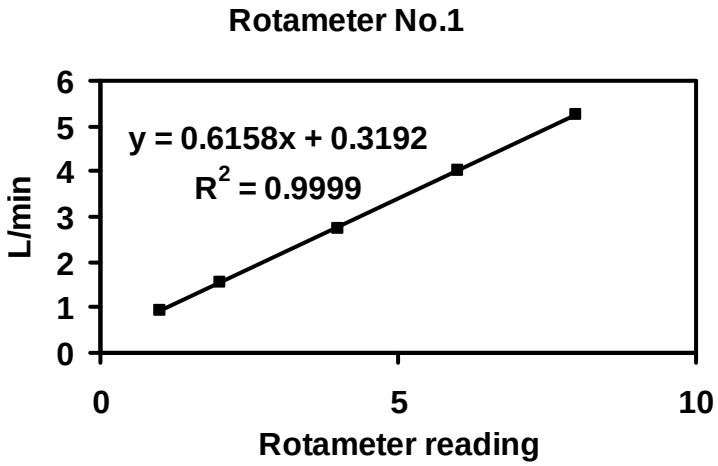

Figure A.6 Calibration curve for gas flow meter number 1, which was used for the air stream.

y: Gas flow rate (L/min)

x: Rotameter reading

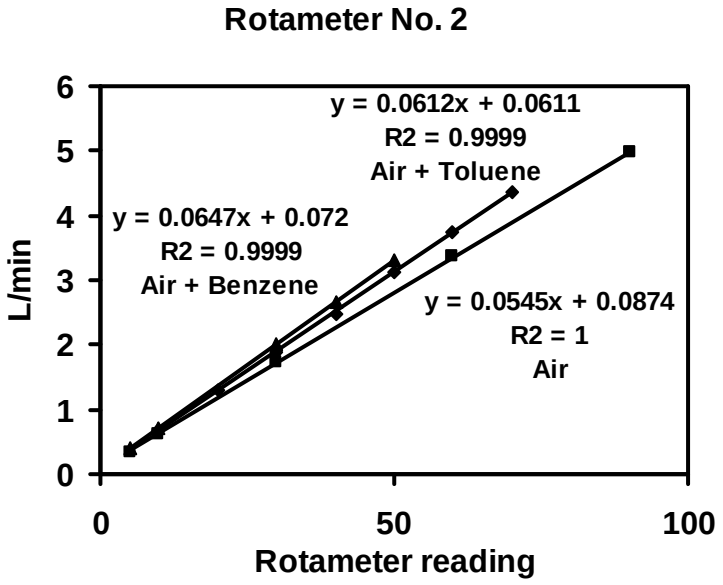

Figure A.7 Calibration curve for gas flow meter number 2, which was used for inlet artificially polluted air stream.

y: Gas flow rate (L/min)

x: Rotameter reading

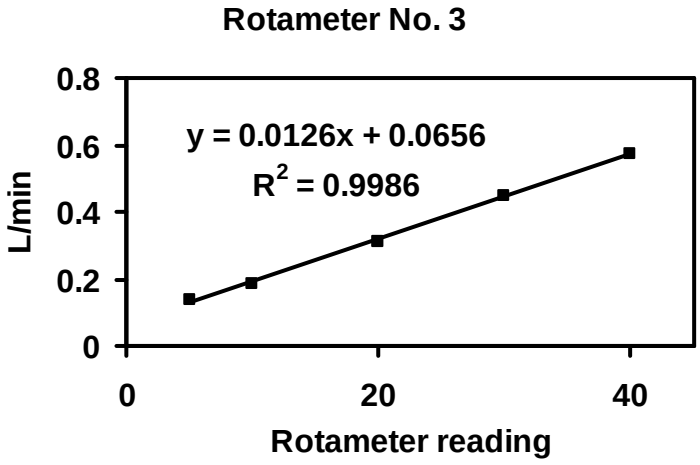

Figure A.8 Calibration curve for gas flow meter number 3, which was used for the outlet air stream.

y: Gas flow rate (L/min)

x: Rotameter reading

Appendix B: Computer programs for modeling sections

B.1 Excel program for growth experiments (old model)

This program is according to the model section of Chapter 2.

Variables	Unit	Definition
MU	h^{-1}	Specific growth rate (μ)
MUmax	h^{-1}	Maximum specific growth rate (μ_{max})
Ks	mg/L	Constant of growth equation
Ki	mg/L	Constant of growth equation
Km	mg/L	Constant of growth equation
DT	h^{-1}	Time step (Δt)
kX1 to 4	mg/L	Four Runge-Kutta (4^{th} order) coefficients for X
kS1 to 4	mg/L	Four Runge-Kutta (4^{th} order) coefficients for S
kC1 to 4	mg/L	Four Runge-Kutta (4^{th} order) coefficients for C
Yxs	mg/mg	Substrate yield factor
Yxc	mg/mg	Oxygen yield factor
kLa	h^{-1}	Oxygen mass transfer coefficient in the liquid phase
Cstar	mg/L	Oxygen saturated concentration in the liquid phase

R, S, and T columns are for X, S, and C (biomass, substrate, and dissolved oxygen concentrations), which start at R3, S3, and T3 with their initial values (X_0, S_0, and C_0)

Col.

A time

B MU=MUmax*S3/(S3+Ks+S3^2/Ki)*T3/(T3+Km)

C kX1=B4*R3*DT

D kS1=(-1/Yxs)*B4*R3*DT

E kC1=((-1/Yxc)*B4*R3+kLa*(Cstar-T3))*DT

F MU=MUmax*(S3+D4/2)/((S3+D4/2)+Ks+(S3+D4/2)^2/Ki)*
(T3+E4/2)/((T3+E4/2)+Km)

G kX2=F4*(R3+C4/2)*DT

H kS2=(-1/Yxs)*F4*(R3+C4/2)*DT

I kC2=((-1/Yxc)*F4*(R3+C4/2)+kLa*(Cstar-(T3+E4/2)))*DT

J MU=MUmax*(S3+H4/2)/((S3+H4/2)+Ks+(S3+H4/2)^2/Ki)*
(T3+I4/2)/((T3+I4/2K)+Km)

K kX3=J4*(R3+G4/2)*DT

L kS3=(-1/Yxs)*J4*(R3+G4/2)*DT

M kC3=((-1/Yxc)*J4*(R3+K4/2)+kLa*(Cstar-(T3+I4/2)))*DT

N MU=MUmax*(S3+L4)/((S3+L4)+Ks+(S3+L4)^2/Ki)*(T3+M4)/((T3+M4)+Km)

O kX4=N4*(R3+K4)*DT

P kS4=(-1/Yxs)*N4*(R3+K4)*DT

Q	kC4=((-1/Yxc)*N4*(R3+O4)+kLa*(Cstar-(T3+M4)))*DT
R	X=R3+(C4+2*(G4+K4)+O4)/6
S	S=MAX(0,S3+(D4+2*(H4+L4)+P4)/6)
T	C=MAX(0,T3+(E4+2*(I4+M4)+Q4)/6)

B.2 Excel program for growth experiments (new model)

This program is according to the model section of Chapter 3.

ky1 to 4	Four Runge-Kutta (4^{th} order) coefficients for y
kGa	Oxygen mass transfer coefficient in the gas phase
H	Henry's constant
ystar	Oxygen concentration in the atmospheric air

V, W, X, and Z columns are for X, S, C, and y (biomass, substrate, dissolved oxygen in the liquid phase, and oxygen in the gas phase concentrations), which start at V3, W3, X3, and Z3 with their initial values (X_0, S_0, C_0, and y_0)

Col.	
A	time
B	MU=MUmax*W3/(W3+Ks+W3^2/Ki)*X3/(X3+Km)
C	kX1=B4*V3*DT
D	kS1=(-1/Yxs)*B4*V3*DT
E	kC1=((-1/Yxc)*B4*V3+kLa*(Z3/H-X3))*DT
F	ky1=(kGa*(ystar-Z3)-kLa*(Z3/H-X3))*DT
G	MU=MUmax*(W3+D4/2)/((W3+D4/2)+Ks+(W3+D4/2)^2/Ki)* (X3+E4/2)/((X3G+E4/2)+Km)
H	kX2 =G4*(V3+C4/2)*DT
I	kS2 =(-1/Yxs)*G4*(V3+C4/2)*DT
J	kC2 =((-1/Yxc)*G4*(V3+C4/2)+kLa*(Z3/H-(X3+E4/2)))*DT
K	ky2 =(kGa*(ystar-(Z3+F4/2))-kLa*((Z3+F4/2)/H-(X3+E4/2)))*DT
L	MU=MUmax*(W3+I4/2)/((W3+I4/2)+Ks+(W3+I4/2)^2/Ki)* (X3+J4/2)/((X3+J4/M2)+Km)
M	kX3 =L4*(V3+H4/2)*DT
N	kS3 =(-1/Yxs)*L4*(V3+H4/2)*DT
O	kC3 =((-1/Yxc)*L4*(V3+M4/2)+kLa*(Z3/H-(X3+J4/2)))*DT
P	ky3 =(kGa*(ystar-(Z3+K4/2))-kLa*((Z3+K4/2)/H-(X3+J4/2)))*DT
Q	MU=MUmax*(W3+N4)/((W3+N4)+Ks+(W3+N4)^2/Ki)* (X3+O4)/((X3+O4)+Km)
R	kX4 =Q4*(V3+M4)*DT

```
S       kS4 =(-1/Yxs)*Q4*(V3+M4)*DT
T       kC4 =((-1/Yxc)*Q4*(V3+R4)+kLa*(Z3/H-(X3+O4)))*DT
U       ky4 =(kGa*(ystar-(Z3+P4))-kLa*((Z3+P4)/H-(X3+O4)))*DT
V       X =V3+(C4+2*(H4+M4)+R4)/6
W       S =MAX(0,W3+(D4+2*(I4+N4)+S4)/6)
X       C =MAX(0,X3+(E4+2*(J4+O4)+T4)/6)
Z       y =MAX(0,Z3+(F4+2*(K4+P4)+U4)/6)
```

B.3 Matlab program for Oxygen Mass Transfer

This program includes three M-files The first M-file is the main program and the next two M-files are auxiliary programs used in the first program.

B.3.1 Main Matlab programming for oxygen mass transfer

This program is according to the model sections of Chapter 4 and 5 and hydrodynamic equations of Chapter 5. It uses text files to read experimental data from.

```
% By: Hossein Nikakhtari, October, 2004
% With or without packing, Absorption or Desorption
% For absorption choose AB=1, For desorption choose AB=2.
% For without packing choose PK=1, For with packing choose PK=2.
% Choose correct experimental data file.
% This program finds the best values for KLa and cstar.

global z t Cnj ynj No yIN DL Deltat Deltaz tDelay ULR UGR TetaGR
global c0  t0 z0 tF zF zFinal tFinal n texp Cexp  ystar AB
%global x

tic

threeD = 1; % 3-D figures
threeD = 2; % No 3-D figures


AB = 1; % Absorption
% AB = 2; % Desorption
% PK = 1; % Without packing
PK = 2; % With packing

Cnj = zeros; % Liquid phase concentrations matrix (g/L)
```

```
ynj = zeros; % Gas phase concentrations matrix (g/L)
t = zeros; % Time (s)
z = zeros;
tpt = zeros; % Time vector for Figure 2
Cnjpt = zeros; % Concentrations matrix for Figure 2
texp = zeros; % Experimental time vector (s)
Cexp = zeros; % Experimental liquid concentrations vector (g/L)
tFig = zeros; % Time vector for Figure 3 and 4
tFigGas = zeros;
CnjFig = zeros; % Liquid Concentrations matrix for Figure 3
ynjFig = zeros; % Gas Concentrations matrix for Figure 4

AR = 6.22E-03;          % Riser cross-sectional area (m2)
AD = 1.74E-03; % Downcomer cross-sectional area (m2)
L = 2*1.30 + 2*0.21; % Length of the circulation loop (m)


if AB == 1
   yIN = 0.2727; % Inlet gas concentration for Absorption (g/L)
else
   yIN = 0; % Inlet gas concentration for Desorption (g/L)
end

ystar = 0.27; % Oxygen saturated concentration in air (g/L)
% c0 = 0.0003275; % g/L
% cstar = 0.0057; % g/L
% Klar = 0.001676; % s-1
Q = 2.58e-5; % Air flow rate (m3/s)
JGR = Q/AR; % Air superficial velocity (m/s)

hp = 1.2; % Packing height (m)
Phis = 0.99; % Packing porosity

if PK == 1
   % without packing
   TetaGR = 3.229*JGR^1.016; % Gas holdup (Eq. 5-12)
   CF = 48.92; % Friction loss variable (m/s, Eq. 5-14)
   Bo = 47; % Bodenstein number
else
   % with packing
   TetaGR = 1.180*JGR^0.743; % Gas holdup (Eq. 5-13)
   CF = 10.48; % Friction loss variable (m/s, Eq. 5-15)
   Bo = 45.45; % Bodenstein number
end

E = (TetaGR/((1-TetaGR)^(-2)+(AR/AD)^2))^0.92; % Gas holdup function (m/s, Eq. 5-
4)
```

```
ULR = CF*E; % Liquid velocity in the riser section (m/s, Eq. 5-3)

DL = ULR*L/Bo; % Axial dispersion coefficient (m2/s, Eq. 5-5)

UGR = JGR/TetaGR; % Gas velocity in the riser section (m/s)


% DL = 0; % without Dispersion
% ULR = 0; % CSTR Method
% UGR = 0;

Deltat = 0.3; % Time step (s)
Deltaz = 0.1; % Height step (m)

z0 = 0; % Initial height (m)
zFinal = 1.4; % Maximum height (m)
% Deltaz = zFinal; % CSTR Method
t0 = 0; % Starting time (s)
% tFinal = 2400; % Desired ending time (s)

HD = 1.39 + 2*0.21; % Downcomer length, including elbows (m)
JLR = ULR*(1-TetaGR); % Liquid superficial velocity in the riser section (m/s)
JLD = JLR*(AR/AD); % Liquid superficial velocity in the downcomer section (m/s, Eq.
5-10)
tDelay = HD/JLD; % Delay time in the downcomer (s, Eq. 5-9)
% tDelay =0; % CSTR Method

% Reading data from the related text file
if PK == 1
   if AB == 1
      fid = fopen('Ox-5-two-Abs.txt'); % Absorption without packing
   else
      fid = fopen('Ox-5-two-Des.txt'); % Desorption without packing
   end
else
   if AB == 1
      fid = fopen('PB-Ox-2-one-Abs.txt'); % Absorption with packing
   else
      fid = fopen('PB-Ox-2-one-Des-1.txt'); % Desorption with packing
   end
end

[expdata, count] = fscanf(fid, '%g %g', [2 inf]); % Experimental data, it has 2 rows.
fclose(fid);
   texp = expdata(1,:); % Vector of time (s)
   Cexp = expdata(2,:)/1000; % Vector of experimental liquid phase concentrations (g/L)
   n = count/2; % Number of experimental data readings
```

```
tFinal = texp(n) % Ending time (s)
c0 = Cexp(1); % Initial liquid phase concentration (g/L)

% Running optimization command of Matlab
No=0; % Counter
[x] = fminsearch ('ConDis', [0.02,0.006])
% Running differential equations program without optimization
% [x] = [0.0011, 0.0062]
% ConDisAMAD

% Fig. of liquid phase concentrations over time (data and model)
for i = 1:n
   plot(texp(i),Cexp(i),'o');
        hold on
end
plot(t,Cnj(:,zF));

grid on
xlabel('Time (s)')
ylabel('Length (m)');
ylabel('Oxygen concentration (g/L)');
title('Liquid Phase');

% Fig. of liquid phase concentrations over time in early times (upto npt s)
npt = 120; % Maximum time for Figure 2 (s)
for i = 1:npt/Deltat
 tpt(i) = t(i);
 Cnjpt(i) = Cnj(i,zF-1);
end

figure(2)
for i = 1:12
   plot(texp(i),Cexp(i),'o');
        hold on
end
plot(tpt,Cnjpt(:));

grid on
xlabel('Time (s)')
ylabel('Length (m)');
ylabel('Oxygen concentration (g/L)');
title('Liquid Phase');

% Writing results in an Excel file
if PK == 1
   if AB == 1
      fid = fopen ('ExcelResults\Abs-noPK.xls','w');
```

```
        fid1 = fopen ('ExcelResults\Abs-noPK-Gas.xls','w');
        fprintf (fid, 'Desorption without packing\n Q =\t %4f\t', Q);
        fprintf (fid, 'm3/s\n');
    else
        fid = fopen ('ExcelResults\Des-noPK.xls','w');
        fprintf (fid, 'Desorption without packing\n Q =\t %4f\t', Q);
        fprintf (fid, 'm3/s\n');
    end
else
    if AB == 1
        fid = fopen ('ExcelResults\Abs-PK.xls','w');
        fid1 = fopen ('ExcelResults\Abs-PK-Gas.xls','w');
        fprintf (fid, 'Absorption with packing\n Q =\t %4f\t', Q);
        fprintf (fid, 'm3/s\n');
    else
        fid = fopen ('ExcelResults\Des-PK.xls','w');
        fprintf (fid, 'Desorption with packing\n Q =\t %4f\t', Q);
        fprintf (fid, 'm3/s\n');
    end
end


fprintf (fid, '\t');
fprintf (fid, '%4f\t', z(:));
fprintf (fid, '\n');
for i=1:5:tF
    fprintf (fid, '%4f\t', (i-1)*Deltat);
    fprintf (fid, '%4f\t', Cnj(i,:));
    fprintf (fid, '\n');
end
for i = 1:20
    fprintf (fid, '%4f\t', texp(i), Cexp(i));
    fprintf (fid, '\n');
end
for i = 21:3:n
    fprintf (fid, '%4f\t', texp(i), Cexp(i));
    fprintf (fid, '\n');
end
fclose(fid)


if AB == 1
    RDeltat = round (1/Deltat)
    for i=1:RDeltat:tF
        fprintf (fid1, '%4f\t', round((i-1)*Deltat));
        fprintf (fid1, '%4f\t', ynj(i,:));
        fprintf (fid1, '\n');
```

```
   end
   fclose(fid1)
end

% A 3-Dimentional picture of the liquid phase concentrations
if threeD == 1
          tFinalFig = tFinal; % s
          tFFig = tFinalFig/Deltat+1;
          for i = 1:(tFFig)
           tFig(i) = t(i);
              for j = 1:zF
               CnjFig(i,j) = Cnj(i,j);
           ynjFig(i,j) = ynj(i,j);
       end
   end
%    for i = 17:(tFFig)
%        tFigGas(i-16) = t(i);
%            for j = 1:zF
%          ynjFig(i-16,j) = ynj(i,j);
%      end
%    end

          figure(3)
          mesh(z,tFig,CnjFig);
          ylabel('Time (s)');
          xlabel('Length (m)');
          zlabel('Concentration (g/L)');
          % title('Liquid Phase');
          az = 100;
          el = 32;
          view(az, el);
          view([10,1,1]);

% A 3-Dimentional picture of the gas phase concentrations
   figure(4)
          mesh(z,tFig,ynjFig);
          ylabel('Time (s)');
          xlabel('Length (m)');
          zlabel('Concentration (g/L)');
          % title('Gas Phase');
          az = 100;
          el = 32;
          view(az, el);
          view([10,1,1]);
          % axis([0 1.5 0 100 1 3])
          % az = 100;
          % el = 32;
```

```
end

% Show some results
TetaGR
ULR
DL
tDelay
time = toc;
time
```

B.3.2 A program for calculation of the Sum of Squared errors

This program is an M-file used in the main program.

```
% Program for calculation of the Sum of Squared errors
% With or Without packing

function SS = ConDis(x)
global z z0 zF t t0 tF c0 yIN  DL Deltaz Deltat ULR UGR TetaGR tDelay
global AL BL EL H BG VG t Cnj ynj texp Cexp n No tFinal zFinal ystar AB
% global x

No = No+1
Klar = x(1); % Overall volumetric mass transfer coefficient (1/s)

if AB == 1
   % Absorption
   cstar = x(2); % Liquid phase equilibrium concentration (g/L)
   if cstar > 0.008
      cstar = 0.008;
   end
   H = ystar/cstar; % Henry's law coefficient (g/L / g/L)
else
   % Desorption
   c0 = x(2); % Liquid phase initial concentration (g/L)
   H = ystar/c0; % Henry's law coefficient (g/L / g/L)
end

% Variables of finite differencing numerical solution for partial
% differential equations (Eqs. 3-13 to 3-17)
AL      = DL*Deltat/Deltaz^2;
BL      = ULR*Deltat/(2*Deltaz);
BG      = UGR*Deltat/(2*Deltaz);
EL      = Klar*Deltat;
VG      = Klar*Deltat*(1-TetaGR)/TetaGR;
```

```
% Variables for time and distance in the solution program
tF = round((tFinal+100)/Deltat+1); % Plus one because of zero time
zF = round(zFinal/Deltaz+1); % Plus one because Z(1) belongs to start point

% Running finite differencing solution program for partial differential equations
ConEqs

% Calculation of SS (Sum of Squared errors)
SS = 0;
j = zF;
for i = 0:tFinal
  for k = 1:n
   if abs(texp(k) - i) < 0.01
      l = round(i/Deltat+1);
      SS = SS + (Cexp(k)-Cnj(l,j))^2;
   end
  end
end
SS
```

B.3.3 Program for solving two partial differential equations simultaneously

This program is finite differencing method to solve two partial differential equations simultaneously (Equations 5.6 and 5.7).

```
% Finite differencing solution program for two partial differential equations (5-6 and 5-7)
% Results of this program are matrixes for the liquid phase and gas phase concentrations
% (Cnj and ynj) rows vary by time, and columns vary by height

function ConEqs
global z z0 zF t t0 tF c0 yIN Deltaz Deltat tDelay AL BL EL H BG VG t Cnj ynj

t(1) = t0;
  i = 1;
  for j = 1:zF
    if j==1
      z(j) = z0;
    else
      z(j) = z(j-1) + Deltaz;
    end
    Cnj(i, j) = c0;
    ynj(i, j) = H*c0;
    ynj(i, j) = yIN; % CSTR Method
  end
```

```
% Variable for delay time (tD)
  tD = round(tDelay/Deltat+1)
  if tD<0
    tD=1;
  end

% Before delay time
  if tDelay > 0
     for i = 2:tD
       t(i) = t(i - 1) + Deltat;
       j = 1;
       Cnj(i, j) = c0;
       ynj(i, j) = yIN;
       for j = 2:zF-1
         Cnj(i, j) = (AL + BL) * Cnj(i - 1, j - 1) + (1 - 2 * AL - EL) * Cnj(i - 1, j) + (AL -
BL) * Cnj(i - 1, j + 1) + EL / H * ynj(i - 1, j);
         %ynj(i, j) = 2 * BG * ynj(i - 1, j - 1) + (1 - VG / H) * ynj(i - 1, j) - 2 * BG * ynj(i
- 1, j + 1) + VG * Cnj(i - 1, j);
         ynj(i, j) = 2 * BG * ynj(i - 1, j - 1) + (1 - VG / H) * ynj(i - 1, j) - 2 * BG * ynj(i -
1, j) + VG * Cnj(i - 1, j);
       end
       j = zF;
       Cnj(i, j) = (AL + BL) * Cnj(i - 1, j - 1) + (1 - AL - BL - EL) * Cnj(i - 1, j) + EL /
H * ynj(i - 1, j);
       ynj(i, j) = 2 * BG * ynj(i - 1, j - 1) + (1 - 2 * BG - VG / H) * ynj(i - 1, j) + VG *
Cnj(i - 1, j);
     end
  end

% After delay time
         for i = tD+1:tF
           t(i) = t(i - 1) + Deltat;
    j = 1;
    Cnj(i, j) = Cnj(i-tD,zF);
    ynj(i, j) = yIN;
    for j = 2:zF-1
        Cnj(i, j) = (AL + BL) * Cnj(i - 1, j - 1) + (1 - 2 * AL - EL) * Cnj(i - 1, j) + (AL -
BL) * Cnj(i - 1, j + 1) + EL / H * ynj(i - 1, j);
      %ynj(i, j) = 2 * BG * ynj(i - 1, j - 1) + (1 - VG / H) * ynj(i - 1, j) - 2 * BG * ynj(i -
1, j + 1) + VG * Cnj(i - 1, j);
      ynj(i, j) = 2 * BG * ynj(i - 1, j - 1) + (1 - VG / H) * ynj(i - 1, j) - 2 * BG * ynj(i - 1,
j + 1) + VG * Cnj(i - 1, j);
      %ynj(i, j) = yIN; % Exact CSTR Method
    end
    j = zF;
```

```
    Cnj(i, j) = (AL + BL) * Cnj(i - 1, j - 1) + (1 - AL - BL - EL) * Cnj(i - 1, j) + EL / H *
ynj(i - 1, j);
    ynj(i, j) = 2 * BG * ynj(i - 1, j - 1) + (1 - 2 * BG - VG / H) * ynj(i - 1, j) + VG *
Cnj(i - 1, j);
    %ynj(i, j) = yIN; % Exact CSTR Method
  End
```

B.4 Matlab program for VOC Mass Transfer

This program also includes three M-files. The first M-file is the main program and next two M-files are similar to the oxygen mass transfer programs (B.3.2 and B.3.1) and are not presented here.

B.4.1 Main Matlab programming for VOC mass transfer

This program is for toluene (or benzene) mass transfer according to the model section of Chapter 6. It uses Excel files to read experimental data from.

```
% By: Hossein Nikakhtari, October, 2004
% Toluene mass transfer in the ELAB (According to the Model in Chapter 6)
% With or without packing, Absorption or Desorption
% It finds the best KLa and cstar
% For absorption choose AB=1, For desorption choose AB=2.
% For without packing choose PK=1, For with packing choose PK=2.
% Choose correct experimental data file.

global z t Cnj ynj No yIN DL Deltat Deltaz tDelay ULR UGR TetaGR
global c0  t0 z0 tF zF zFinal tFinal n texp Cexp  ystar AB H
% global x

tic
% Choose the process
AB = 1; % Absorption
% AB = 2; % Desorption
% PK = 1; % Without packing
PK = 2; % With packing

threeD = 1; % 3-D figures
threeD = 2; % No 3-D figures
```

```
xlsout = 1; % You want Excel output
% xlsout = 2; % You don't want Excel output

Cnj = zeros; % Liquid phase concentrations matrix (g/L)
ynj = zeros; % Gas phase concentrations matrix (g/L)
t = zeros; % Time (s)
tpt = zeros; % Time vector for Figure 2
Cnjpt = zeros; % Concentrations matrix for Figure 2
texp = zeros; % Experimental time vector (s)
Cexp = zeros; % Experimental liquid concentrations vector (g/L)
texpgas = zeros;
yexp = zeros;
tFig = zeros; % Time vector for Figure 4 and 5
CnjFig = zeros; % Liquid Concentrations matrix for Figure 4
ynjFig = zeros; % Gas Concentrations matrix for Figure 5

% Reading experimental data from an appropriate excel file
if PK == 1
   if AB == 1
      expdata = xlsread('Tol-2nd50.xls', 1, 'F12:G45'); % Absorption without packing
      tFinal = xlsread('Tol-2nd50.xls', 1, 'F7') % s
      gasdata = xlsread('Tol-2nd50.xls', 1, 'K62:L90'); % Absorption without packing,
just for fig 3
   else
      expdata = xlsread('Tol-50.xls', 1, 'M12:N45'); % Desorption without packing
      tFinal = xlsread('Tol-50.xls', 1, 'M7') % s
      gasdata = xlsread('Tol-50.xls', 1, 'K101:L125'); % Desorption without packing, just
for fig 3
   end
else
   if AB == 1
      expdata = xlsread('PB-Tol-40-2nd.xls', 1, 'F12:G45'); % Absorption with packing
      tFinal = xlsread('PB-Tol-40-2nd.xls', 1, 'F7') % s
      gasdata = xlsread('PB-Tol-40-2nd.xls', 1, 'K62:L90'); % Absorption with packing,
just for fig 3
   else
      expdata = xlsread('PB-Tol-70.xls', 1, 'M12:N45'); % Desorption with packing
      tFinal = xlsread('PB-Tol-70.xls', 1, 'M7') % s
      gasdata = xlsread('PB-Tol-70.xls', 1, 'K101:L125'); % Desorption with packing, just
for fig 3
   end
end

texp = expdata(:,1); % Vector of time (s)
Cexp = expdata(:,2)/1000; % Vector of experimental liquid phase concentrations (g/L)
% c0 = Cexp(1); % Initial liquid phase concentration (g/L)
```

```
% Reading gas phase experimental data if there is any
if gasdata(1,1) > 0
   texpgas = gasdata(:,1); % Vector of time for gas phase data (s)
   yexp = gasdata(:,2)/1000; % Vector of experimental gas phase concentrations (g/L)
end

if AB == 1
   yIN = 0.13; % Inlet gas concentration for Absorption (g/L)
else
   yIN = 0; % Inlet gas concentration for Desorption (g/L)
end

ystar = 0.13; % Toluene saturated concentration in air (g/L)
% H = 0.284; % Henry's constant for toluene (g/L / g/L)
Q = 4.18e-5; % Air flow rate (m3/s)

Deltat = 0.3; % Time step (s)
Deltaz = 0.1; % Height step (m)

z0 = 0; % Initial height (m)
zFinal = 1.4; % Maximum height (m)
t0 = 0; % Starting time (s)
% tFinal = 2400; % Desired ending time (s)

hp = 1.2; % Packing height (m)
Phis = 0.99; % Packing porosity

AR = 6.22E-03;          % Riser cross-sectional area (m2)
AD = 1.74E-03; % Downcomer cross-sectional area (m2)
L = 2*1.39 + 2*0.21; % Length of the circulation loop (m)

JGR = Q/AR; % Air superficial velocity (m/s)

if PK == 1
   % without packing
   TetaGR = 3.229*JGR^1.016; % Gas holdup
   CF = 48.92; % Friction loss variable (m/s)
   Bo = 47; % Bodenstein number
else
   % with packing
   TetaGR = 1.180*JGR^0.743; % Gas holdup
   CF = 10.48; % Friction loss variable (m/s)
   Bo = 45.45; % Bodenstein number
end

E = (TetaGR/((1-TetaGR)^(-2)+(AR/AD)^2))^0.92; % Gas holdup function (m/s)
```

```
ULR = CF*E; % Liquid velocity in the riser section (m/s)

DL = ULR*L/Bo; % Axial dispersion coefficient (m2/s)

UGR = JGR/TetaGR; % Gas velocity in the riser section (m/s)


HD = 1.30 + 2*0.21; % Downcomer length, including elbows (m)
JLR = ULR*(1-TetaGR); % Liquid superficial velocity in the riser section (m/s)
JLD = JLR*(AR/AD); % Liquid superficial velocity in the downcomer section (m/s)
tDelay = HD/JLD; % Delay time in the downcomer (s)

% Running optimization command of Matlab
No=0; % Counter
[x] = fminsearch ('ConDisxls', [0.002, 1, Cexp(1)])
% Running differential equations program without optimization
% [x] = [0.0011, 0.0062]
% ConDisAMAD

Time1 = toc

% Fig. of liquid phase concentrations over time (data and model)
figure(1)
plot(texp(:),Cexp(:),'o');
hold on
plot(t,Cnj(:,zF));
grid on
xlabel('Time (s)')
ylabel('Length (m)');
ylabel('Concentration (g/L)');
title('Liquid Phase');

% Fig. of liquid phase concentrations over time in early times (upto npt s)
npt = 300; % Maximum time for Figure 2 (s)
for i = 1:npt/Deltat
   tpt(i) = t(i);
   Cnjpt(i) = Cnj(i,zF-1);
end
figure(2)
for i = 1:3
   plot(texp(i),Cexp(i),'o');
   hold on
end
plot(tpt,Cnjpt(:));
grid on
xlabel('Time (s)')
ylabel('Length (m)');
```

```
ylabel('Concentration (g/L)');
title('Liquid Phase');

% Fig. of gas phase concentrations over time
if gasdata(1,1) > 0
   figure(3)
   plot(texpgas(:),yexp(:),'o');
   hold on
   plot(t,ynj(:,zF));
   grid on
   xlabel('Time (s)')
   ylabel('Length (m)');
   ylabel('Concentration (g/L)');
   title('Gas Phase');
end

% Writing results in an Excel file
if xlsout == 1;
          if PK == 1
      if AB == 1
           fid = fopen ('ExcelResults\Abs-noPK.xls','w');
              fid1 = fopen ('ExcelResults\Abs-noPK-Gas.xls','w');
      else
           fid = fopen ('ExcelResults\Des-noPK.xls','w');
      end
   else
      if AB == 1
           fid = fopen ('ExcelResults\Abs-PK.xls','w');
      else
        fid = fopen ('ExcelResults\Des-PK.xls','w');
            end
         end

         for i=1:10:tF
      fprintf (fid, '%4f\t', i-1);
      fprintf (fid, '%3.2e\t', Cnj(i,:));
      fprintf (fid, '\n');
         end
         fclose(fid)

         if (AB == 1) & (PK == 1)
      for i=1:10:tF
         fprintf (fid1, '%4f\t', i-1);
         fprintf (fid1, '%3.2e\t', ynj(i,:));
         fprintf (fid1, '\n');
      end
      fclose(fid1)
```

```
        end
end

% A 3-Dimentional picture of the liquid phase concentrations
if threeD == 1
        tFinalFig = tFinal; % s
        tFFig = tFinalFig/Deltat+1;
        for i = 1:(tFFig)
      tFig(i) = t(i);
            for j = 1:zF
         CnjFig(i,j) = Cnj(i,j);
         ynjFig(i,j) = ynj(i,j);
            end
        end
        figure(4)
        mesh(z,tFig,CnjFig);
        ylabel('Time (s)');
        xlabel('Length (m)');
        zlabel('Concentration (g/L)');
        % title('Liquid Phase');
        az = 100;
        el = 32;
        view(az, el);
        view([10,1,1]);

% A 3-Dimentional picture of the gas phase concentrations
   figure(5)
        mesh(z,tFig,ynjFig)
        ylabel('Time (s)')
        xlabel('Length (m)');
        zlabel('Concentration (g/L)');
        % title('Gas Phase');
        az = 100;
        el = 32;
        view(az, el);
        view([10,1,1]);
        % axis([0 1.5 0 100 1 3])
        % az = 100;
        % el = 32;
end

% Show some results
H
% TetaGR
% ULR
% DL
% tDelay
```

```
Time2 = toc
```

B.5 Matlab program for Phenol Mass Transfer

This program also includes three M-files. The first M-file is the main program and is similar to the main program for other VOCs (B.4.1), but the next two auxiliary M-files are different for the case of phenol (explained earlier in 6.5.3) and are presented here.

B.5.1 Program for calculation of Sum of Squared errors

```
% Program for calculation of the Sum of Squared errors
% for the case of phenol mass transfer
% With or Without packing

function SS = ConDis(x)
global z z0 zF t t0 tF c0 yIN  DL Deltaz1 Deltat ULR UGR TetaGR tDelay t Cnj ynj
global texp Cexp n No tFinal zFinal ystar AB EL VG
global x

No = No+1
Klar = x; % Overall volumetric mass transfer coefficient (s-1)

% Variables of finite differencing numerical solution for partial
% differential equations
EL      = Klar*Deltat;
VG      = Klar*Deltat*(1-TetaGR)/TetaGR;

% Running finite differencing solution program for partial differential equations
ConEqs

% Calculation of SS (Sum of Squared errors)
SS = 0;
j = zF;
for i = 0:tFinal
  for k = 1:n
   if abs(texp(k) - i) < 0.01
      l = round(i/Deltat+1);
      SS = SS + 1e6 * (Cexp(k)-Cnj(l,j))^2;
   end
```

```
  end
end
SS
```

B.5.2 Program for solving two partial differential equations simultaneously for the case of phenol

As explained earlier (section 6.5.3) the solving method used for two partial differential equations (Equations 6.9 and 6.10) is different for the case of phenol, and a different program was used, which is presented here.

```
% Finite differencing solution program for two partial differential equations (6-9 and 6-
% 10) for the case of phenol mass transfer with a variable height step
% (nn times of the previous one) as it was discussed in Chapter 6.
% Results of this program are matrixes for the liquid phase and gas phase concentrations
% (Cnj and ynj) rows vary by time, and columns vary by height.

function ConEqs
global z z0 zF t t0 tF c0 yIN Deltaz1 Deltat tDelay H t Cnj ynj
global zFinal tFinal DL ULR UGR TetaGR EL VG

t(1) = t0;
Deltaz = Deltaz1;
zF = 1;
z(zF) = z0 + Deltaz;
nn = 2;

while z(zF) < zFinal-nn*Deltaz
  Deltaz = nn * Deltaz;
  zF = zF + 1;
  z(zF) = z(zF-1) + Deltaz;
end
DeltazF = zFinal - z(zF);
zF = zF + 1;
z(zF) = zFinal;

% Variables for time and distance as it is used in this program
tF = round(tFinal/Deltat+1); % Plus one because of zero time
tD = round(tDelay/Deltat+1); % Plus one because of zero time

i = 1;
for j = 1:zF
        Cnj(i, j) = c0;
        ynj(i, j) = yIN;
end
```

```
% Before delay time (tD)
for i = 2:tD
        t(i) = t(i - 1) + Deltat;
  j = 1;
  Deltaz = Deltaz1;
        AL      = DL*Deltat/Deltaz^2;
        BL      = ULR*Deltat/(2*Deltaz);
        BG      = UGR*Deltat/(2*Deltaz);

  Cnj(i, j) = (AL + BL) * c0 + (1 - 2 * AL - EL) * Cnj(i - 1, j) + (AL - BL) * Cnj(i - 1, j
+ 1) + EL / H * ynj(i - 1, j);
  ynj(i, j) = yIN;

  for j = 2:zF-1
    Deltaz = nn * Deltaz;
                AL      = DL*Deltat/Deltaz^2;
                BL      = ULR*Deltat/(2*Deltaz);
                BG      = UGR*Deltat/(2*Deltaz);

    Cnj(i, j) = (AL + BL) * Cnj(i - 1, j - 1) + (1 - 2 * AL - EL) * Cnj(i - 1, j) + (AL - BL)
* Cnj(i - 1, j + 1) + EL / H * ynj(i - 1, j);
        ynj(i, j) = 2 * BG * ynj(i - 1, j - 1) + (1 - 2 * BG - VG / H) * ynj(i - 1, j) + VG *
Cnj(i - 1, j);
  end

  j = zF;
  Deltaz = DeltazF;
        AL      = DL*Deltat/Deltaz^2;
        BL      = ULR*Deltat/(2*Deltaz);
        BG      = UGR*Deltat/(2*Deltaz);

  Cnj(i, j) = (AL + BL) * Cnj(i - 1, j - 1) + (1 - AL - BL - EL) * Cnj(i - 1, j) + EL / H *
ynj(i - 1, j);
  ynj(i, j) = 2 * BG * ynj(i - 1, j - 1) + (1 - 2 * BG - VG / H) * ynj(i - 1, j) + VG * Cnj(i -
1, j);
end

% After delay time (tD)
for i = tD+1:tF
  t(i) = t(i - 1) + Deltat;
  j = 1;
  Deltaz = Deltaz1;
        AL      = DL*Deltat/Deltaz^2;
        BL      = ULR*Deltat/(2*Deltaz);
        BG      = UGR*Deltat/(2*Deltaz);
```

```
  Cnj(i, j) = (AL + BL) * Cnj(i-tD,zF) + (1 - 2 * AL - EL) * Cnj(i - 1, j) + (AL - BL) *
Cnj(i - 1, j + 1) + EL / H * ynj(i - 1, j);
  ynj(i, j) = yIN;

  for j = 2:zF-1
    Deltaz = nn * Deltaz;
                AL      = DL*Deltat/Deltaz^2;
                BL      = ULR*Deltat/(2*Deltaz);
                BG      = UGR*Deltat/(2*Deltaz);

    Cnj(i, j) = (AL + BL) * Cnj(i - 1, j - 1) + (1 - 2 * AL - EL) * Cnj(i - 1, j) + (AL - BL)
* Cnj(i - 1, j + 1) + EL / H * ynj(i - 1, j);
                ynj(i, j) = 2 * BG * ynj(i - 1, j - 1) + (1 - 2 * BG - VG / H) * ynj(i - 1, j) +
VG * Cnj(i - 1, j);
  end

  j = zF;
  Deltaz = DeltazF;
        AL      = DL*Deltat/Deltaz^2;
        BL      = ULR*Deltat/(2*Deltaz);
        BG      = UGR*Deltat/(2*Deltaz);

  Cnj(i, j) = (AL + BL) * Cnj(i - 1, j - 1) + (1 - AL - BL - EL) * Cnj(i - 1, j) + EL / H *
ynj(i - 1, j);
  ynj(i, j) = 2 * BG * ynj(i - 1, j - 1) + (1 - 2 * BG - VG / H) * ynj(i - 1, j) + VG * Cnj(i -
1, j);
end
```

B.6 Matlab program for Bioremediation

This program includes two M-files. The first M-file is the main program and the second M-file is an auxiliary program for solving diferential equations.

B.6.1 Main Matlab programming for bioremediation process

This program is according to the model section of Chapter 7.

```
% Main Matlab programming for bioremediation experiments (According to the
% Model in Chapter 7)
% By: Hossein Nikakhtari, November 2005
```

```
global MUmax Ks Ki Yxs H ULR UGR TetaGR DL KLa Snot dSnot ynot Xnot Xbio
global Sout Xout yout dSout n

tic
'Program started'
n = 0; % Counter
t = zeros; % Time (s)
X = zeros; % Free biomass concentration (mg/L)
S = zeros; % Substrate (phenol) concentration in the liquid phase (mg/L)
y = zeros; % Phenol concentration in the gas phase (mg/L)

AR = 6.22e-3; % Riser cross-sectional area (m2)
AD = 1.74e-3; % Downcomer cross-sectional area (m2)
L = 2*1.30 + 2*0.21; % Length of the circulation loop (m)

Wp = 0.3994; % Packing weight (kg)
Rop = 5139; % Packing density (kg/m3)
Dp = 5e-4; % Packing diameter (m)
Delta = 5.8e-4; % Biofilm thickness (m)
Robio = 300; % Biofilm density (kg/m3)
Alfa = 0.112; % Active biomass in biofilm correction factor
VR = 1.42 * AR; % Riser section volume (m3)
Xbio = 4e3*Wp*Delta*Robio*Alfa/(Rop*Dp*VR); % Active biomass in biofilm
                                                % (mg/L, Eq. 7.11)
H = 1.82e-5; % Henry's coefficient for phenol (mg/L / mg/L)

MUmax = 0.170/3600; % Maximum specific growth rate (s-1)
Ki = 470; % Growth equation constant (mg/L)
Ks = 1; % Growth equation constant (mg/L)
Yxs = 0.0881; % Substrate yield factor (mg/mg)

Q = 9.23e-5; % Air flow rate (m3/s)
JGR = Q/AR; % Air superficial velocity (m/s)

hp = 1.2; % Packing height (m)
Phis = 0.99; % Packing porosity

TetaGR = 1.460*JGR^0.784; % Gas holdup with packing (Eq. 7.5)
CF = 10.8; % Friction loss variable with packing (m/s)
Bo = 45.5; % Bodenstein number with packing
E = (TetaGR/((1-TetaGR)^(-2)+(AR/AD)^2))^0.92; % Gas holdup function
                                                % (m/s, Eq. 7.7)
ULR = CF*E; % Liquid velocity in the riser section (m/s, Eq. 7.6)

DL = ULR*L/Bo; % Axial dispersion coefficient (m2/s, Eq. 7.8)
% DL = 0.0000043;
```

```
TetaLR = 1 - TetaGR; % Liquid holdup
UGR = JGR / TetaGR; % Gas velocity in the riser section (m/s)
JLR = ULR * TetaLR; % Liquid superficial velocity (m/s)
F = JLR * AR; % Liquid flow rate in the ELAB (m3/s)
Fo = 1.67e-6; % Liquid make up, coming in or going out of the ELAB (m3/s)

KLa = 0.0001382; % Phenol mass transfer coefficient in the liquid (s-1)

dXnot = 0; % Inlet dX/dz (Eq. 7.14)
dSnot = 0; % Inlet dS/dz (Eq. 7.16)
ynot = 0.8; % Inlet y (mg/L, Eq. 7.17)
Snot=0; % Inlet S (mg/L, Eq. 7.15)
Xnot = 80; % Inlet y (mg/L, Eq. 7.13)
Xout=1;
Xoutold=0;

while abs(Xoutold-Xout)>0.001
   n=n+1;
        Xoutold = Xout;

   options = odeset('RelTol',1e-3,'AbsTol',[1e-3 1e-3 1e-3 1e-3 1e-3]);
        [z,y] = ode45('difeqsELAB',[0 1.4],[Snot dSnot Xnot dXnot ynot],options);

   Xnot = Xout*F/(F+Fo); % (Eq. 7.18)
   Snot = Sout*F/(F+Fo); % (Eq. 7.19)

   % type elapsed time on the screen
   t(n) = n*8/3600;
   X(n) = Xout;
   S(n) = Sout;
   if round(n/100) == n/100
      time = round (toc)
   end
end

% Writing steady state results on Excel
fid = fopen ('ExcelResults\Riser.xls','w');
for i=1:size(z,1)
   fprintf (fid, '%4f\t', z(i),'%3.2e\t',y(i,1),y(i,3),y(i,5));
   fprintf (fid,'\n');
end
fclose(fid);
% Writing transient part results on Excel
fid1 = fopen ('ExcelResults\Transient.xls','w');
for i=1:n
   fprintf (fid1, '%4f\t', t(i),'%3.2e\t',X(i),S(i));
   fprintf (fid1,'\n');
```

```
end
fclose(fid);

% Fig. of steady state concentrations of X, S, and y vs. height of the column
plot(z,y(:,1),'-',z,y(:,3),'-.',z,y(:,5),'.');
xlabel('Length (m)');
ylabel('Concentration (mg/L)');

% Fig. of transient concentration of X vs. time
figure(2)
plot (t,X,'.');
xlabel('Time (h)');
ylabel('Biomass Concentration (mg/L)');

% Fig. of transient concentration of S vs. time
figure(3)
plot (t,S,'.');
xlabel('Time (h)');
ylabel('Substrate Concentration (mg/L)');

% Fig. of steady state concentrations of S and y vs. height of the column
figure(4)
plot(z,y(:,1),'-',z,y(:,5),'.');
xlabel('Length (m)');
ylabel('Concentration (mg/L)');

% type results for iteration number, outlet concentrations, and elapsed time
n
Sout
Xout
yout
toc
```

B.6.2 A program for solving three differential equations simultenously

This program is for solving three differential equations (Equations 7.1, 7.2, and 7.3) simultaneously using Matlab codes.

```
% differential equations used in the Main programming of the bioremediation
% (according to the model in Chapter 7)
% By: Hossein Nikakhtari
% November 2005

function dy = difeqsELAB(z,y)
global MUmax Ks Ki Yxs H ULR UGR TetaGR DL KLa Snot dSnot ynot Xnot Xbio
```

```
global Sout Xout yout dSout n

MU = MUmax * ( y(1) / (y(1) + Ks + y(1)^2 / Ki)); % Specific growth rate
                                                  % (1/s, Eq. 7.4)
XT = Xbio + Xnot; % Total biomass (mg/L, Eq. 7.10)
Sstar =  y(5)/H; % Equilibrium substrate concentration
            % (mg/L, Eq. 7.9)
dy = zeros(5,1); % A column vector

   dy(1) = y(2); % y(1)= S
        dy(2) = -1/DL*(ULR*y(2) - KLa*(Sstar-y(1)) + MU*XT/Yxs); % y(2)= dS/dz,
                                                                 % Eq. 7.1

   dy(3) = y(4); % y(3)= X
        dy(4) = -1/DL*(ULR*y(4) - MU*XT); % y(4)= dX/dz, Eq. 7.2

   dy(5) = -1/UGR*(KLa*(Sstar-y(1))*(1-TetaGR)/TetaGR); % y(5)= y, Eq. 7.3

Sout= y(1); % Outlet S (mg/L)
Xout= y(3); % Outlet X (mg/L)
yout= y(5); % Outlet y (mg/L)
dSout= y(2); % Outlet dS/dz
```